Autoignition Studies on Bio-Derived Fuels in a Constant Volume Combustion Chamber

A Thesis
Presented in Partial Fulfilment of the Requirements for the
Degree of Master of Science
with a
Major in Mechanical Engineering
in the
College of Graduate Studies
University of Idaho

by
Richard Leathers

Major Professor: Kamal Kumar, Ph.D.
Committee Members: Steven Beyerlein, Ph.D.; Daniel Cordon, Ph.D.;
John Crepeau, Ph. D.; Chih-Jen Sung, Ph. D.
Department Administrator: Steven Beyerlein, Ph.D.

December 2017

Authorization to Submit a Thesis

This thesis of Richard Leathers, submitted for the degree of Master of Science with a Major in Mechanical Engineering and titled “Autoignition Studies on Bio-Derived Fuels in a Constant Volume Combustion Chamber," has been reviewed in final form. Permission, as indicated by the signatures and dates below, is now granted to submit final copies to the College of Graduate Studies for approval.

Major Professor: _____ Date: _____
Kamal Kumar, Ph.D.

Committee Members: _____ Date: _____
Steven Beyerlein, Ph.D.

_____ Date: _____
Daniel Cordon, Ph.D.

_____ Date: _____
John Crepeau, Ph.D.

_____ Date: _____
Chih-Jen Sung, Ph.D.

Department Administrator: _____ Date: _____
Steven Beyerlein, Ph.D.

Abstract

This thesis reports three works on experimental investigation into the autoignition behavior of bio-derived fuels. Understanding the autoignition behavior of current and future fuels is essential for their clean and efficient use in future energy system. Fuel sprays were injected into a quiescent, pressurized, and preheated air in a constant volume combustion chamber using the Waukesha Fuel Ignition Tester. Autoignition times were determined using the absolute pressure rise and rate of pressure rise within the combustion chamber. Data for potential biofuels has been obtained in the different temperature range of 680 K to 820K and at a pressure of 24 bar. The experimental results provided the Derived Cetane Number (DCN) of the fuel or blend. The DCN is a valuable metric in classifying the about ignition propensity of a fuel. A representative correlation for the DCN as a function of a fuel volumetric blending ratio has been provided where appropriate.

Additionally, the exhaust emissions of the different biofuels have also been studied using non-dispersive infrared analyzers for species like CO, CO_2, O_2, & HC. A chemiluminescence detector was used to measure NO_x emissions. A global equivalence ratio of the fuel or blend was derived from the exhaust gas analysis. Using the global equivalence ratio, the experiments were simulated using a zero-dimensional, constant volume, homogenous reactor model with detailed reaction mechanisms.

The work focused on biofuels such as *n*-butanol, methyl decanoate, and biodiesel made at the University of Idaho's biological engineering facility. *n*-Butanol was chosen for study because it is a potential second-generation biofuel that has certain benefits over ethanol. Methyl decanoate is a fatty acid methyl ester commonly used as a biodiesel surrogate. Biodiesel produced from corn, canola, and soy feedstocks were studied. The fatty acid profiles of the

aforementioned biodiesel fuels were known. This rendered an investigation into the influence of the degree of saturation on the autoignition results.

This work has a significance to both the lab and field. Results like the DCN representative correlation will be useful in determining what mixture of bio-fuel one can use in a certain system. Moreover, the FIT data can be used as a tool to support the validation of chemical mechanisms. Accurate chemical mechanisms are essential for allowing predictive capability in computational models. A first step towards investigating under what conditions the FIT can support the validation of chemical mechanisms has been done via a rudimentary 0-D , constant volume, reactor model that does not consider any physical effects. In general, the agreement between the experimental results and the simulated are results is fair, but could be improved upon. It has been concluded that the homogenous reactor assumption is not entirely accurate for experiments were the ignition delay is short; this is suspected to be because the physical effects of the fuel spray dominate the autoignition behavior. Comparisons between the experimental results and the 0-D computational model may be valid for results with long ignition delay times. Future work is needed in determining the spray parameters in the FIT and developing a full computational model of the reactor that includes all the effects.

Acknowledgments

I wish to express my gratitude to Dr. Steven Beyerlein. His support and guidance throughout my graduate career has been essential to my success. I would like to thank Dr. Chih-Jen Sung for his insightful feedback. His paper revisions were critical in the development of this research. I wish express my appreciation to Dr. Steven Penoncello and Dr. John Crepeau for being inspirational instructors. I owe my deepest gratitude to my mentor and friend, Dr. Kamal Kumar. His guidance into the world of combustion and instruction in the laboratory have been indispensable. Without his continuous optimism, enthusiasm, encouragement and support this study would hardly have been completed. I am indebted to many of my colleagues for their help in this work. I would like to thank Dr. Dev Shrestha and Chad Dunkle for making the biodiesel fuels for the biodiesel study. I wish to express my thanks to Samuel Stuhlman for his help with the biodiesel and methyl deaconate study. Lastly, I would like to thank the University Of Idaho College Of Graduate Studies and the Mechanical Engineering department for the tuition support they provided throughout my graduate career.

Dedication

For my Father, Richard Lee Leathers II.

To my parents, Julie and David Stubbs,
my little brother, Devan Leathers,
the rest of my family, and all my friends.
Your unconditional love and support and have always been there for me.
Thank you so much.

Table of Contents

List of Figures

List of Tables

List of Equations

Introduction

Biomass derived fuels are becoming increasingly viable and economically feasible for use in the transportation and energy production sectors. In general, advances in biomass conversion technologies have allowed for more sustainable production of the various bio-fuels and also permit non-edible feed stocks to be used. This is important to recognize and take advantage of, because the adverse impacts of fossil fuel usage on economic well-being, energy security, as well as climate and human health are becoming increasingly apparent. Currently 80% of the world's energy demand is met by petroleum based fuels, ~60% of that is exhausted by the transportation sector [1]. Additionally, the global energy demand is expected to grow by 37% by 2040 [1]. The adoption of renewable fuels to displace petroleum derived fuels in internal combustion engines should therefore be a high priority. These future fuels should be sustainable, economically viable, and environmentally friendly if they are to displace petroleum derived fuels.

There are three classes of biofuels, or rather classes of feedstock biofuels are derived from: first generation, second generation, and third generation. First generation biofuels use starch, sugars, fats, and vegetable oils as a feedstock to produce biodiesel (fatty acid methyl esters from esterification) and other types of fuels. First generation feedstocks can also be for the production of biogas (methane rich gas from anaerobic digestion of organic materials), alcohols (ethanol, butanol, and propanol from fermentation of starches and cellulose), and syngas [1]. First generation biofuels are less sustainable than other classifications of biofuels because arable and fodder farm land is used to produce the fuel feedstocks, competing with food industry [2].

Second generation biofuels are derived from cellulosic biomass (cellulose, hemicellulose, and lignin) [1]. Cellulosic biomass consist of wood waste or the uneatable parts of a crop (corn stock instead of corn). Second generation biofuels are more economical than first because of the larger abundance of feedstock [3]. It is the second generation biofuels that are called carbon neutral or carbon negative with respect to their impact on the carbon footprint [3]. Second generation biofuel conversion technologies can be categorized as thermochemical or biochemical processes. Thermochemical conversion technologies include: gasification, direct combustion, liquefaction, and pyrolysis. The more common biochemical processes include anaerobic digestion and fermentation. Transesterification of non-edible plant oils into biodiesel can be considered biochemical conversion

Third generation biofuels refer to algae based biofuels. A large variety of fuels and valuable chemicals can be produced with third generation technologies such as: bio-methane, biodiesel, bio-ethanol, bio-butanol, and bio-derived jet fuel [1]. Third generation biofuels have a much higher quality yield of biofuel, around 10 times more than the best traditional feedstock [1]. This is because algae lack the complex cell structures found in higher plants and can produce useful quantities of polysaccharides (sugars) and triacylglycerides (fats) that are the raw materials for biofuel [4]. The challenges associated with algae bio-stock is cultivation of microalgae on a large scale. They require ample amounts of water, phosphorus, potassium, and nitrogen [4]. The production of algae fertilizers is energy intensive and, in itself, can generate more greenhouse gasses than the product can contribute to mitigating [4]. Algae feedstock, can be converted into a fuel source through means of thermochemical and biochemical techniques. The biochemical techniques associated with algae feedstocks are anaerobic digestion, fermentation, and photocatalytic production of hydrogen [1].

Currently, the most sustainable and economical options in biofuel lie in second generation biofuels. The large challenges associated with the biofuel industry are the availability and quality of feedstocks. Also, efforts are needed with the sustainable development of bio-based refinery and biofuel production facilities [1]. The road to clean and sustainable energy does not stop at the fuel source and production method. Understanding combustion processes of petroleum and bioderived fuels is essential for efficient and clean utilization of fuels in IC engines and power generation systems.

Designing these advanced engines and systems requires the use of intensive experimentation and modeling efforts that couple the flow/physical effects of the system with the fuels chemistry. This enables predictions of detailed performance parameters related to the design before it is built. Chemical kinetics and reaction mechanisms are what describes the rate and sequence of elementary reactions the fuel undergoes in its transformation from reactants to products. To better develop these reaction mechanisms, data from fundamental combustion experiments are needed. Fundamental combustion experiments are well characterized mathematically, and limit the influence of physical effects on the combustion process.

The work herein focuses on adding to the availability of data on bioderived fuels and their blends with gasoline and diesel surrogate fuels. This work provided autoignition data for potential biofuels in the different temperature range of 680 K to 820K and at a pressure of 24 bar. The fuel injection duration was held constant at 5.0 milliseconds. Besides the autoignition times, the Derived Cetane Number (DCN) of the fuel or blend was found. Moreover, exhaust gas emissions measurement from the tests have been evaluated.

This thesis is divided into chapters that are categorized broadly on the basis of type of fuels investigated. Chapter 1 contains a detailed description of the experimental apparatus and

testing procedures. First, the Fuel Ignition Tester (FIT) is described and autoignition measurement methods are given. Additionally, the data processing procedures/equations are given and the averaged operating conditions are summarized. Second, the emissions measurement tools and methods are given and described. Next, the 0-D computational model that is used to provide the simulated comparisons is discussed. Finally, the error analysis methods are given and discussed.

Chapter 2 contains the experimental and computational results of a renewable fuel study focusing on gasoline like fuels. The renewable fuel, *n*-butanol, along with the primary reference fuels (PRFs) of gasoline, *n*-heptane and *iso*-octane, are studied. *n*-Butanol is a 4-carbon alcohol with benefits over ethanol. The experimental results are compared to numerical results as well as others work from the literature. Note that this work was initiated by Dr. Quanhong Xu in 2012 at the University of Connecticut (Storrs). Dr. Xu set up the test matrix and did preliminary studies with the FIT. All of the experimental data reported in this thesis were collected by the author, at the University of Idaho from the summer of 2016 to the fall of 2017. Additionally, the author wrote a manuscript that is under consideration for publication, and is the corresponding author.

Chapter 3 details the experimental and computational results of a renewable fuel study focusing on diesel like fuels. The biodiesel ester, methyl decaonate, and diesel surrogate, *n*-decane, are studied. Methyl Decanoate is a constituent of biodiesel and also commonly used as a surrogate for detailed chemical kinetic modeling for real biodiesel. The experimental results are compared to numerical results.

Chapter 4 covers three biodiesel fuels that were produced in-house from canola, corn, and soybean. These biofuels were made through transesterification. The constituents differ in

terms of chain length and unsaturation, both molecular traits affect the ignition delays and DCNs of the fuels. The three biofuels produced for this study have similar chain lengths, but different degrees of unsaturation. A previous paper by Stuhlman et al. [5] , a member of this research group, presented initial work on the DCNs of the three biodiesel fuels at the WSSCI Fall Meeting, 2017. Since then, temperature dependence studies have been completed by the author. Also, a method is proposed of determining the average biodiesel chain length and degree of unsaturation, allowing for a quantitative comparison in the ignition delay times/ DCN to be made. This work provides insights into the autoignition behaviors of plant derived biodiesels at different temperatures.

Conference presentation and journal publications related to this M.S. thesis are:

1) Chapter 2: Q. Xu, R. Leathers, D. Savage, K. Kumar, and C.J. Sung. "Influence of Blending n-Butanol with iso-Octane and n-Heptane on Ignition Delay Times in a Fuel Ignition Tester", Energy and Fuels, (Submitted).
2) Chapter 3: R. Leathers, S. Stuhlman, K. Kumar, S. Beyerlein and C.J. Sung "Influence of Blending Methyl Decanoate with n-Decane on Ignition Delay Times in a Fuel Ignition Tester", Paper 29KI-0008, Fall Technical Meeting of the Western States Section of the Combustion Institute, University of Wyoming, Laramie, October 2-3, 2017.

Chapter 1 : Methods

1.1 Fuel Ignition Tester (FIT)

A constant volume combustion chamber known as the Fuel Ignition Tester was used for the autoignition studies reported in this work. The Fuel Ignition Tester, manufactured by Waukesha Engine Dresser, Inc., is a bench-top, constant volume combustion chamber. It is an apparatus used to obtain the Derived Cetane Number (DCN) of a liquid fuel in conformance with the ASTM D7170 standard [6]. The DCN is a valuable metric that gives information on the autoignition propensity of a fuel. The combustion chamber consists of a cylindrical block with a volume of 0.60±0.03 L, with external heating elements, heat shield, and electrically actuated intake and exhaust valves. There is an opening at the top to accommodate a fuel injection nozzle assembly. The bottom of the combustion chamber is equipped with ports for various sensors, intake, and the exhaust connections.

The injector is a standard one-hole nozzle injector conforming to DIN 73372 standard [7]. The DIN standard gives the dimensions of nozzles size T and U. Additionally, the standard is said to apply to long hole nozzles (type A), short hole nozzles (type C), and pin hole nozzles (type B). Unfortunately, the size and the type of the nozzle in the FIT is not known. The average temperature of the fuel injected from the tests reported here is 308.1 K with a standard deviation of 0.06 K. The system is microprocessor controlled and equipped with high speed in-cylinder pressure data acquisition system in addition to standard pressure and temperature instrumentation.

A schematic of the setup is provided in Fig. 1.1. Combustion air is introduced into the chamber at 24 bar and heated to the desired temperature. The air temperature was measured using one probe in the approximate middle of the chamber on the center axis. Similarly, one

probe measured the wall temperature in the middle of the chamber. Typical operating temperatures are in the range of 695–860 K. Once the oxidizer pressure and temperature reach steady conditions, fuel is injected into the quiescent oxidizer, leading to an autoignition event.

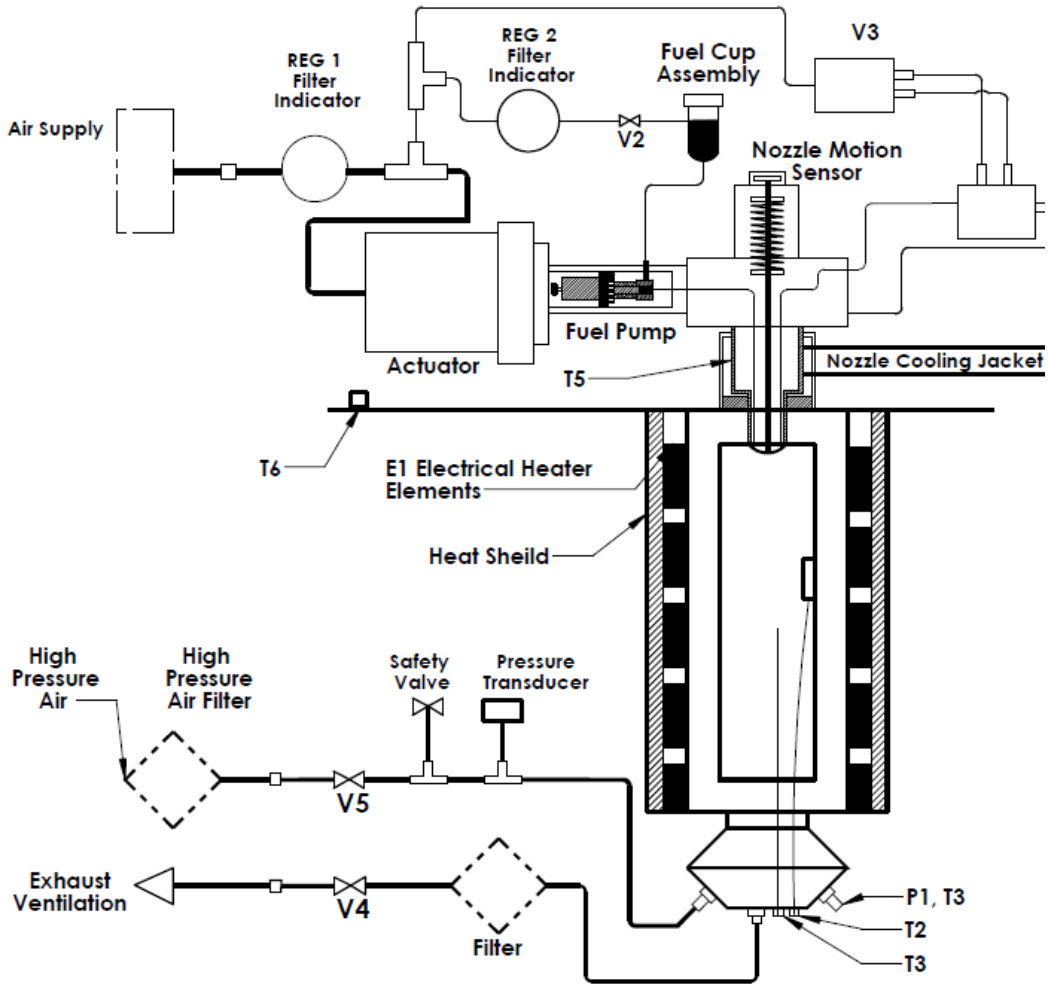

Figure 1.1: Schematic of the Fuel Ignition Tester (FIT).

A plot of an ignition event for pure *iso*-octane fuel and the associated rate of pressure rise is shown in Fig. 1.2. Fig. 1.2 also serves to illustrate the definitions of various ignition delays used in this work. The ignition delay time, τ_{onset}, is the ASTM ignition criteria (time where the chamber pressure is 0.2 bar above the initial charge pressure). τ_1 is the first stage ignition delay time, based on the time consistent with the first rate of pressure rise maximum. Similarly, the $\tau_{overall}$ ignition delay time measurement is based on the second rate of pressure rise maximum. Note that if two stage ignition behavior was not observed then the one and only pressure rise maximum was used for the ignition delay time; for these cases the ignition delay time is $\tau_{overall}$. The time between the first and overall ignition delay time is called the induction time, or simply τ_2 for this work.

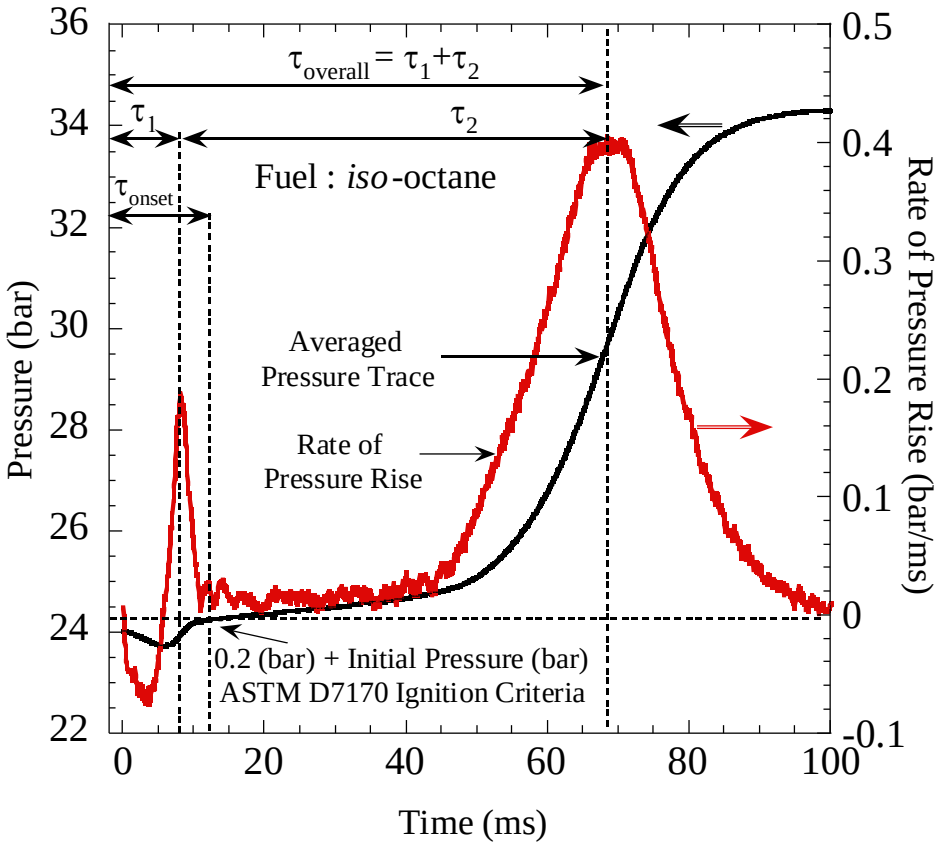

Figure 1.2: Definitions of ignition delays based on rate of, and absolute pressure rise.

The fuels used in this study were attained from different sources. *n*-Butanol was obtained from Fisher Scientific (99.95% purity), *n*-heptane was obtained from OmniSolv (99% purity), and *iso*-octane (2,2,4-trimethylpentane) was obtained from Tokyo Chemical Industry (99.0% purity). *n*-Decane used in the experiments was obtained from Fisher Scientific (99.95% purity) and methyl decanoate was obtained from Tokyo Chemical Industry (98.0% purity). The fatty acid profiles of the biodiesel fuels are provided in Table 4.1 of Chapter 4.

The FIT utilizes a unique way of determining the DCN of a fuel sample. A test comprises of 25 injections. Each fuel injection is analogous to a single shot, compression ignition, combustion event. The fuel auto-ignites when injected, and the time from the start of injection to the beginning of combustion defines the ignition delay time. For the FIT, the onset of ignition, or Ignition Delay (ID), in millisecond, is defined as the time from the start of injection to a point where the chamber pressure is 0.2 bar above the initial charge pressure. The recorded IDs from the 25 injections were averaged, and then correlated to a DCN value, using Equation 1.1 [6, 8]:

$$DCN_{FIT} = \frac{171}{ID} \tag{1.1}$$

This method of determining the DCN is in accordance with the ASTM D7170 method [6]. Additionally, to enable comparison with other work, the first and second maximum rates of pressure rise are also used to define the first stage ignition delay (τ_1) and the overall ignition delay ($\tau_{overall}$), respectively, as demonstrated in Fig. 1.2. Note that the first and overall ignition delay times were attained from the maximums of the average rate of pressure rise trace.

The FIT unit has two adjustable controls, the duration of the fuel injection period, and the wall temperature set point. The injection duration is controlled by slightly varying the injection pressure via the fuel pump rack position. The injection pressure and the amount it varies is

unknown. The injection duration is measured using a motion sensor mounted injector nozzle needle extension pin. Different fuels have different physical characteristics, the position of the fuel pump rack needs to be adjusted to enable the duration of the injection to remain constant (5 *ms*) for each fuel and blend. The wall set point temperature is the calibration control of the unit. By having a higher wall temperature set point, the chamber air will be hotter. Generally, greater the air temperature, the shorter the ignition delay. For this work the calibration wall set point temperature varied between 848.8 K and 849.6 K.

The ASTM D7170 standard has outlined two calibration points for two different reference fuels for the FIT unit: *n*-heptane and methylcyclohexane. For *n*-heptane, the FIT is considered calibrated when the mean ignition delay is 3.15±0.04 *ms* over 3 tests (75 injections) with a mean injection period of 5 *ms.* Using the calibration wall set point temperature for *n*-heptane, the calibration is then validated using methylcyclohexane, for which the acceptable mean ignition delays are 10.1±0.6 *ms*. Methylcyclohexane, meeting the purification specification, was tested after the first calibration and gave a mean ignition delay of 8.03 *ms*. The methylcyclohexane test did not meet the accepted reference value. However, as mentioned by the D7170 standard, failure to meet the MCH specification is not a one off occurrence and for these cases, the ignition delay was typically 1 to 1.5 ms shorter [6]. For this work, the *n*-heptane calibration specification was the only specification used to consider the FIT calibrated. Calibration checks were done for every air cylinder change and at the start of every testing day. For the data reported here, a minimum of three sets of 25 injections were gathered for each blend. The set with the smallest difference from the average of all the sets was chosen for the characteristic data set of that blend.

1.2 Exhaust Gas Analysis

To preform simulations that are representative of the experiments, the global equivalence ratio must be known. The FIT lacks certain equipment needed to determine this parameter gravimetrically. Also, it has been observed that the FIT has certain inherent fuel losses that cannot be accounted for; these losses are namely leaks around the fuel injection pump rack and vaporization upon purging the fuel lines. As such, a gravimetric analysis method of determining the equivalence ratio was not perused. Instead, the exhaust gas compositions were used to approximate the global equivalence ratios.

Exhaust species were determined using a ZRE model analyzer manufactured by California Analytical Instruments. The ZRE analyzer was used to measure CO, CO_2, and hydrocarbons (HC) in the sample using non-dispersive infrared analyzers. Additionally, the NO concentration in the FIT exhaust was also measured. The NO measurements were carried out with a model CLA-600 chemiluminescence detector. The emissions measurements were used to calculate the global equivalence ratio present in the FIT. Additional air-to-fuel ratio measurements were also carried out using a Horiba MEXA-584L automotive emissions analyzer as a validation. The air-to-fuel equivalence ratio, λ, was derived from the exhaust gas composition using equation 1.2 [9] and converted to a fuel-to-air equivalence ratio value using equation 1.3.

$$\lambda = \frac{[CO_2] + \frac{[CO]}{2} + [O_2] + \left\{\left(\frac{H_{CV}}{4} \times \frac{3.5}{3.5 + \frac{[CO]}{[CO_2]}} - \frac{O_{CV}}{2}\right) \times ([CO_2] + [CO])\right\}}{\left(1 + \frac{H_{CV}}{4} - \frac{O_{CV}}{2}\right) \times \{([CO_2] + [CO]) + (K_1 \times [HC])\}} \tag{1.2}$$

$$\phi = 1/\lambda \tag{1.3}$$

It may be noted that the equivalence ratio calculation is dependent on the fuels' hydrogen to carbon ratio (H_{CV}) as well as the oxygen to carbon ratio(O_{CV}); the ratios used are given in Table 1.1. All concentration values in Equation 2 are given in % volume except for HC which is given in ppm-vol. The constant K_1 (6×10^{-4}) is used to convert hydrocarbons in ppm to an *n*-hexane, % volume, equivalent.

Table 1.1: Hydrogen to carbon ratios and oxygen to carbon ratios of the various fuels/blends tested with the emissions analyzer.

	R_{cv}	R_{ov}
n-butanol	2.500	0.25
n-heptane	2.875	0.000
iso-octane	2.250	0.000
R_B=60 *with n*-heptane	2.437	0.177
R_B=60 *with iso*-octane	2.433	0.183
methyl decanoate	2.000	0.182
n-decane	2.200	0.000
R_{MD}=60 *with n*-decane	2.085	0.105

The method for collecting the samples from the FIT exhaust was straightforward. A vessel (lined with an inert silonite coating) was vacuumed out using a vacuum pump rated for an ultimate pressure of 1.1×10^{-3} Torr. With the inlet and outlet valves of the vessel closed, the FIT exhaust line was connected upstream of the vessel inlet valve. The fuel sample was run through the FIT, as in a normal test. After the injection period of the fuel was locked in, around 5 milliseconds, the exhaust was ready for collection. The sample was gathered by opening the vessel inlet valve while exhaust products were flowing out of the FIT exhaust port line, the

exhaust was split into two streams. One filled the vessel and the other one vented to fume hood. Only a portion of the exhaust gas from one FIT injection was needed to fill the silonite vessel to a pressure of about 90 kPa. Typically, 7 samples were able to be collected for a given 25 run cycle.

The exhaust products trapped in the vessel were then moved to the gas analyzers via an oil-free gas sampling pump. The sample line was connected directly to the CLA, which had its own flow regulator. The flow to the ZRE analyzer was regulated using a rotameter. The readings from the analyzers were monitored via a real time plot. After steady state readings were seen, the results were recorded at 10 Hz to a spreadsheet for the remainder of the qualifying flow time. It took approximately 1 minute for the analyzers to reach steady state, leaving approximately 45 seconds of logged values. The emissions values reported in this work are the averages of the injections that had an injection duration reading of 5 *ms*.

A question arose of whether or not the FIT exhaust sample is diluted with air. It was suspected that dilution of the exhaust sample could come about if the FIT purged its chamber with air while the exhaust valve open. It was found that the FIT does not purge its chamber with air while exhausting. This was verified by setting up a test where the air supply to the chamber could be shut off and brought to atmospheric pressure when desired; an exhaust gas analysis test was set up, but instead of letting the FIT operate normally, the chamber air supply was shut off and brought to atmospheric pressure just before the exhaust cycle. The emissions were collected and were found to be consistent with the tests done while letting the FIT operate normally. This test showed that dilution of the exhaust is not an issue but pointed out that the FIT only exhausts to atmospheric pressure. This means that there is a portion exhaust in the chamber for the subsequent test. Only 4% of the chamber air is suspected to be exhaust gas. As

will be shown by the exhaust analyses, the exhaust gas is very fuel-lean: ~18% oxygen and ~79%. Therefore, the implications of this behavior are assumed minimal and are not considered further.

1.3 Zero-Dimensional Reactor Model

An objective of this work is to compare the experimentally observed pressure-time evolution profiles to those obtained from numerical simulations. The simplest approach of carrying out homogeneous constant volume reactive simulations was adopted. The FIT experiments were simulated based on zero-dimensional homogeneous kinetics calculations using CHEMKIN® PRO [10]. The different mechanisms used are discussed in their relevant chapters. The reactor can be described by three governing equations. The simplified conservation energy equation of the model is given in equation 1.4.

$$C_v \frac{dT}{dt} + v \sum_{k=1}^{K} e_k \dot{\omega}_k W_k = 0 \tag{1.4}$$

Where,

C_v = The specific heat at constant volume.

T = The temperature of the gas.

v = The specific volume of the gas.

K = The total number of chemical species.

e_k = The specific energy of the kth species.

$\dot{\omega}_k$ = The production rate of the kth species.

W_k = The molecular weight of the kth species.

The mass conservation equation is given in equation 1.5.

$$\frac{dY_k}{dt} = v\dot{\omega}_k W_k \tag{1.5}$$

Where,

Y_k = The mass fraction of the kth species.

The equation relating pressure to temperature takes the form:

$$P = \frac{\rho RT}{\bar{W}} \tag{1.6}$$

The equations are simple and allow for large reaction mechanisms to be used with little consideration to the computational cost of the simulation. While beneficial in this sense, the simulation lacks all the detail related to the fuel spray, breakup, and vaporization relevant to the FIT experiments.

A previous study with direct-injection into a constant volume combustion chamber by Allen et al. [11] concluded that a homogenous combustion model was reasonably accurate for ignition delays greater than 5 *ms*. Similarly, Bogin et al. [12] reported that reasonable agreement between experimental data and 0-D simulations was achieved in an IQT for large *n*-alkanes with ignition delay times of ~40ms or greater [12].The minimum ignition delay time for assuming well mixed combustion differs in both works, likely due to differences in the CVCC apparatuses.

The FIT will therefore have its own homogenous mixing time for certain fuels and conditions. The characteristic mixing / homogenous time is unknown and requires further investigation. Full spray models were made to investigate this with limited success. It was concluded that basic experimentation with the FIT injection nozzle is needed to preform characteristic simulations of the FIT. The comparisons between the zero-dimensional model

and the experiments are left open to interpretation. However, relevant discussion is given where appropriate.

1.4 Uncertainty / Error Analyses

It is advantageous to know what uncertainties/errors may be associated with preforming these analyses. Uncertainties can come about from: the combustion air used, the volumetric blending of the fuel samples, the injection duration of the 25 injections that make up a test, and the initial air temperature preceding each injection. The statistical traits surrounding each of these parameters is discussed here. Moreover, the methods used to quantify the scatter for each data point is given.

The combustion air used for the experiment is bottled breathing grade dry air and should have no other constituents beside oxygen and nitrogen. The oxygen mole fraction of the combustion air has been measured for the oxidizer. The average oxygen mole fraction and standard deviation was found to be 20.9% and 0.2% respectively.

The volumetric blending of the fuels was performed using Fisherbrand pipettes. The largest uncertainty belongs to the 50 ml and 40 ml pipette at ±0.05 ml. The uncertainties of the smaller pipets are ±0.03 ml. The samples made were typically 100 ml. Usually three measurements using the pipettes were made per sample. Assuming two measurements were made with 40 ml pipette and one with the 20 ml pipette, the total uncertainty can be found as using the root-sum-squares method. For this example, the total uncertainty is ±0.08 ml. This insinuates an error of ~±0.1% of the total 100 ml sample.

As mentioned previously, multiple sets of 25 injections has been done for each test condition. The characteristic set (the one chosen to be reported) was chosen based off the relative quality of statistical parameters describing the test set. These are namely the average &

standard deviations of the injection duration and ignition delay time. The reported test with the largest average injection duration difference from 5*ms* is the 25% methyl decanoate / 75% *n*-decane blend at 5.07*ms* (SDV=0.05*ms*). The reported test with the greatest injection duration standard deviation is the 40% butanol & 60 % *iso*-octane blend at 0.16 ms (AVG=4.97*ms*). The examples given, even though outliers, show that the injection duration is very well maintained around 5*ms* and typically has a small standard deviation. Some fuels/ tested temperatures exhibited more scatter than others. Therefore, when injection duration differences were miniscule between data sets, choices based of the ignition delay time standard deviation were relative to that set.

A lot of data has been obtained and processed throughout this work. To quantify the scatter seen in the tests, the standard deviation was calculated for all of the reported values. In the tables throughout this work, the standard deviation will be noted as SDV. For the ignition delay times and DCNs, the population standard deviation was used for the calculation. For exhaust gas analysis results, the sample standard deviation was used. The plots through this work display error bars where appropriate. Theses error bars are the length of one standard deviation.

Chapter 2 : Influence of Blending *n*-Butanol with *iso*-Octane and *n*-Heptane on Ignition Delay Times in a Fuel Ignition Tester

Submitted to *Energy and Fuels*

2.1 Introduction and *n*-Butanol Discussion

Biomass derived butanol has been a topic of research. It has been shown that bio-butanol meets the requirements for transitioning into circulation with minimal changes to fuel handling infrastructure [13-16]. Also, bio-butanol production can utilize existing ethanol infrastructure [14]. An example of this is the BP and DuPont joint venture Butamax®. They are adding bio-isobutanol production capability to an acquired ethanol facility in Scandia, Kansas [17]. Bio-butanol can be produced via processes such as fermentation or the use of microbial strains using the same agricultural feedstocks as ethanol [14]. Butanol, compared to lower carbon number alcohols like ethanol, has been shown to tolerate water contamination, and is less corrosive [16]. Butanol (29.2 MJ L^{-1}) has a higher energy density than ethanol (19.6 MJ L^{-1}) or methanol [13, 14]. Production of butanol using second generation lignocellulosic feedstocks, such as wood chips, are becoming economically viable [15]. Butanol production using second generation feedstocks ensures that arable farm land is used for food rather than fuel production. Another benefit of using bio-butanol, as with any use of a fuel derived from biomass, is it would displace the CO_2 emissions resulting from petroleum derived fuels (trapped within the earth) with that from biomass. Butanol, with proper blending, can be used in compression ignition and spark ignition combustion systems [14]. While the energy density of butanol is higher than ethanol or methanol, it is still lower than conventional petroleum based hydrocarbons. Therefore, the brake specific fuel consumption of a butanol-fueled Internal Combustion (IC) engine would be slightly higher than that of an engine running with petroleum derived fuels.

As with any potential alternative fuel, its efficient and clean utilization in IC engines is dependent on the ability to predict the global combustion properties and the detailed species evolution during oxidation. The development of predictive capabilities, like a detailed reaction mechanism, is dependent on experimental and computational efforts. The potential use of *n*-butanol as an IC engine fuel, both in spark ignition and compression combustion systems, has spurred an increase in fundamental combustion research related to *n*-butanol combustion, on both experimental and computational fronts. The development and validation of comprehensive reaction mechanisms is supported by fundamental experimental data from diverse, well characterized experiments, which are complementary in nature and cover a wide range of thermophysical conditions. Such experiments that have been conducted with *n*-butanol include shock tubes [18-23], laminar non-premixed flames [24-30], outwardly propagating flames [31-35], steady premixed flames [29, 36-38], jet stirred reactors [29, 39-43], rapid compression machines [44-47], and constant volume combustion chambers [11, 48-52] like the fuel ignition tester (FIT) [53] and ignition quality tester (IQT) [12, 54, 55]. Beside these fundamental experiments, theoretical studies concerning the chemical kinetics of *n*-butanol combustion have also been carried out. These include the thermochemistry of species relevant to *n*-butanol combustion [56], rate constants for hydrogen abstraction by radicals at different carbon atom sites [57, 58], and the decomposition kinetics of butanol derived radicals [59]. In addition to the fundamental combustion experiments and theoretical studies, there have also been applied studies investigating the effect of blending butanol with conventional petroleum derived fuels. The applied studies have been done in systems such as spark ignition [60-62], compression ignition [63-67], and homogenous charge compression ignition (HCCI) [68-72]. The work done on *n*-butanol has recently been reviewed by Trindade and dos Santos [16].

Baumgardner et al. [53] have done a similar study to this work. The autoignition behavior of *n*-butanol and the primary reference fuels (PRFs), *n*-heptane and *iso*-octane, along with blends of *n*-heptane/*n*-butanol were studied in an FIT and an HCCI engine. Derived Cetane Number (DCN) values were determined from the FIT experimental work for the PRFs, *n*-butanol, and blends. The work focused on determining if the FIT can be used to predict/explain differences in HCCI performance. A point corresponding to the fraction of low temperature heat release was used as a comparative ignition delay metric for the FIT and HCCI engine. It was shown that the fraction of low temperature heat release found from FIT experiments could be used to predict the crank angle at 50% heat release (CA50) [53]. This metric was developed to better characterize autoignition behavior of fuels where traditional metrics, such as the octane number and cetane number, are not directly applicable concerning homogeneous premixed or partially premixed conditions. It was found that the fraction of low temperature heat release correlated well with the crank angle of maximum heat release and showed promise of being used as an indicator of the CA50 location [53].

As discussed, various experiments have been done with pure *n*-butanol. While *n*-butanol could potentially be used as a complete replacement in conventional combustion systems, it is more likely that it will make its way into distribution by way of occurring as an additive. As a result of this, blend studies are important and are a focus of this work. Given that *n*-butanol is a possible substitute for gasoline, it is essential to acquire fundamental ignition data on *n*-butanol and gasoline PRF constituent blends under conditions similar to IC engines. The two neat PRF's chosen are *n*-heptane and *iso*-octane. They represent extremes on the octane index, which gives a measure of the knock resistance, and represent the *n*-alkane and *iso*-alkane chemical classes, respectively.

The FIT provides a means of studying combustion under high pressure, and low-to-intermediate temperature conditions. The conditions within the FIT are most similar to direct-injection compression ignition engines. The first aim of this work is to investigate the influence of blending ratio on DCN. The fuels tested here are primarily used in spark ignition engines, with the exception of *n*-heptane. For this reason, the octane index would be the ideal metric to test for. However, the FIT is designed to test for the cetane number. To remain true to the equipment's purpose, the DCN was obtained instead of the octane number. In addition to obtaining the DCN, the first stage ignition delay and the total "hot" ignition delay events were investigated using the first and second maximums of the rate of combustion pressure rise as the delay time definitions respectively [73]. Furthermore, temperature dependence experiments were completed for the three pure fuels to further investigate the first stage and overall ignition delay characteristics as a function of temperature.

The second focus of this work is to compare the experimental data to homogenous constant volume simulations using reaction mechanisms that have been previously validated. In order to make the simulations as representative of the FIT as possible, exhaust products from the FIT were used to determine the global equivalence ratios. The exhaust emissions data also provide some key insights into fuel oxidation. A 0-dimensional, constant volume, homogenous, and adiabatic reactor is used to provide a rudimentary model of the FIT. Obviously, the homogenous assumption is not true for experiments with short ignition delay times. However, for tests with long ignition delay times, the fuel spray has a longer mixing time and the homogenous assumption become more legitimate. The comparisons can be assumed reasonably valid since the global equivalence ratio used in the simulation is representative of the corresponding FIT

experiment. The chemical kinetic models used in this work have been previously validated with rapid compression machine data for low temperature homogeneous autoignition [73].

2.2 *n*-Butanol and PRF Reaction Mechanism

The experimental results in this study were simulated using a detailed chemical kinetic scheme for *n*-butanol and the primary reference fuels for gasoline, namely, *n*-heptane and *iso*-octane. The mechanism was previously used for homogenous autoignition simulations in a rapid compression machine study [73]. This mechanism was derived from a systematic merger of previously reported schemes for *n*-butanol by Sarathy et al. [74], *n*-heptane by Karwat et al. [75], and *iso*-octane by Lawrence Livermore National Laboratory (Version 3) [76-79], and consists of 2385 species and 9515 reactions. For the R_B=60 blends and pure fuels, the initial conditions used for the simulations corresponded to the average pressure and temperature from the FIT experiments, namely 24.01 bar and 812 K, respectively. The equivalence ratios used for the R_B=60 blends and pure fuels were deduced using the exhaust gas composition measurements, discussed earlier. In addition, the temperature dependence studies were modeled with the initial conditions corresponding to the matching experimental air temperature. An average pressure of 24.01 bar was used.

2.3 *n*-Butanol Results and Discussion

2.3-1 Ignition Delay Times

The characteristic experimental pressure trace data of the pure fuels, along with the derived mean pressure traces and rates of pressure rise, are helpful in gaining an understanding of how each fuel behaves when subjected to a low temperature autoignition environment. Fig. 2.1 shows the raw and processed data of each pure fuel. The post combustion chamber pressure of *n*-heptane, Fig. 2.1(a), and *iso*-octane, Fig. 2.1(b), are similar, each near 34 bar. This is most likely because the two fuels have a similar carbon number and therefore similar energy density. The energy density of: *n*-heptane is -32,690 MJ/m^3, *iso*-octane is -33,433 MJ/m^3, and *n*-butanol is -29,107 MJ/m^3 [80]. On the contrary, the post combustion chamber pressure for *n*-butanol, Fig. 2.1(c), is lesser than the primary reference fuels, around 32 bar; this is consistent with the fact that it has a lesser energy density than the PRFs. In addition, as seen from Fig. 2.1, *n*-heptane shows the tightest grouping of individual test pressure traces, followed by *n*-butanol, and then *iso*-octane.

It is fitting that the raw pressure traces of iso-octane are shown in Fig.2 (b) since the pure iso-octane tests possess the most scatter compared to the rest of fuels and blends shown here. The inherent scatter associated with iso-octane was unavoidable and is unexplained. Even with the considerable scatter associated with the pure iso-octane tests, it can be seen that the averaged pressure trace is reasonably effective at capturing and characterizing the shape, slope, and locations of the individual pressure traces; this supports that this method of processing the FIT data is suitable. The scatter associated with a certain test is, to some extent, quantified by the overall ignition delay standard deviations given in Tables 2.1 & 2.2.

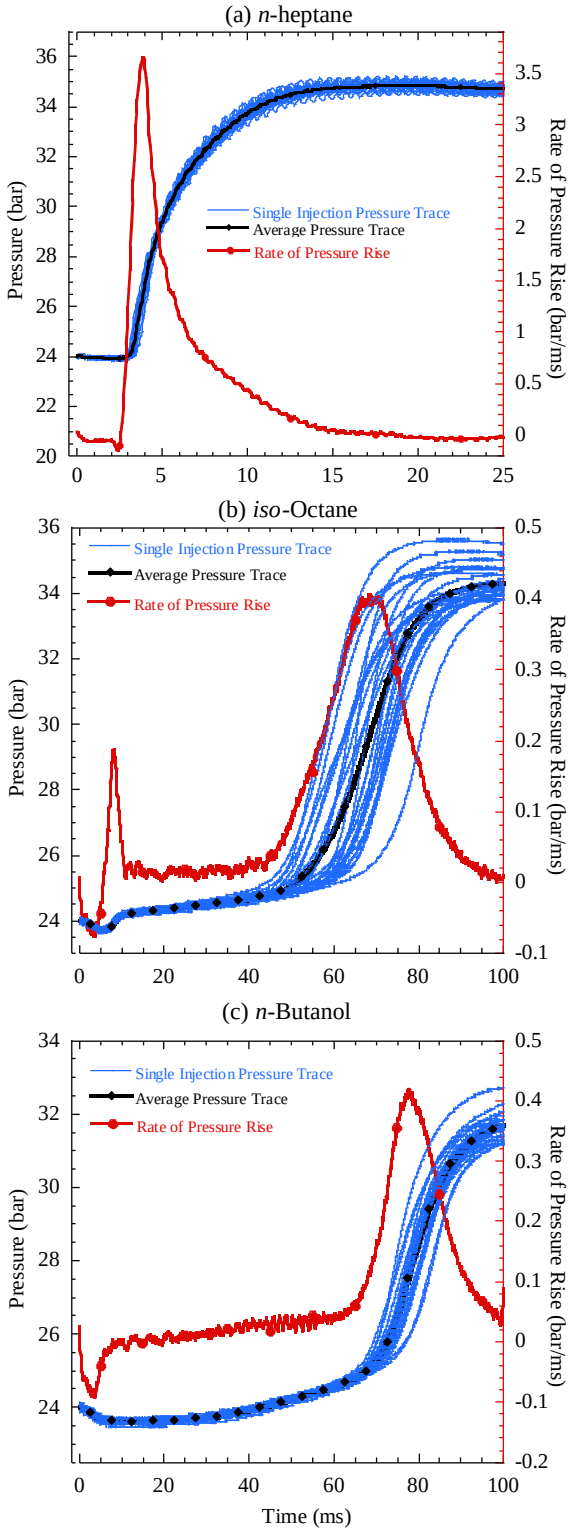

Figure 2.1: The 25 experimental pressure trace data for the pure fuels along with the averaged pressure traces and rates of pressure rise for (c) *n*-butanol.

At this temperature, the rate of pressure rise of n-heptane, Fig. 2(a), shows only one maximum, the overall ignition event. For iso-octane, Fig. 2(b), the first and second stage ignition points are easily discernable. On the other hand, the first stage ignition points of n-butanol, Fig. 2(c), and some n-butanol/iso-octane blends (discussed later), are difficult to pick out. For these cases, the rate of pressure rise for n-butanol shows a region of preignition heat release where the rate of pressure rise is positive and increasing. However, the rate of pressure rise profile does not show a discernable maximum point to be deemed the first stage ignition; for cases like this, the first stage ignition delay was left unidentified. The fact that n-butanol exhibits significant preignition heat release in a semi-linear fashion suggests that the fuel air mixture is being consumed by flame propagation.

The influence of *n*-butanol blending ratio on the autoignition characteristics of binary blends of *n*-butanol/*n*-heptane and *n*-butanol/*iso*-octane is shown in Figs. 2.2(a) and 2.2(b), respectively. Fig. 2.2(a) shows that addition of *n*-butanol (R_B) into the straight chain alkane (*n*-heptane) significantly slows down its reactivity, and also leads to an extended region of slow rate of pressure rise prior to the main ignition event. A similar variation in R_B for *iso*-octane leads to a relatively moderate decrease in second-stage reactivity as shown in Fig. 2.2(b). For *n*-butanol/*iso*-octane blends, the strongest influence of blending appears at relatively low R_B with almost negligible variations in overall ignition delay times for $R_B > 20\%$. Note however, that an increasing R_B continues to significantly impact the first-stage ignition delay times for *n*-butanol/*iso*-octane blends. The pressure traces in Figs. 2.2(a) and (b) also indicate that the addition of *n*-butanol reduces the pressure rise associated with the first stage ignition. The reduction in the maximum pressure with increasing R_B is also consistent with the lower energy density of *n*-butanol (~3,900 MJ/m^3 lower) [80].

(a) Averaged Traces for *n*-Butanol / *n*-Heptane Blends

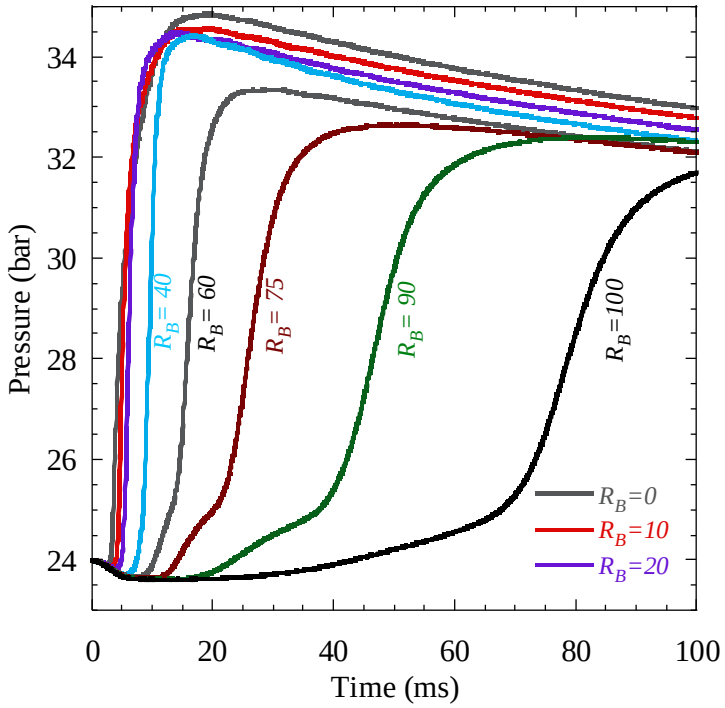

(b) Averaged Traces for *n*-Butanol / *iso*-Octane Blends

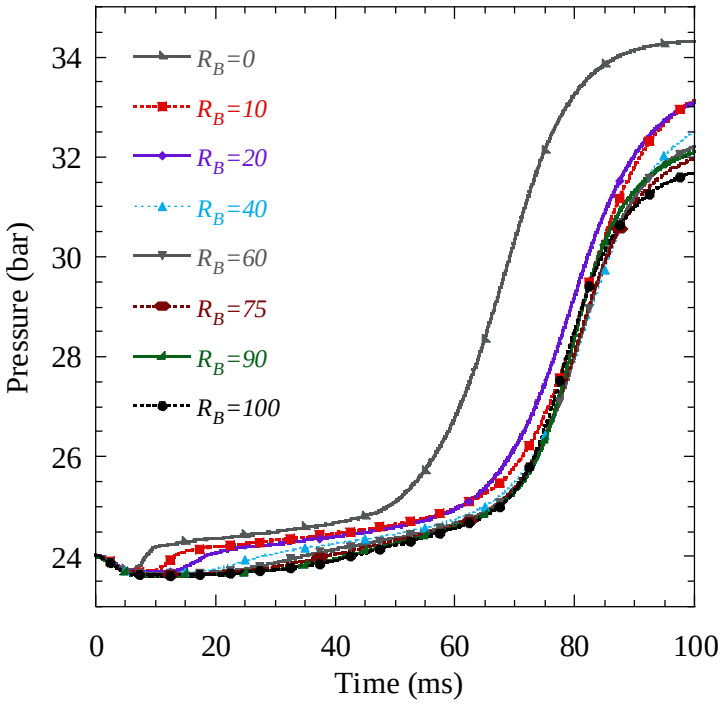

Figure 2.2: (a) Averaged pressure traces for *n*-butanol/*n*-heptane blends. (b) Averaged pressure traces for *n*-butanol/*iso*-octane blends.

The first-stage and the overall ignition delay times based on the maximum rate of pressure rise locations for *n*-butanol/*n*-heptane and *n*-butanol/*iso*-octane blends are shown in Figs. 2.3(a) and 2.3(b), respectively. As noted earlier, the blending of *n*-butanol into *n*-heptane leads to a sharp increase for both first- and second-stage ignition delays, while the effect is not as pronounced for *n*-butanol addition to *iso*-octane. It can be seen from Fig. 2.3(a) that the first stage ignition delay increases with R_B and roughly follows the exponential trend of the overall ignition delay. Conversely, in Fig. 2.3(b), the first stage ignition delay of the low R_B *n*-butanol/*iso*-octane blends show a linear increase.

The derived cetane numbers using Equation 1.1 for the two binary blends as a function of the volumetric blending ratio (R_B) are shown in Figs. 2.4(a) and 2.4(b). As shown, the DCN decreases in a monotonic, non-linear fashion for both the blends as a function of R_B. The extent of the absolute variation in DCN's for *n*-butanol/*n*-heptane blends is considerably larger than that for *n*-butanol/*iso*-octane blends. Furthermore, the DCN variation trend can adequately be captured by a fitting function of the form:

$$DCN\ (R_B/100) = DCN_{base} - (DCN_{base} - DCN_{n-butanol}) \times \left(\frac{\ln(1 + R_B/100)}{\ln(2)}\right)^n \qquad (2.1)$$

where the base fuel is either *n*-heptane or *iso*-octane and n is a fitting parameter. The proposed fit forces the endpoints to match up with the experimentally observed DCN of the neat components. In addition, the R^2 values are 0.9993 and 0.9968 for Figs. 2.4(a) and 2.4(b), respectively.

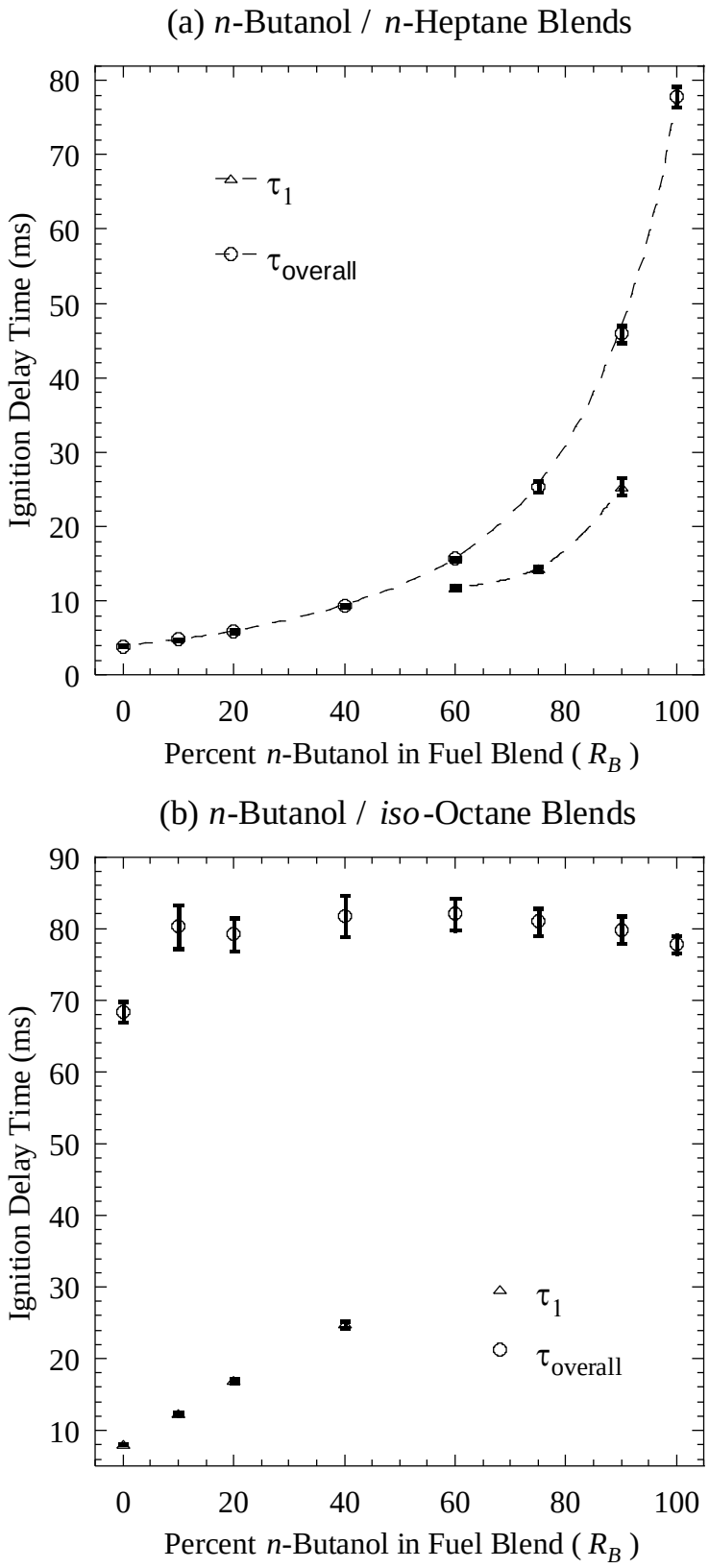

Figure 2.3: Ignition delay time as a function of volumetric blending ratio for (a) *n*-butanol/*n*-heptane blends and (b) *n*-butanol/*iso*-octane blends.

The present experimental DCNs and ignition delay times of pure fuels and binary blends are listed in Table 2.1. The variability in the set of 25 tests used to calculate the reported DCN is shown in Fig. 2.5. The center line represents the median of the data. The top and bottom of the boxes mark the limits of ± 25% of the DCN population. The lines extending from the top and bottom of each box marks the minimum and maximum values within the data set. Points whose value are either greater than the upper quartile plus 1.5 times the inner quartile distance or lower than lower quartile minus 1.5 times the inner quartile distance are outliers and displayed as individual points.

A comparison of the DCN values obtained from the current experimental work with selected results reported in the literature is provided in Fig. 2.6. Both FIT [81] (ASTM D7170) and IQT [82] (ASTM D6890) results are shown. The results attained from this work correspond well with other FIT studies with the exception of the $R_B = 20$ blend in *n*-heptane. In particular, IQT studies compare well with the current work for low R_B *n*-butanol/*n*-heptane blends, but deviate significantly for volumetric mixture of and greater than 40%.

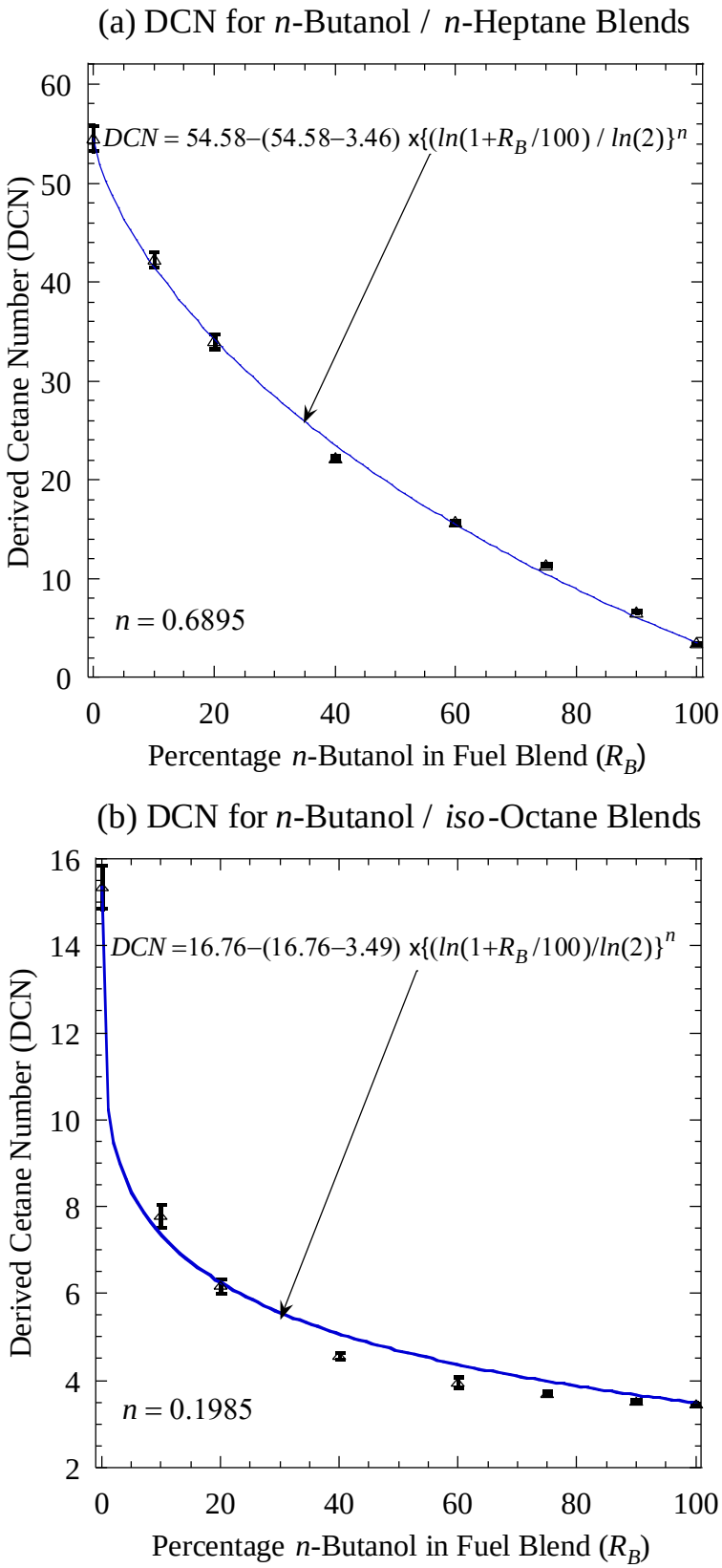

Figure 2.4: DCN as a function of volumetric blending ratio for (a) *n*-butanol/*n*-heptane blends and (b) *n*-butanol/*iso*-octane blends.

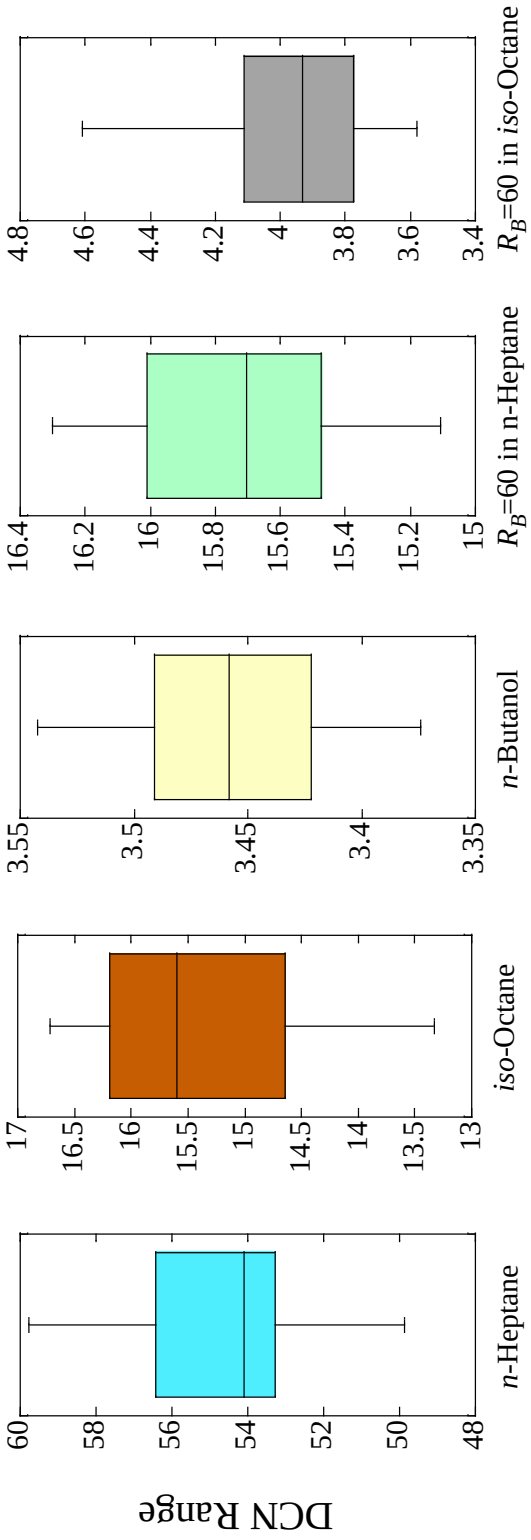

Figure 2.5: Variability in the 25 tests used to obtain DCN

Table 2.1 Experimental DCNs and ignition delay times of pure fuels and binary blends.

Fuel	R_B	DCN	SDV	τ_1	SDV	$\tau_{overall}$	SDV	Air Temperature
	(% Vol)			(ms)	(ms)	(ms)	(ms)	(K)
n-butanol		3.5	0.05			77.8	2.70	812.1
n-heptane		54.6	2.58			3.9	0.26	812.3
iso-octane		15.4	0.98	8.1	0.36	68.4	6.05	812.2
n-butanol/*n*-heptane blends	10	42.3	1.47			4.8	0.24	812.1
	20	34.1	1.37			6.0	0.32	811.5
	40	22.2	0.53			9.4	0.35	811.8
	60	15.7	0.34	11.8	0.46	15.7	0.47	811.2
	75	11.4	0.25	14.4	0.79	25.4	1.42	811.3
	90	6.7	0.18	25.4	2.18	45.9	2.25	811.5
n-butanol/*iso*-octane blends	10	7.8	0.53	12.4	0.80	80.3	4.61	812.4
	20	6.2	0.31	17.0	0.89	79.2	5.79	811.5
	40	4.6	0.15	24.8	1.89	81.7	4.57	812.5
	60	4.0	0.24			82.0	3.65	812.3
	75	3.7	0.08			81.0	3.83	812.6
	90	3.5	0.06			79.9	2.49	812.3

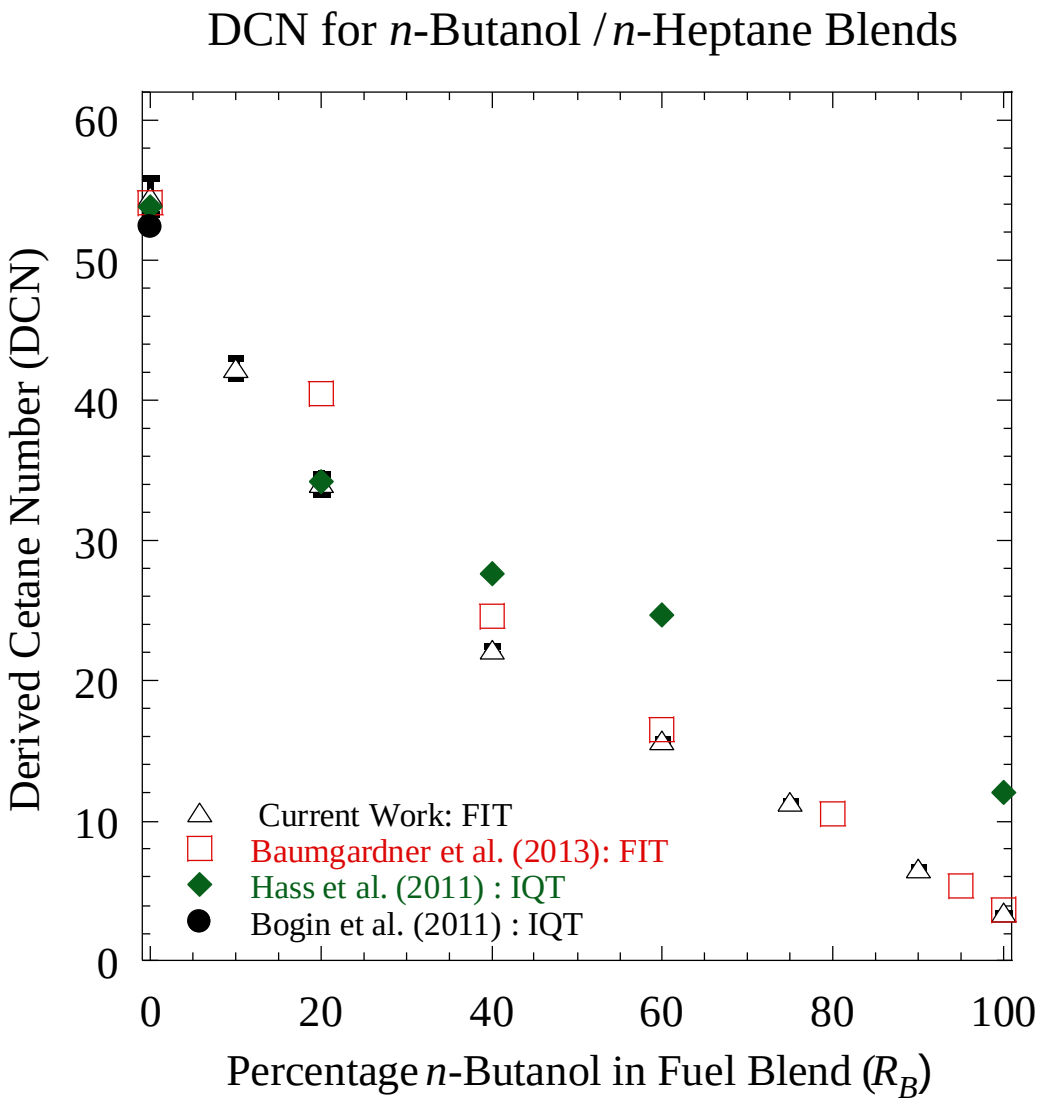

Figure 2.6: DCN comparison as a function of volumetric blending ratio for *n*-butanol/*n*-heptane blends. Comparative data was gathered from Baumgardner et al. [53], Hass et al. [55], and Bogin et al. [12]

2.3-2 Influence of Oxidizer Temperature

The dependence of ignition delay time on the oxidizer temperature has also been obtained for the three pure fuels. While the data gathered for each fuel would ideally span the temperature range allowed by the FIT (693–864 K), the ignition event has to be within the FIT's data acquisition window. Table 2.2 lists the experimental results obtained herein.

Table 2.2: Dependence of ignition delay on oxidizer temperature.

Air Temperature	Pressure	Estimated Equivalence Ratio (ϕ)	τ_1	SDV	$\tau_{overall}$	SDV
(K)	(bar)	(-)	(ms)	(ms)	(ms)	(ms)
n-heptane						
678.2	24.0	0.112	53.0	2.38	70.2	4.20
690.4	24.0	0.114	24.8	1.37	31.1	1.87
713.7	24.0	0.118			17.9	0.61
738.8	24.0	0.122			12.0	0.32
762.2	24.0	0.126			7.6	0.50
787.5	24.0	0.130			5.2	0.30
812.3	24.0	0.134			3.9	0.26
iso-octane						
796.5	24.0	0.123	9.6	0.46	86.1	8.58
806.3	24.0	0.124	9.2	0.40	73.3	5.94
812.2	24.0	0.125	8.1	0.36	68.4	6.05
815.8	24.0	0.126	8.0	0.48	64.0	5.10
826.0	24.0	0.127	7.4	0.46	56.2	3.84
n-butanol						
808.6	24.0	0.104			82.7	2.72
812.1	24.0	0.104			77.8	2.71
815.7	24.0	0.104			76.6	3.31
820.2	24.0	0.105			68.9	2.08
825.1	24.0	0.106			67.0	2.66

Figs. 2.7(a) and 2.7(b) show the pressure traces and ignition delay times of *n*-heptane at different temperatures, respectively. It can be seen from Fig. 2.7 that the ignition event of *n*-heptane exhibits a monotonic decrease in ignition delay with increasing temperature. Negative temperature coefficient (NTC) behavior was not observed for the tested temperature range. Fig. 2.7(b) also shows an exponential decrease in ignition delay with increasing temperature.

Fig. 2.7(a) shows a couple more things of note. The post combustion peak pressure of the three hottest tests show an increasing trend with decreasing temperature. The maximum pressures are 35.37 bar, 34.93 bar, and 34.75 bar for test with average air temperatures of 762.2 K, 787.5 K, and 812.3 K, respectively. It is also noted that the average fuel injection duration of the three tests are: 4.95 *ms*, 5.01 *ms*, and 4.96 *ms*. The small injection duration difference between the three tests does not fully explain the trend seen. Since the pressure and volume are held constant, the increase in air temperature should lead to a slightly larger global equivalence ratio as the number of moles of oxidizer is reduced on account of increasing the temperature. This should have resulted in increased post combustion pressure as the oxidizer temperature was increased. This anomaly is likely to have a chemical kinetic explanation related to the low-temperature fuel chemistry. Moreover, it is seen from Fig. 2.7(a) that the post combustion peak pressure drops off drastically for temperatures of 678.2 K and 690.4 K, which have maximum pressure of 32.52 bar and 33.54 bar, respectively, most likely on account of incomplete combustion.

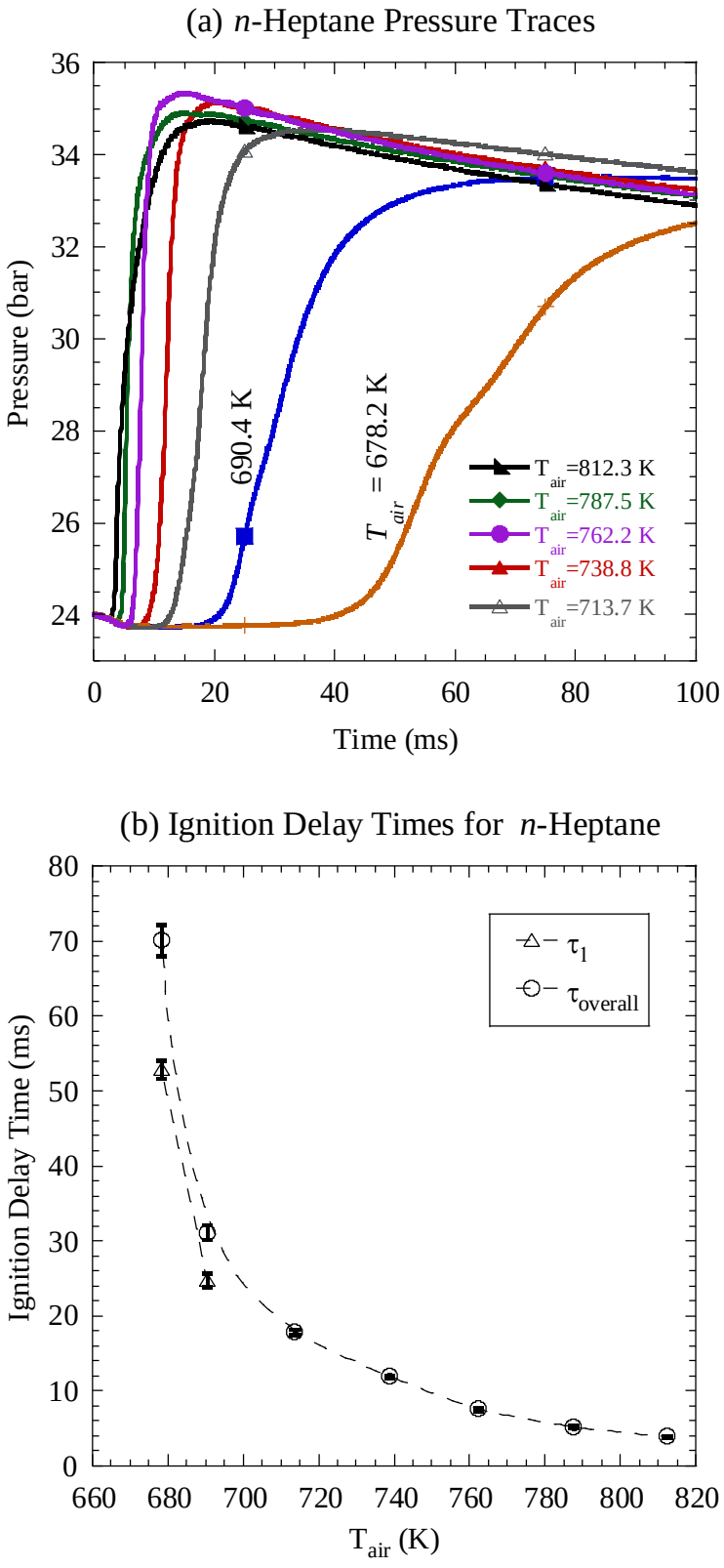

Figure 2.7: (a) Averaged pressure traces for *n*-heptane with varying initial air temperatures and (b) ignition delay times for *n*-heptane as a function of initial air temperature.

As shown in Fig 2.7(a), a two-stage ignition behavior is observed for *n*-heptane tests with the two lowest averaged air temperature: 678.2 K and 690.4 K. This two-stage ignition behavior at an average air temperature of 678.2 K is better viewed in Fig. 2.8. It can be seen that the average pressure trace captures the characteristics of the individual pressure traces characteristics' well. Interestingly, one or two individual pressure traces do not exhibit two-stage ignition behavior. The average rate of pressure rise curve shows two maximums, with the first being more pronounced than the second. For the two tests having average air temperatures of 678.2 K and 690.4 K, the largest and first rate of pressure rise maximum is identified as the first stage delay, τ_1. The second, less pronounced maximum, is used to identify the overall ignition delay, $\tau_{overall}$. The first stage pressure rise is greater than the second stage. Typically, the opposite is observed as in Fig. 1(b). Optical diagnostics would be helpful in determining the cause of this behavior.

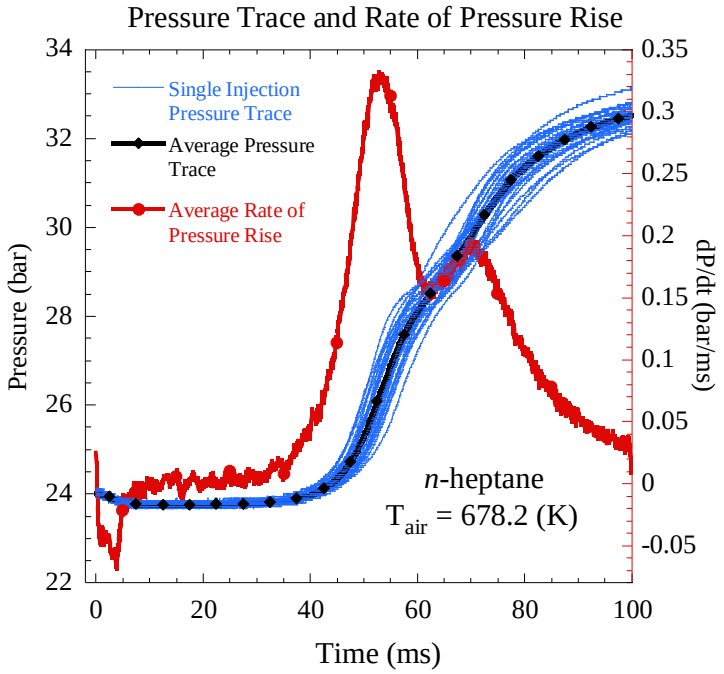

Figure 2.8: Experimental pressure traces, averaged pressure trace, and rate of pressure rise for *n*-heptane with an initial air temperature of 678.2 K.

Figs. 2.9(a) and 2.9(b) show the pressure traces and ignition delay times of *iso*-octane at different temperatures. As seen in Fig. 2.9(a) the ignition delay time decreases in a monotonic fashion with increasing temperature. However, the location of the first-stage pressure rise (around 25 *ms*), changes very little. The peak pressures display a trend similar to the *n*-heptane cases. The ignition delay behavior is better understood from Fig. 2.9(b). Both the overall and first-stage ignition delays decrease with increasing temperature. However, the rate of change with temperature is significantly larger for the overall ignition delay as compared to the first-stage ignition delay. The small decrease in the first stage ignition delay time, compared to the overall ignition delay time, with increasing temperature is consistent with RCM results [83].

Figs. 2.10(a) and 2.10(b) show the pressure traces and ignition delay times of *n*-butanol at different temperatures. Like the other two neat fuels, *n*-butanol shows a monotonic decrease in ignition delay with increasing temperature. No first stage ignition delay was observed over the range of temperatures covered in this work. It can be seen from Fig. 2.10(a) that the pressure traces are very similar up until around 25 *ms.* The point of deviation may be a good point of reference for the induction time since there is no obvious first-stage ignition delay to base a measurement on. The slopes of the pressure traces are very similar. In addition, the post combustion peak pressure indicates a decreasing trend with decreasing temperature. In Fig. 2.10(b), the shape of the overall ignition delay temperature variation curve is not as smooth as the other two fuels. Moving from low temperature to high temperature initial conditions, the slope of the ignition delay curve is slightly reduced around the 815.7 K averaged air temperature test. Note that the 815.7 K air temperature test shown here is one of four sets of tests that were done, this one was chosen to be reported because of its smaller standard deviation of injection duration and charge pressure. For this reason, it is unlikely that this point is an outlier.

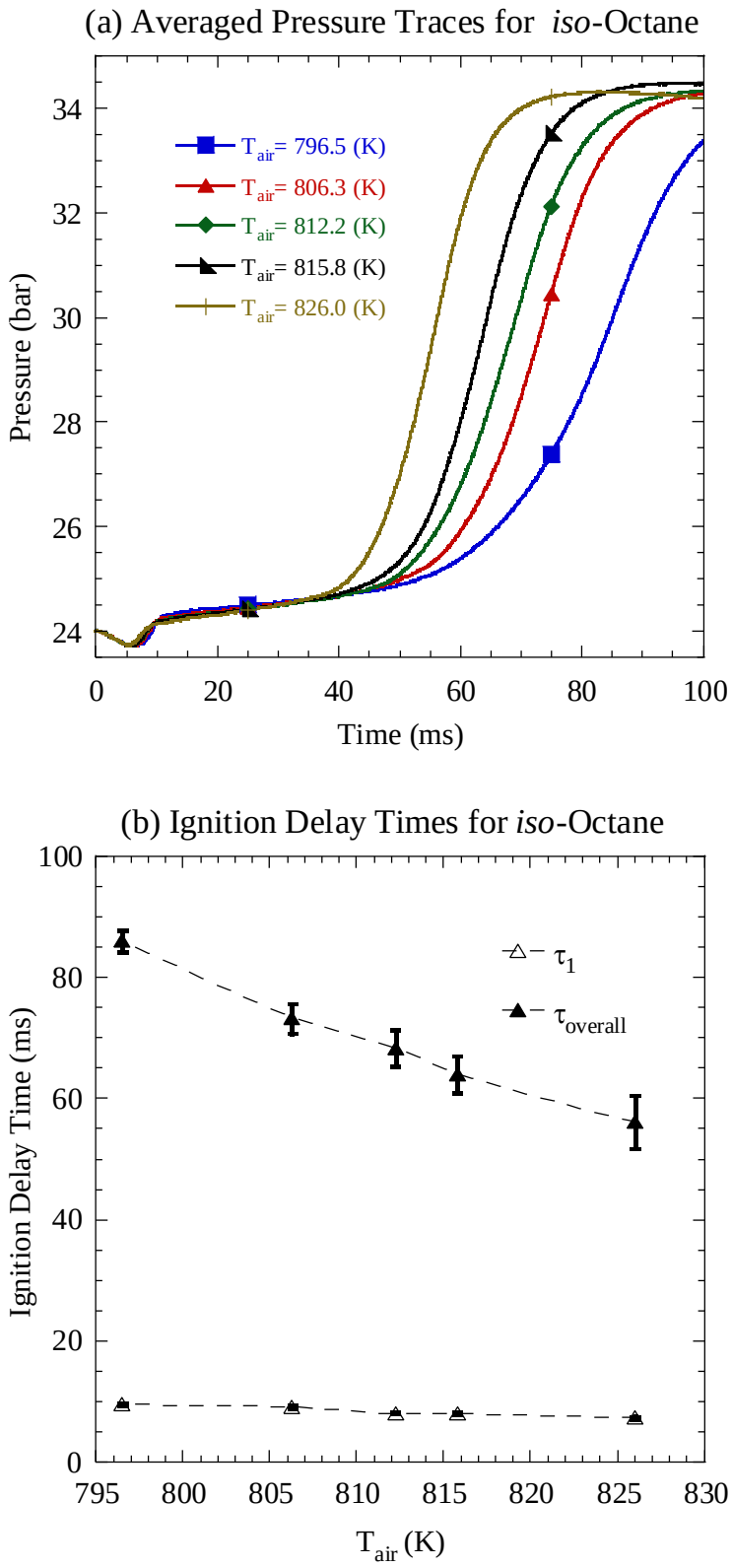

Figure 2.9: (a) Averaged pressure traces for *iso*-octane with varying initial air temperatures and (b) Ignition delay times for *iso*-octane as a function of initial air temperature.

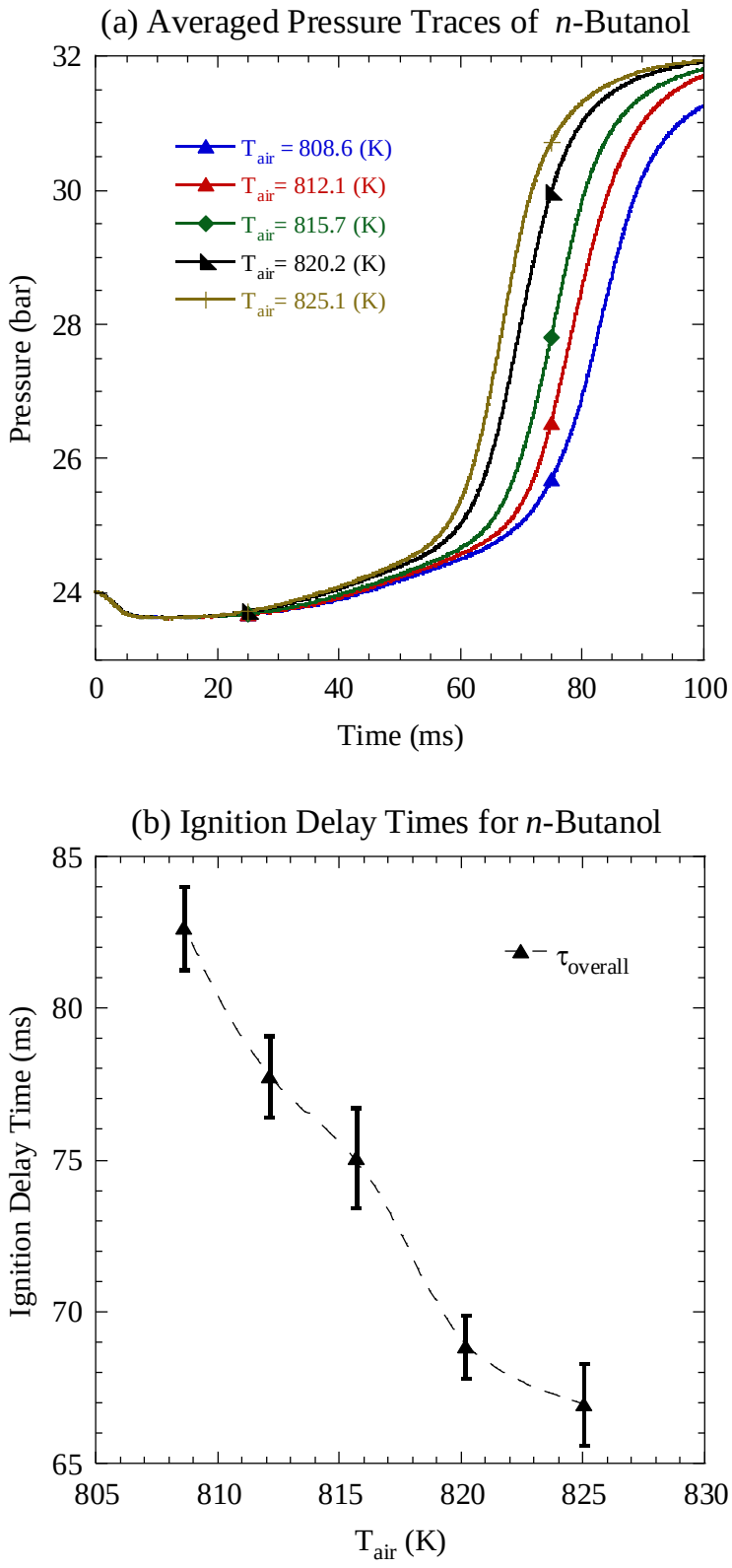

Figure 2.10: (a) Averaged pressure traces for *n*-butanol with varying initial air temperatures and (b) Ignition delay times for *n*-butanol as a function of initial air temperature.

Additional comparison between the current experimental results and that from other constant volume combustion apparatus are shown in Fig. 2.11. The plots show the temperature dependence trend for *n*-heptane and *n*-butanol ignition delay times. Note that due to unavailability of data under identical pressure conditions the results from the literature sources have been scaled to 24 bar. The scaling assumes an inverse dependence of ignition delay time on pressure. The plots in Fig. 2.11(a) show that there is a good agreement between the FIT and IQT ignition delay times. However the results of Allen et al. [11] are in variance with both the FIT and IQT. This comparison suggests that the FIT behaves more like the IQT and not Allen et al.'s CVCC [11]. Similar comparative results for n-butanol fuel are presented in Fig. 2.11(b). The *n*-butanol results from the study of Hou et al. [84] are significantly faster than the current FIT data. This difference is to be expected as the apparatus of Hou et al. [84] has very different operating conditions in terms of the fuel temperature and injector parameters.

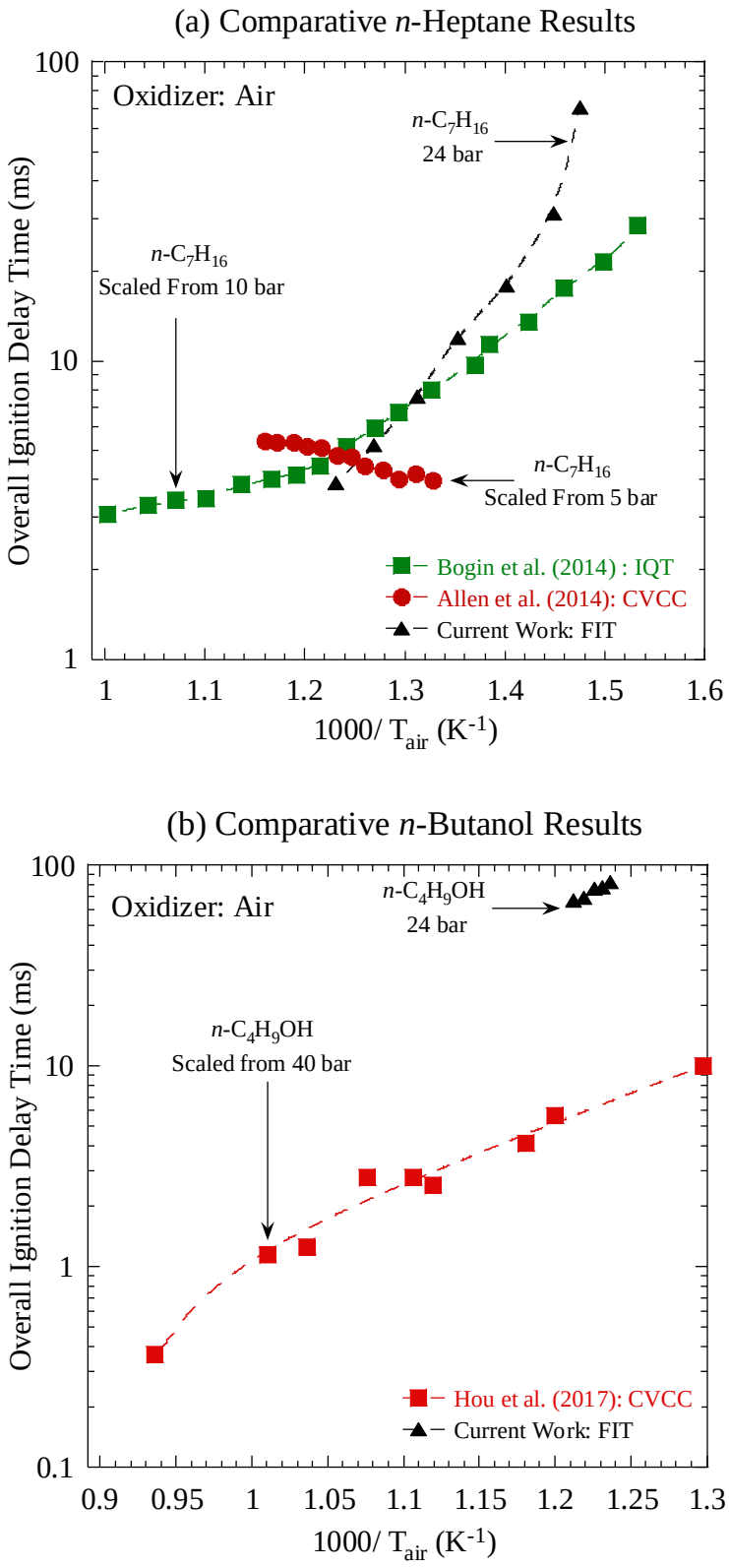

Figure 2.11: (a) Comparison of ignition delay times scaled to 24 bar as a function of varying oxidizer temperatures in various experimental configurations. for (a) *n*-heptane and (b) *n*-butanol.

2.3-3 Exhaust Emissions

The results of the exhaust gas composition measurements are shown in Figs. 2.12(a) and 2.12(b). The graphs represent the averaged volume % emissions results and the averaged volume ppm emissions results, respectively, for the 5 tested blends: pure *n*-butanol, pure *n*-heptane, pure *iso*-octane, 60% *n*-butanol in *n*-butanol/*n*-heptane, and 60% *n*-butanol in *n*-butanol/*iso*-octane. Only injections with a measured fuel injection duration of 5 *ms* are shown here. The results are somewhat expected but informative nonetheless. Regarding the neat *n*-heptane, Figs. 2.12(a) and 2.12(b) show that it undergoes near complete combustion with little to no production of CO. *n*-Heptane combustion also produced the most nitric oxide. For *iso*-octane, CO_2 production was less than that of *n*-heptane. As expected, for *iso*-octane, a significant amount of CO was produced; this is consistent with incomplete combustion. A greater extent of incomplete combustion is expected for iso-octane and n-butanol because their ignition delay times are long compared to the experimental window of 100 ms, shortly after which the chamber is evacuated and the gas composition frozen. The neat *n*-butanol showed the largest residual O_2 after combustion, likely due to its fuel bound oxygen atoms. Additionally, *n*-butanol produced the least amount of CO_2 and the greatest amount CO; this could indicate a relatively greater extent of incomplete combustion for *n*-butanol than *iso*-octane. Although the hydrocarbon readings are very similar for all fuels/blends, the residual hydrocarbon is greatest for *iso*-octane.

The values for the estimated global equivalence ratio based on the exhaust gas composition measurements are shown in Table 2.3. It was found that the equivalence ratio is strongly dependent on the fuel injection duration. The results presented in Table 2.3 correspond to a fixed injection duration of 5 *ms* for each neat fuel or fuel blend. As expected, *n*-butanol was

found to have the lowest equivalence ratio. It is interesting to note that the $R_B = 60$ blend with *iso*-octane has a slightly higher equivalence ratio than the $R_B = 60$ blend with *n*-heptane. Baumgardner et al. [53] conducted equivalence ratio tests for n-butanol and the PRFs in an FIT. The equivalence ratios were obtained by gravimetrically weighing the fuel before and after each set of injections and using the ideal gas law to calculate the amount of air in the chamber. This method produced equivalence ratios of ~0.5 for the PRFs and ~0.2 for pure butanol. The exhaust gas composition measurement done here produced equivalence ratios smaller than when done by gravimetric analysis.

Table 2.3: Exhaust gas composition measurements and estimated global equivalence ratios for various fuel blends.

	n-heptane	*iso*-octane	*n*-butanol	R_B= 60 with *n*-heptane	R_B= 60 with *iso*-octane
O_2 (Vol-%) SDV	18.12 0.07	18.46 0.03	18.83 0.08	18.62 0.05	18.51 0.01
CO_2 (Vol-%) SDV	1.78 0.05	1.53 0.08	1.20 0.06	1.42 0.04	1.48 0.02
CO (Vol-ppm) SDV	5.28 8.94	1427.25 372.52	2370.61 34.22	891.92 133.17	1719.97 355.29
NO_x (Vol-ppm) SDV	345.67 22.71	6.73 2.00	0.00 0.00	0.21 0.09	0.00 0.00
HC (Vol-ppm) SDV	25.20 1.32	44.92 8.54	29.40 8.32	24.23 5.04	22.02 7.99
Estimated Equivalence Ratio	0.134	0.125	0.104	0.111	0.120

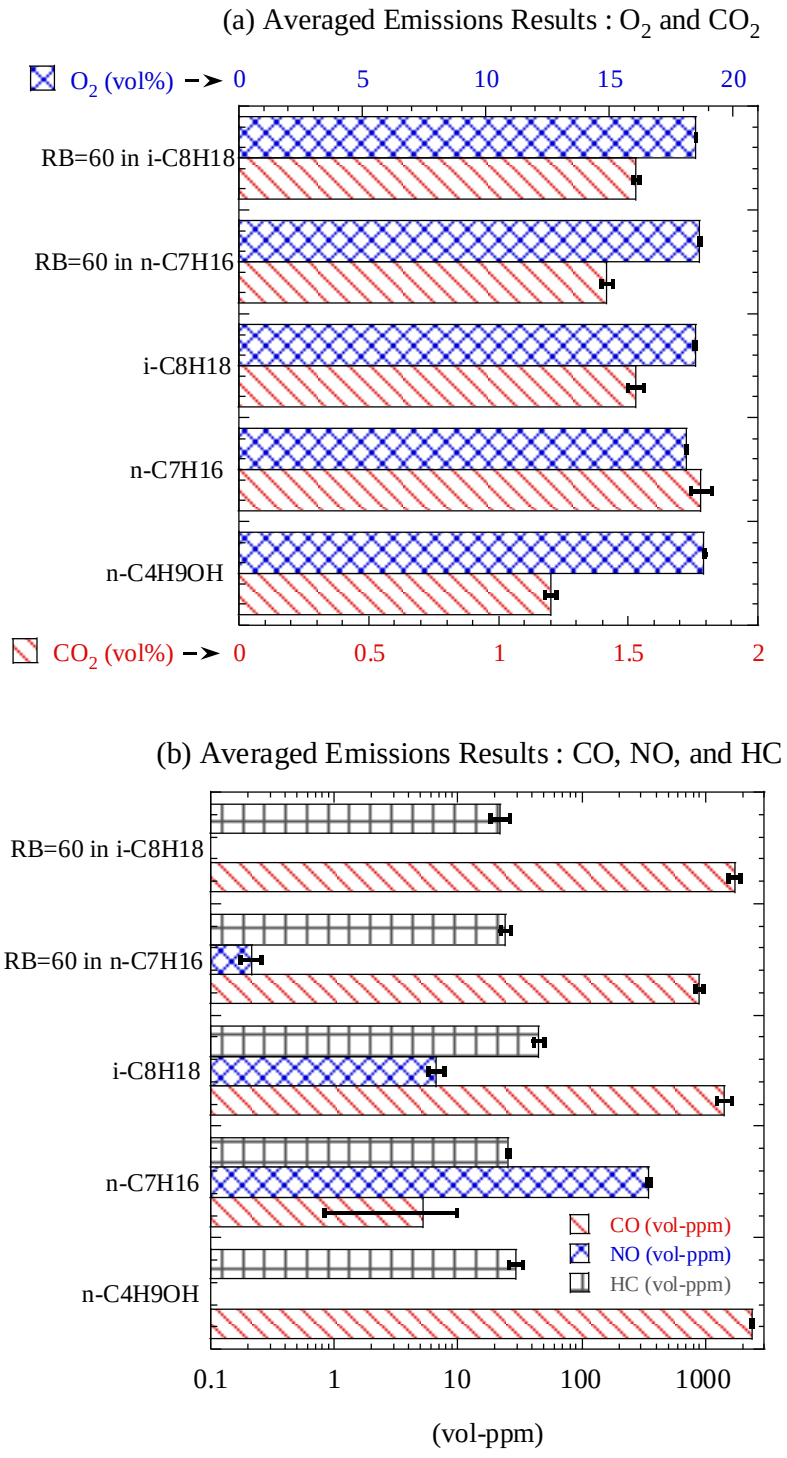

Figure 2.12: (a) Oxygen and carbon dioxide concentrations in the raw FIT exhaust at the calibration temperature of $T \approx 812\ K$. (b) Nitric oxide, hydrocarbons, and carbon monoxide concentrations in the raw FIT exhaust at the calibration temperature of $T \approx 812\ K$.

2.3-4 Ignition Delay Simulation Comparison

Figs. 2.13(a) and 2.13(b) compare the experimental and simulated pressure traces for neat fuels and binary fuel blends of $R_B = 60$, respectively. The agreement between the experimental and simulated pressure traces is reasonable considering that physical effects related to the spray, vaporization, and non-uniform fuel distributions are not included in the simulations. Additionally, the post-ignition rate of pressure rise and the locations of maximum rates of pressure rise also have a fair level of agreement. The above conclusions apply to both the neat components and the binary blends with the exception of pure *iso*-octane whose simulated ignition delay time is not within the window of the experimental test-duration. There is a noteworthy similarity in the post-combustion peak pressures in both the simulated and experimental pressure traces seen in Fig. 2.13(a) and 2.13(b). The comparison gives reason to believe that the estimated equivalence ratios are reliable.

Regarding n-heptane in Fig. 13(a), the experiments show only a single ignition event while the simulations predict a two-stage ignition. The ignition delay time of n-heptane is short enough that mixing likely plays a key role in the ignition process. A recent study performed by Dahms et al. [85] establishes a conceptual model for turbulent ignition in high-pressure spray flames. After injection, first stage ignition occurs in localized lean mixture regions initiating a cool flame wave that propagates through the mixture [85]. Following this, high temperature ignition occurs in rich mixture regions which form steep gradients to initiate the propagation of a turbulent flame [85]. Because of this, the overall ignition delay time is shorter than for homogeneous ignition [85]. This behavior is likely occurring for experiments in the FIT where the ignition delay is short and may cause masking of the first stage ignition in the measured pressure history.

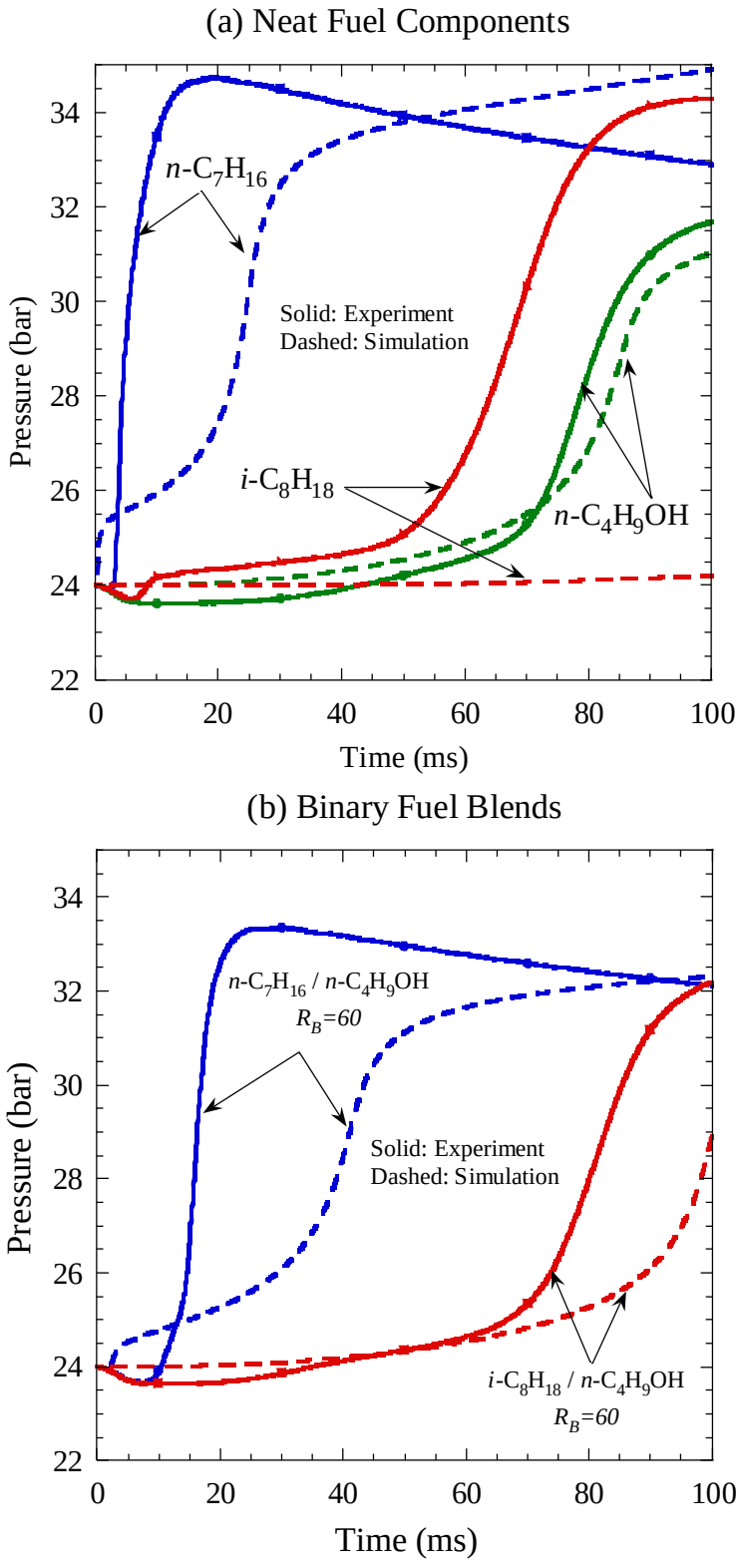

Figure 2.13: (a) Comparison of experimental and simulated pressure traces for *n*-heptane ($\phi = 0.134$), *iso*-octane ($\phi = 0.125$), and *n*-butanol ($\phi = 0.104$) all at $T \approx 812\ K$. (b) Comparison of experimental and simulated pressure traces for *n*-heptane/*n*-butanol ($\phi = 0.111$), *iso*-octane/*n*-butanol ($\phi = 0.120$) each with R_B=60 and all at $T \approx 812\ K$.

Figs. 2.14(a), 2.14(b), and 2.14(c) compare the experimental and simulated overall ignition delay times at different temperatures for *n*-heptane, *iso*-octane, and *n*-butanol, respectively. From Fig. 2.14(a), it can be seen that, in general, the simulation under-predicts the first stage ignition delay and over-predicts the overall ignition delay results of *n*-heptane from the FIT, while the simulated results follow a very similar trend to the experiments. In addition, the experimental and simulated trends are seen to stay reasonably parallel. It is likely that the physical delay has something to do with the offset seen.

For *iso*-octane, as seen in Fig. 2.14(b), the simulation over-predicts the overall ignition delay and does not predict a first stage ignition event. However, the simulations show a similar slope as the experimental trend. Furthermore, the simulated overall ignition delays of *n*-butanol closely match the experimental results in Fig. 2.14(c). Interestingly, the simulations slightly under-predict the overall ignition delay at the hottest tested temperature and over-predict the overall ignition delays slightly for tests at other temperatures. No first stage ignition events were observed from the experiments or simulations for pure *n*-butanol. Furthermore, similar to the experimental results, the simulations also show no NTC behavior.

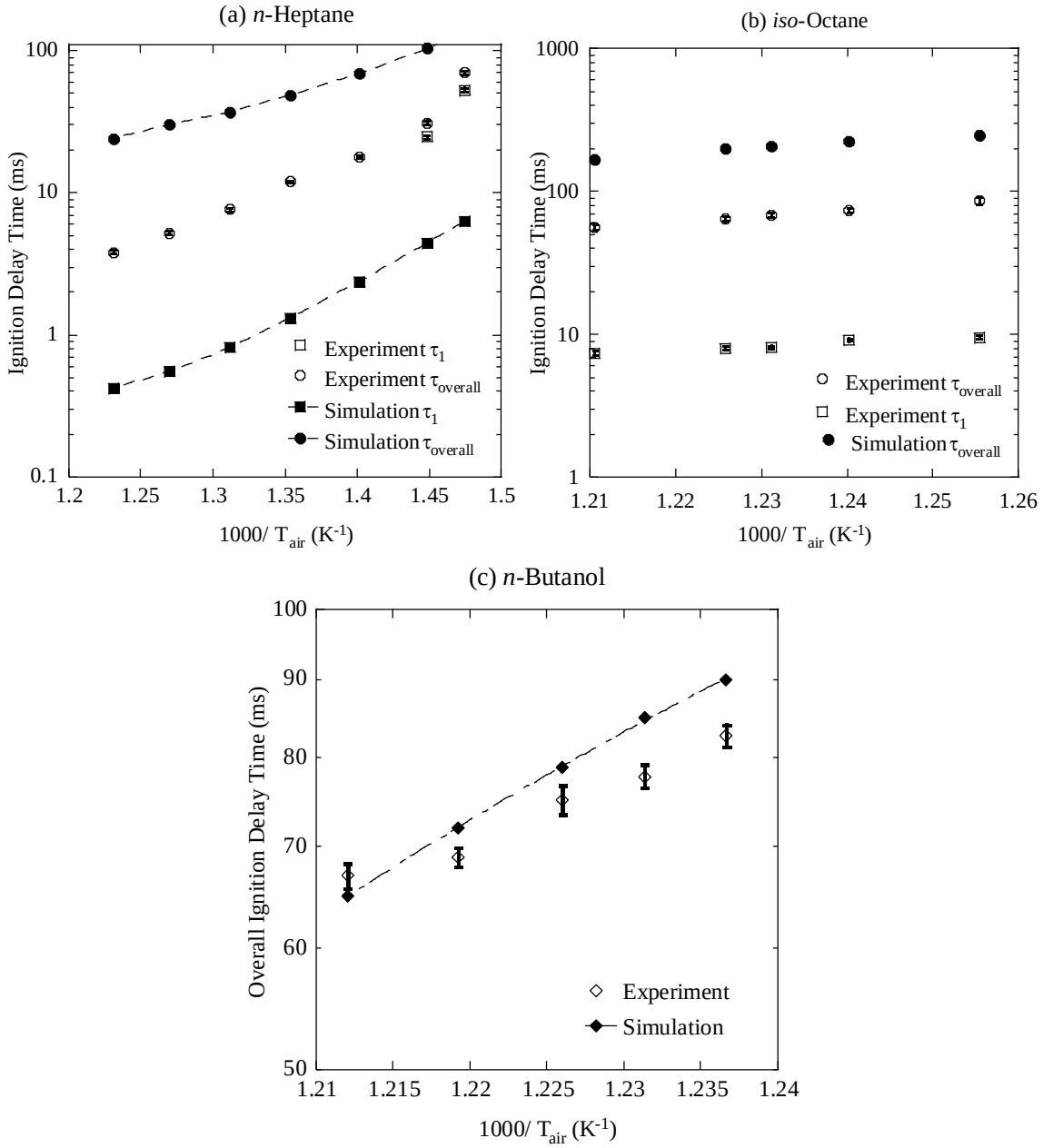

Figure 2.14: Overall & first stage ignition delay comparison between experimental and simulated results for (c) *n*-butanol.

2.4 Concluding Remarks on *n*-butanol PRF study

The autoignition characteristics of *n*-butanol, gasoline PRF constituents, and PRF/*n*-butanol binary blends have been obtained in a constant volume combustion chamber at a fixed fuel injection duration and oxidizer temperature. Addition of *n*-butanol to both *n*-heptane and *iso*-octane was found to reduce reactivity when compared to pure PRF components. The inhibition effect of *n*-butanol was observed for both the first- and second-stage ignition delay times. A correlation for the DCN variation with the volumetric proportion of *n*-butanol blended with either *n*-heptane or *iso*-octane has also been obtained and demonstrated. The DCN representative correlation will be useful in determining what mixture of bio-fuel one can use in a certain system.

The dependence of ignition delay on the oxidizer temperature was obtained for three pure fuels. Neither the experiments nor the simulation showed definitive NTC behavior. The lack of NTC behavior in the experiments (for *n*-heptane) is believed to be because of the relatively high initial chamber pressure and physical effects related to the spray. The lack of NTC behavior from the mechanism is believed to be because of the low global equivalence ratio. Simulations at an equivalence ratio of 0.5, for *n*-heptane, showed NTC behavior in the tested temperature region. Additionally, the dependence on oxidizer tests nicely showed chemically controlled two stage ignition for *n*-heptane at the lowest tested temperature 678 K. It was determined that physical effects from experiments with short ignition delay times might mask this two-stage ignition behavior.

Exhaust gas composition measurements further validated the positive relationship between complete combustion and nitric oxide production. The extreme sensitivity of nitric oxide production to the extent of complete combustion was also shown. A greater extent of

incomplete combustion is expected for *iso*-octane and *n*-butanol because their ignition delay times are long compared to the experimental window of 100 ms, shortly after which the chamber is evacuated and the gas composition frozen. Using the results from the exhaust gas amylase, the global equivalence ratios were found. The equivalence ratios found using the exhaust gas composition method are smaller than those predicted by a gravimetric analysis of the fuel before and after the injections. This is believed to be because the gravimetric analysis does not account for inherent fuel losses in the system.

A first step towards investigating under what conditions the FIT can support the validation of chemical mechanisms has been done via a rudimentary 0-D, constant volume, reactor model that does not consider any physical effects. In general, the agreement between the experimental results and the simulated are results is fair for the overall ignition delay times, rates of pressure rise, and absolute pressure rise, except for pure *iso*-octane. The case of the *iso*-octane experiments poor agreement with eh simulation is believed to be due to the low equivalence ratio. It has been concluded that the homogenous reactor assumption is not entirely accurate for experiments were the ignition delay is short; this is suspected to be because the physical effects of the fuel spray dominate the autoignition behavior.

Chapter 3 : Ignition Delay Times of Methyl Decanote and n-Decane in a Constant Volume Combustion Chamber

Presented at the WSSCI 2017 Fall Meeting in Laramie WY

3.1 Introduction

Biodiesel is a very attractive alternative for use in diesel engines considering the: reduction in CO_2 emissions, biodegradability, and energy dependence. Biodiesel is a potentially renewable fuel and has advantageous fuel properties like lubricity and a high flash point [86]. The production of biodiesel has nearly quadrupled over the past decade from 250 million gallons in 2006 to 1,268 million gallons in 2016 [87]. The ASTM standard [88] defines biodiesel as, "a fuel comprised of mono-alkyl esters of long chain fatty acids derived from vegetable oils or animal fats, designated B100". Biodiesel is most commonly produced with a lipid feedstock via transesterification with an alcohol, typically methanol [89]. Usually the local availability of feedstock determines the choice of raw materials that goes into producing biodiesel. The choice of feedstock in turn determines the fatty-acid composition of the biodiesel and it is the compositional profile that is influential in combustion and ignition performance [90, 91]. Typical mono-alkyl esters common in corn, canola, and soybean derived biodiesel are shown in Fig. 3.1.

Biodiesel offers the possibility of significant CO_2 emissions reduction; this possibility is due to the renewable nature of the feedstocks. Another environmental plus associated with biodiesel is that it is readily biodegradable in both soil and aquatic environments. Soil contaminated from a biodiesel fuel spill can restore itself in 4-6 weeks to a degree that can support plant germination [92]. There are however some drawbacks associated with biodiesel fuels. A study by the U.S. Environmental Protection Agency (EPA) showed that a 20 percent blend of soybean derived biodiesel in a base fuel led to a 2 percent increase in NOx emissions

while showing a 10 percent decrease in particulate matter [93]. In a different study, the emission of ultrafine particulate matter from Rapeseed Methyl Ester (RME) biodiesel was distinctly higher when compared to conventional diesel [94]. Biodiesel is ideal alternative for use in diesel engines considering the: reduction in CO_2 emissions, biodegradability, and energy dependence. Biodiesel will be even more environmentally appealing when NO_x and ultrafine particulate emissions resulting from biodiesel combustion are reduced.

Methyl decanoate is one of the fatty acid methyl esters that occurs in biodiesel; its molecular structure is shown in Fig. 3.2. Methyl Decanoate is most commonly produced from transesterification of coconut and palm feedstocks [95]. It is a long alkyl chain with 11 carbon atoms. Since biodiesel contains a number of alkyl ester compounds, typically ranging in carbon numbers of 12 to 24, it has been common to use a single- or reduced- component surrogate to model biodiesel. Methyl decanoate is one such surrogate [86, 96]. It is advantageous to use a surrogate to model biodiesel since there are usually a large number of mono-alkyl esters present in biodiesel and the carbon numbers of the mono-alkyl esters have a large range. Given that methyl decanoate is a constituent of biodiesel and commonly used biodiesel surrogate, it is essential to acquire fundamental ignition data on blends of methyl decanoate and neat diesel constituent under conditions similar to compression ignition engines.

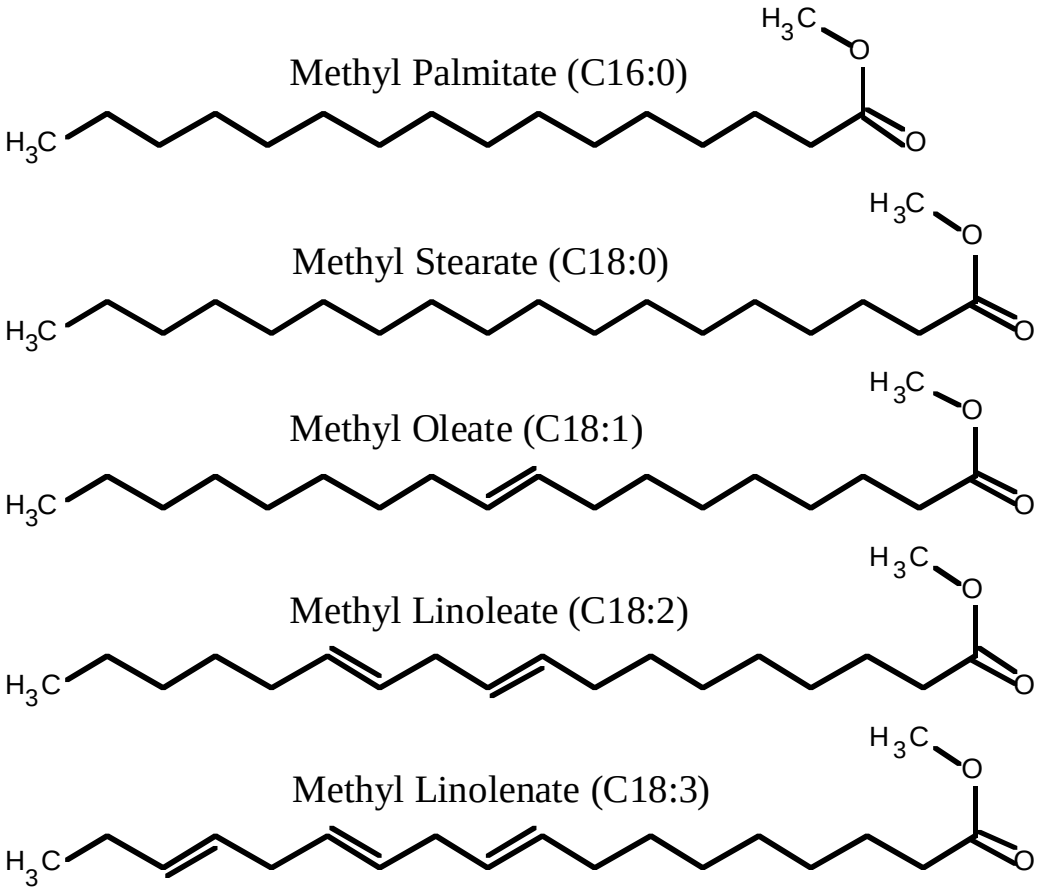

Figure 3.1: Different mono alkane fuel structures common in derived biodiesel.

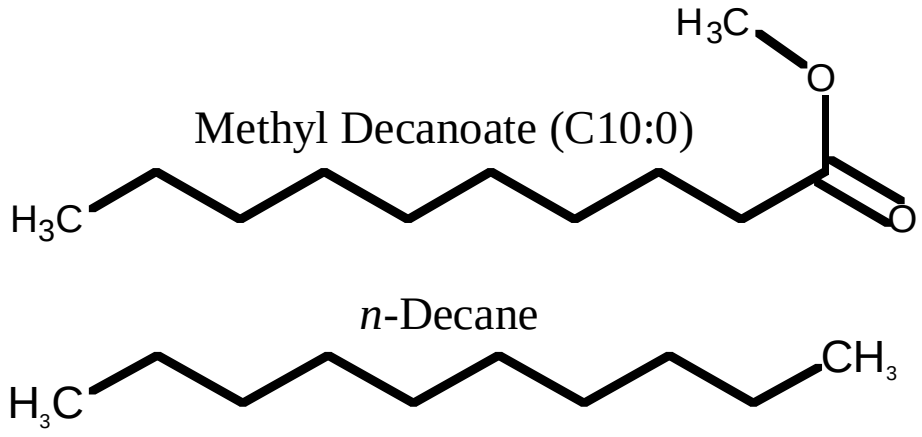

Figure 3.2: Methyl Decanoate and *n*-Decane Fuel structures.

Biodiesels' efficient and clean utilization in engines is dependent on the ability to predict the global combustion properties and the detailed species evolution during oxidation. The development of predictive capabilities, like a detailed reaction mechanism, is dependent on experimental and computational efforts. An increase in fundamental combustion research related to methyl decanoate combustion has been seen, on both experimental and computational fronts. The development and validation of comprehensive reaction mechanisms is supported by fundamental experimental data from diverse, well characterized experiments, which are complementary in nature and cover a wide range of thermophysical conditions. Such experiments that have been conducted with methyl decanoate include shock tubes [86, 97-100], steady premixed flames [36, 101, 102], laminar non-premixed flames [103-107], jet stirred reactors [108], and reduced gravity experiments [109, 110]. Surprisingly, no work was found concerning methyl decanoate and rapid compression machines (RCMs) or methyl decanoate and constant volume combustion chambers (CVCC) in the literature. In addition to the fundamental combustion experiments, there have also been applied studies investigating methyl decanoate and investigating the effect of blending methyl decanoate with conventional diesel fuels. The applied studies have been done in systems such as compression ignition [111-116] and homogenous charge compression ignition engines (HCCI) [117].

In general, pure biodiesel can be used as a fuel or it can be blended with petroleum derived fuels [89]. Consequently, it is important to develop a fundamental understanding of the autoignition characteristics of both petro and bio derived diesel fuels. The fuel, *n*-decane, is representative of a typical conventional diesel fuel constituent and is therefore chosen for this study, its molecular make up is shown in Fig. 3.2. This study focuses on broadening the experimental understanding of conventional and alternative diesel fuel constituent blends.

A Fuel Ignition Tester (FIT) apparatus is used to obtain the ignition delay times resulting from fuel injection at elevated pressure and low-to-intermediate temperature conditions. The thermodynamic conditions within the FIT are similar to direct-injection compression ignition engines. The objective of this work is to examine the influence of blending methyl decanoate to *n*-decane on the derived cetane number (DCN). In addition, the first stage ignition delay and the total "hot" ignition delay events were obtained using the first and second maximums of the rate of combustion pressure rise as the delay time definitions respectively [118]. The influence of oxidizer temperature on the ignition delay times was also investigated. This work also compares the experimental results to numerical calculations. Homogenous constant volume simulations were carried out using chemical kinetic mechanisms reported in the literature. The global equivalence ratios used in the simulations were deduced from measurements of exhaust products from the FIT. The validity of the zero dimensional simulations to model a constant volume combustion chamber autoignition, under certain conditions, with spray has been previously demonstrated by Allen et al. [11].

3.2 Computational Methods

The experimental results in this study were simulated using detailed chemical kinetic schemes for the neat fuels and their blends. Pure fuels were simulated using the LLNL C_8-C_{16} *n*-alkane [119] and LLNL methyl decanoate [96] mechanisms, respectively. The aforementioned mechanisms for the pure fuels include both low and high temperature sub-mechanisms. Mechanisms that can model binary mixtures of *n*-decane and methyl decanoate were scarce, and only one was found in the literature. This blend mechanism developed by Ranzi et al. [120] was used to model the R_{MD}=60 conditions.

Numerical Simulations based on zero-dimensional homogeneous kinetics model were carried out using CHEMKIN® PRO [121]. The initial conditions used for the simulations corresponded to the average pressure and temperature from the FIT experiments, namely 24.0 bar and 812.7 K, respectively. The equivalence ratios were deduced using the exhaust gas composition measurements, discussed earlier. In addition, the effect of oxidizer temperature was modeled using the same averaged pressure and the corresponding experimental air temperature.

3.3 Results and Discussion

3.3-1 Ignition Delay Times

Experimental pressure traces for *n*-decane and methyl decanoate are shown in Fig. 3.3. This figure also shows the rate of pressure rise which was obtained from the average of the raw pressure traces. As seen from the figure, the ignition delay (both τ_{onset} and $\tau_{overall}$) of methyl decanoate is slightly longer than *n*-decane. The peak post-combustion pressure is higher for *n*-decane when compared to methyl decanoate. This is consistent with the lower energy density of methyl decanoate as compared to *n*-decane. However, methyl decanoate exhibits a greater rate of combustion pressure rise (1.36 bar/*ms* larger) than *n*-decane.

Both fuels show a tight grouping of individual test pressure traces, with the scatter in methyl decanoate traces being somewhat lesser after combustion. A representative pressure trace is derived based on the averaging of the 25 individual traces. The averaged pressure trace is an effective approach to characterize the shape, slopes, and locations of peak pressures for the fuels under test. Note, that the averaged trace is difficult to discern in Fig. 3.3 due to the overlap with the other 25 traces. A clearer representation of the averaged pressure traces can be seen in Fig. 3.4.

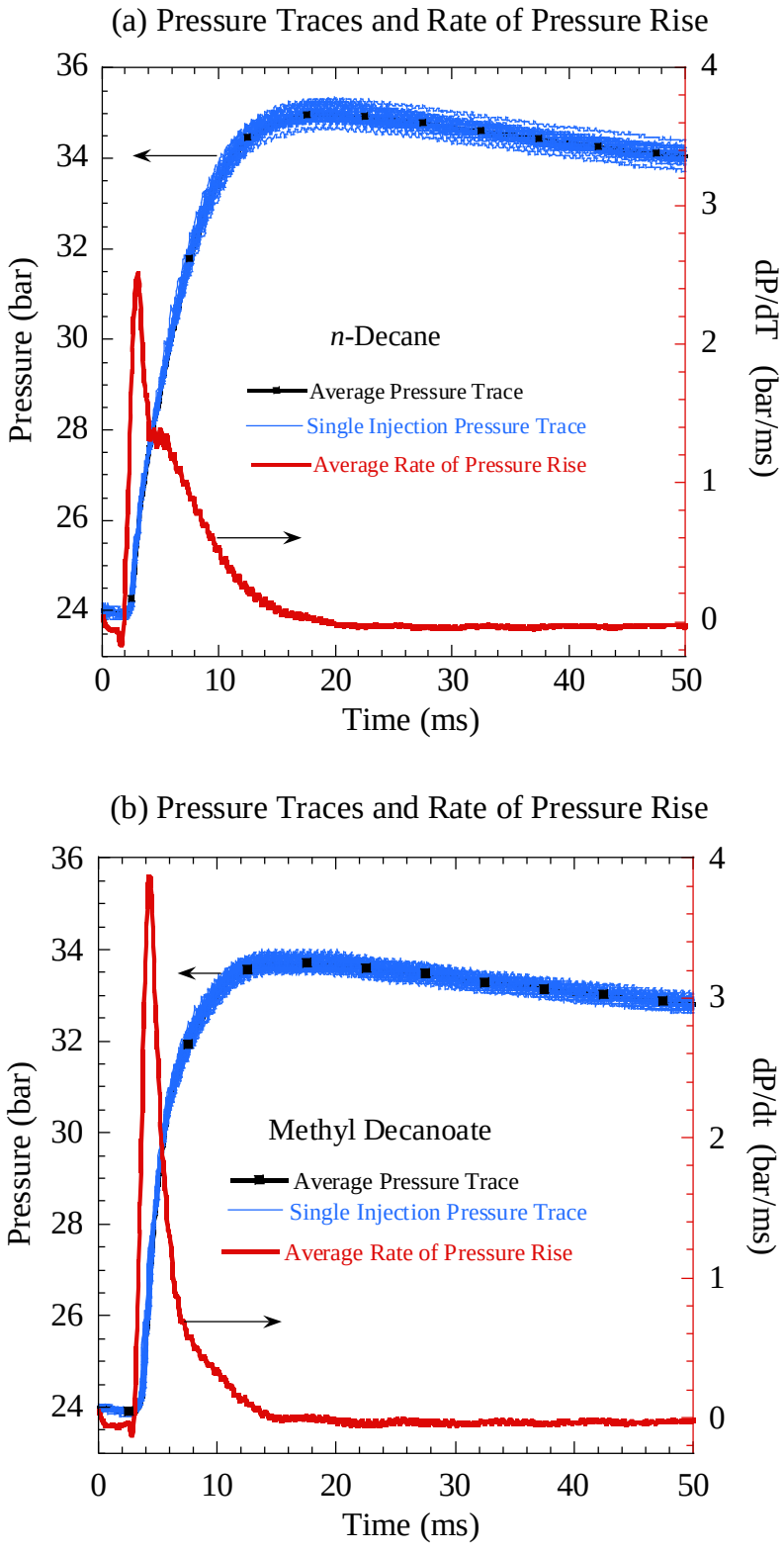

Figure 3.3: Experimental pressure trace data for the pure fuels along with the averaged pressure traces and rates of pressure rise for (a) n-decane and (b) methyl decanoate.

The influence of blending methyl decanoate in *n*-decane on the autoignition characteristics is shown in Figs. 3.4(a) and 3.4(b) on different time scales. Figure 3.4(a) shows that there is a decrease in the peak combustion pressure with increasing methyl decanoate content, consistent with its lower energy density. The energy density of methyl decanoate is -32,150 MJ/m^3 [122]. The energy density of *n*-decane is -34,581 MJ/m^3 [80]. Figure 3.4(b) shows that the addition of methyl decanoate into *n*-decane monotonically slows down its reactivity, although it is over the span of a millisecond. Figure 3.4(b) also shows another clear trend; the rate of pressure rise increases with R_{MD} causing crossover to occur among the averaged pressure traces around 3.5→5ms. This crossover occurs after the τ_{onset} and $\tau_{overall}$ definitions of ignition delay.

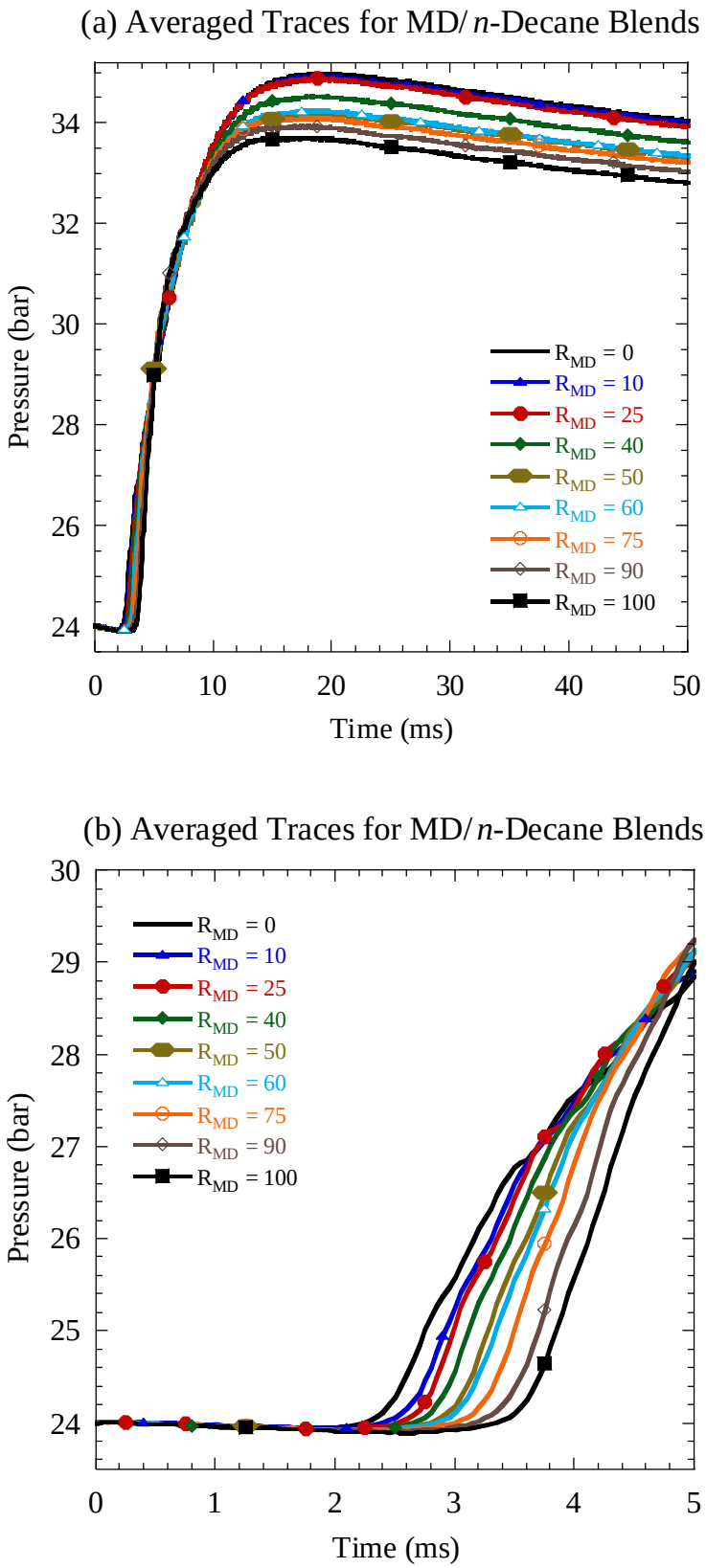

Figure 3.4: (a) Averaged pressure traces for methyl decanoate/ *n*-decane blends. (b) First five milliseconds of averaged pressure traces for methyl decanoate / *n*-decane blends.

The overall ignition delay times based on the maximum rate of pressure rise and the DCN for methyl decanoate / *n*-decane blends are shown in Figs. 3.5(a); they are also given in Table 3.1. The ignition delay time of the blend ($\tau_{overall}$) increases as the methyl decanoate proportion (R_{MD}) is increased. A near linear relationship between the overall ignition delay and the proportion of methyl decanoate appears to hold, as seen from Fig. 3.5(a). The variability in the 25 tests used to obtain the DCN reported here is shown in Fig. 3.6. It is seen that the data sets follow a reasonably normal distribution with R_{MD}=60 being the most skewed. The inter quartile range of the plots typically span 3 DCN units.

Table 3.1: Experimental DCNs and ignition delay times of *n*-decane, methyl decanoate, and the *n*-decane/ methyl decanoate blends

Fuel	R_B	DCN	SDV	$\tau_{overall}$	SDV	Pressure	Air Temperature
	(% Vol)			(ms)	(ms)	(bar)	(K)
n-decane		72.1	2.68	3.05	0.33	24.0	812.8
Methyl decanoate		48.9	1.73	3.250	0.23	24.0	813.0
n-decane/methyl decanoate blends	10	66.9	2.87	3.350	0.24	24.0	812.7
	25	65.0	1.76	3.45	0.21	24.0	813.1
	40	62.0	1.96	3.650	0.33	24.0	812.1
	50	58.6	2.24	3.7	0.21	24.0	813.0
	60	57.3	2.02	3.900	0.29	24.0	812.3
	75	54.5	1.73	4.1	0.24	24.0	812.2
	90	51.2	2.13	4.25	0.26	24.0	812.8

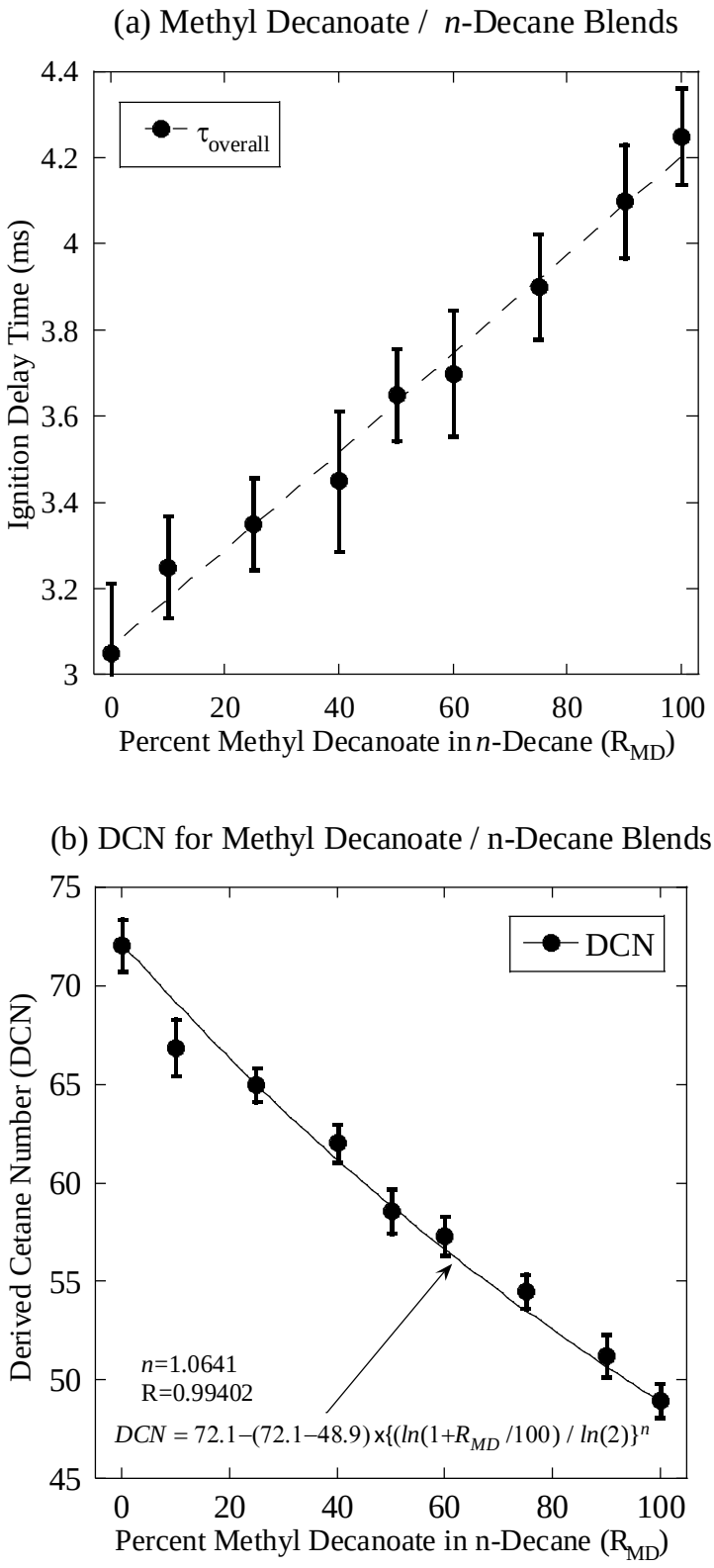

Figure 3.5: (a) Overall ignition delay times and (b) DCN as a function of volumetric blending ratio.

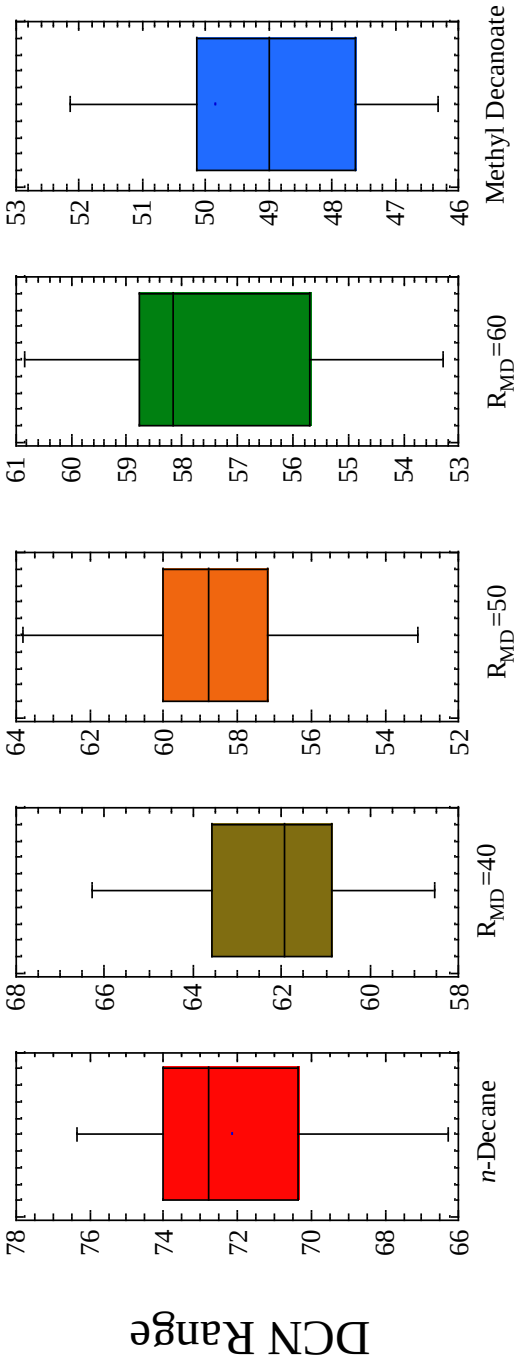

Figure 3.6: Variability in the 25 tests used to obtain the DCN.

The derived cetane numbers for the binary blends, as a function of the volumetric blending ratio(R_{MD}) are shown in Fig 3.5(b). As shown, the DCN decreases monotonically as a function of R_{MD}. Furthermore, the DCN variation trend can adequately be captured by a fitting function of the form the same as Equation 2.1, however the parameters are different. Equation 3.1 shows the DCN function as a function of the volumetric blending ratio for methyl decanoate/ *n*-decane blends.

$$DCN\ (R_{MD}/100) = 72.1 - (72.1 - 48.9) \times \left(\frac{\ln(1 + R_{MD}/100)}{\ln(2)}\right)^{1.064} \tag{3.1}$$

The form of the fitting function ensures that the end points correspond to the experimentally observed DCN of the neat components. This property makes this functional form preferable over a simple inverse relationship that would appear to be valid based on Fig. 3.5(a).

3.3-2 Influence of Oxidizer Temperature

The dependence of ignition delay time on the oxidizer temperature has also been obtained for the two pure fuels. The results are presented in Table 3.2. Figs. 3.7(a) and 3.7(b) show the pressure traces and ignition delay times of *n*-decane at different temperatures, respectively. As shown in Fig. 3.7 the *n*-decane ignition delay time exhibits a monotonically decreasing trend as a function of the oxidizer temperature, for the conditions tested. No evidence of a prominent two-stage ignition is found in the pressure traces for the FIT tests for *n*-decane. However, it can be seen from Fig. 3.7(a) that the post combustion peak pressure of the four tests with the highest oxidizer temperature show a decreasing trend with an increase in temperature. The minimal difference in the duration of fuel injection alone cannot account for the observed trend. An increase in air temperature for a fixed volume and pressure should lead to a slightly larger global

equivalence ratio since the number of moles of oxidizer is reduced. Consequently, an increase in the post combustion pressure is expected since the system is globally lean. The contrary peak pressure trend may be related to the reduced reactivity on account of the low-temperature chemistry observed for *n*-alkanes in a similar temperature window. Additionally, it is seen from Fig. 3.7(a) that the post-combustion peak pressure drops off for the pressure trace with the lowest initial oxidizer temperature; most likely on account of incomplete combustion.

(a) *n*-Decane Pressure Traces

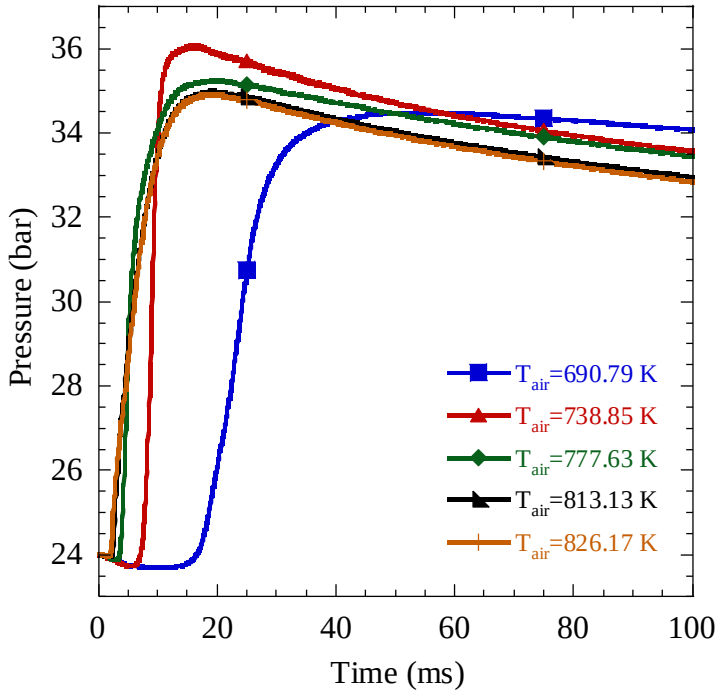

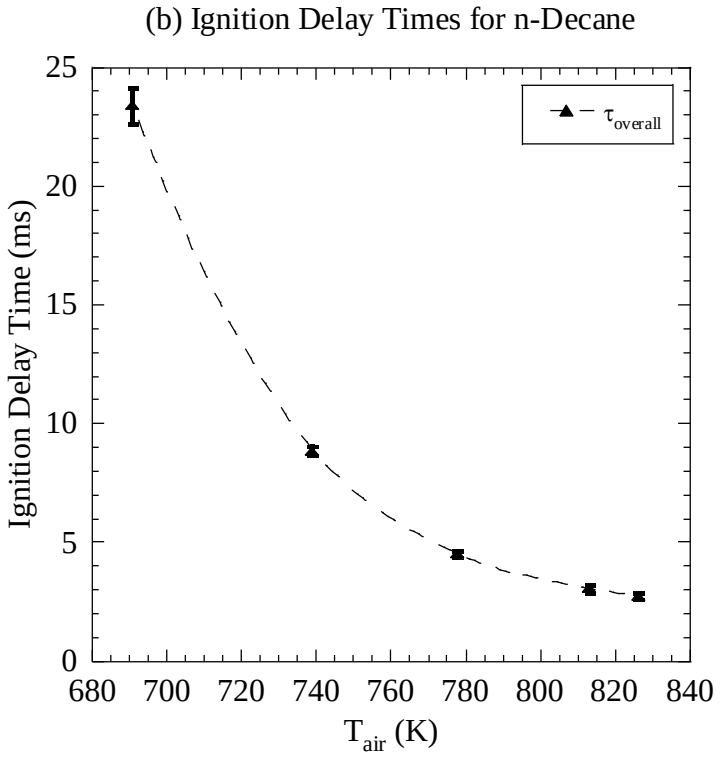

Figure 3.7: (a) Averaged pressure traces for *n*-decane with varying initial air temperature and (b) ignition delay times for *n*-decane as a function of initial air temperature.

The dependence of ignition delay time on the oxidizer temperature for the pure fuel, methyl decanoate, is shown in Figs. 3.8(a) and 3.8(b) and given in Table 3.2. Fig. 3.8(a) shows that the ignition event of methyl decanoate exhibits a monotonic decrease in ignition delay with increasing temperature. Negative temperature coefficient (NTC) behavior was not observed for the tested temperature range. Fig. 3.8(b) also shows a sharp decrease in ignition delay with increasing temperature. Similar to *n*-decane, methyl decanoate shows an increasing trend in combustion peak pressure with decreasing temperature, for the three hottest tests. The combustion peak pressure falls off rapidly for the two pressure traces with the lowest initial oxidizer temperature.

Table 3.2: Experimental temperature dependence of ignition delays for *n*-decane and methyl decanoate

Air Temperature	Pressure	τ_1	SDV	$\tau_{overall}$	SDV
(K)	(bar)	(ms)	(ms)	(ms)	(ms)
n-Decane					
690.79	24.0			23.4	0.75
738.85	24.0			8.85	0.19
777.63	24.0			4.5	0.13
813.13	24.0			3.05	0.16
827.0	24.0			2.75	0.13
Methyl Decanoate					
690.82	24.0	23.4	1.28	39.7	4.53
728.91	24.0			15	0.46
767.52	24.0			7.35	0.28
812.83	24.0			4.25	0.23
825.57	24.0			3.65	0.24

(a) MD Pressure Traces

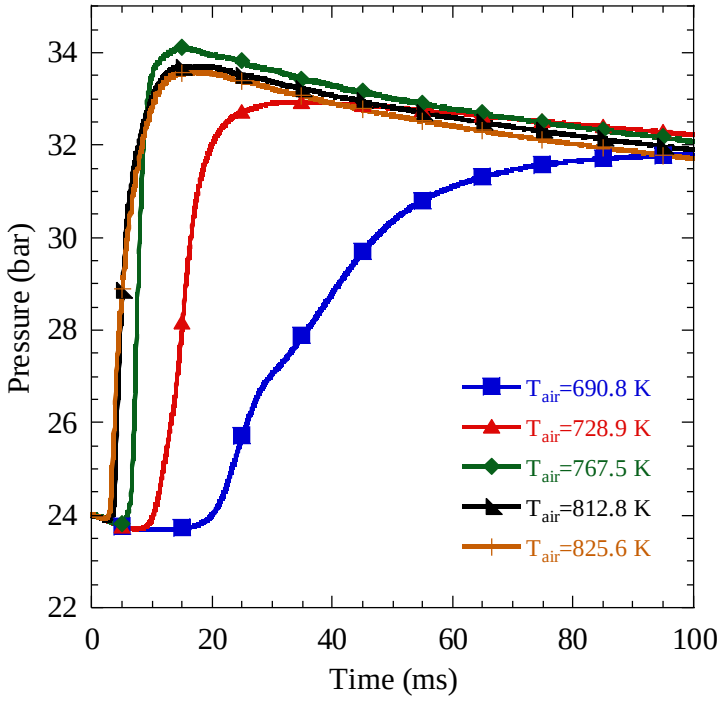

(b) Ignition Delay Times for MD

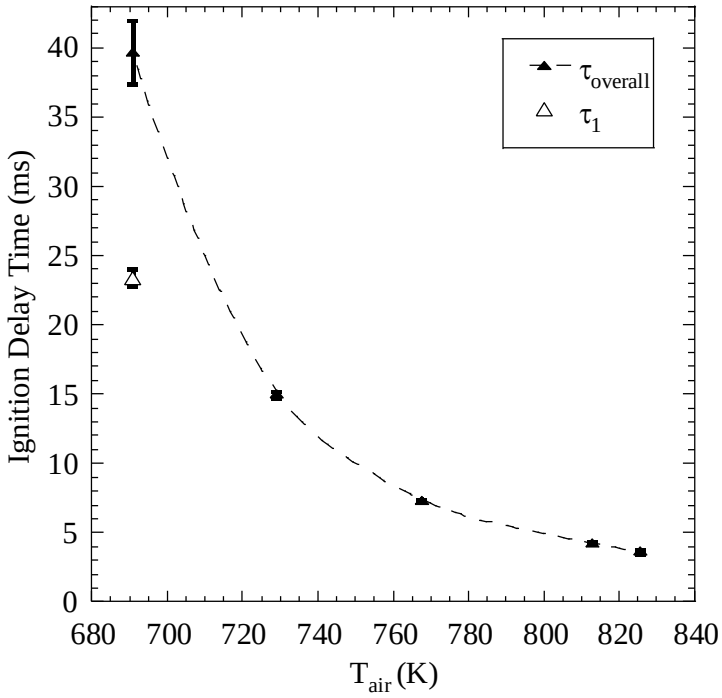

Figure 3.8: (a) Averaged pressure traces for methyl decanoate with varying initial air temperatures and (b) ignition delay times for methyl decanoate as a function of initial air temperature.

3.3-3 Pure Fuels and Blend (R_{MD}=60) Exhaust Emissions

The results of the exhaust gas composition measurements are shown in Figs. 3.9(a) and 3.9(b). The graphs represent the averaged volume % emissions results and the averaged volume ppm emissions results, respectively, for the two neat fuels and their blend. Regarding the neat *n*-decane, Figs. 3.9(a) and 3.9(b) show that it undergoes near complete combustion with no production of CO. *n*-Decane combustion also produced the most nitric oxide (548 ppm, about 130 ppm more than pure methyl decanoate). For methyl decanoate, CO_2 production was less than that of *n*-decane but very similar to the $R_{MD} = 60$ blend. For pure methyl decanoate, a very small amount of CO was produced; this is consistent with complete combustion. Additionally, methyl decanoate showed the largest residual O_2 after combustion (around 0.5% more than pure *n*-decane and 0.1 % more than the $R_{MD} = 60$ blend, likely due to its fuel bound oxygen atoms. The averaged exhaust gas composition measurements and the estimated global equivalence ratios based on the exhaust gas composition measurements, and calculated from Equations 1.1 & 1.2, are shown in Table 3.3. As expected, the pure methyl decanoate was found to have the lowest equivalence ratio likely because it has oxygen in its molecular makeup.

Table 3.3: Exhaust gas composition measurements and estimated global equivalence ratios for *n*-decane, methyl decanoate, and a volumetric blend of 60% methyl decanoate / 40% *n*-decane.

	Pure MD	Pure *n*-Decane	60% MD 40% *n*-Decane
O_2 (Vol-%) SDV	18.52 0.12	18.1 0.11	18.41 0.08
CO_2 (Vol-%) SDV	1.71 0.09	1.82 0.07	1.71 0.07
CO (Vol-ppm) SDV	1.56 2.32	0 0	0 0
NO_x (Vol-ppm) SDV	415.7 34.2	548.39 46.2	451.83 31.3
HC (Vol-ppm) SDV	3.03 2.19	14.94 1.30	4.99 2.46
Equivalence Ratio	0.115	0.136	0.120

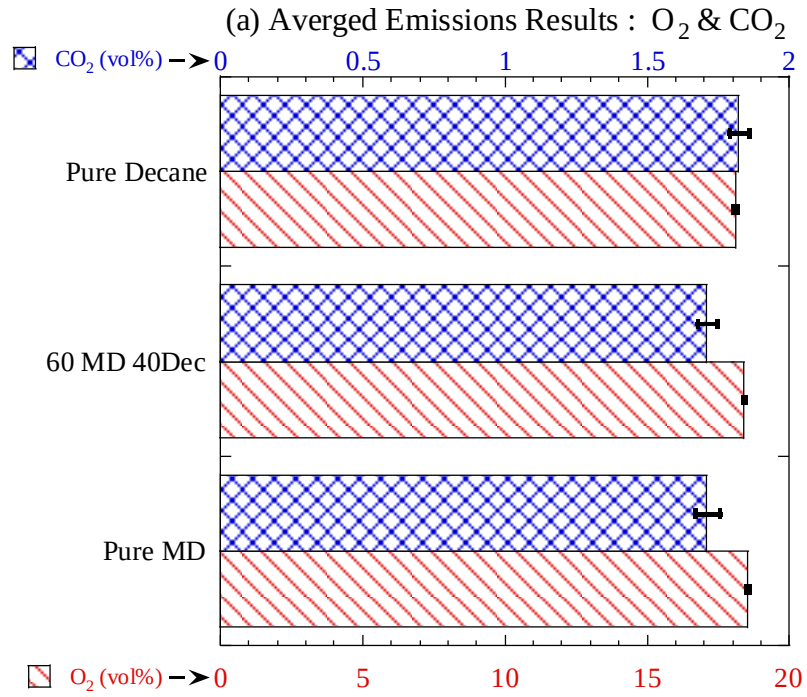

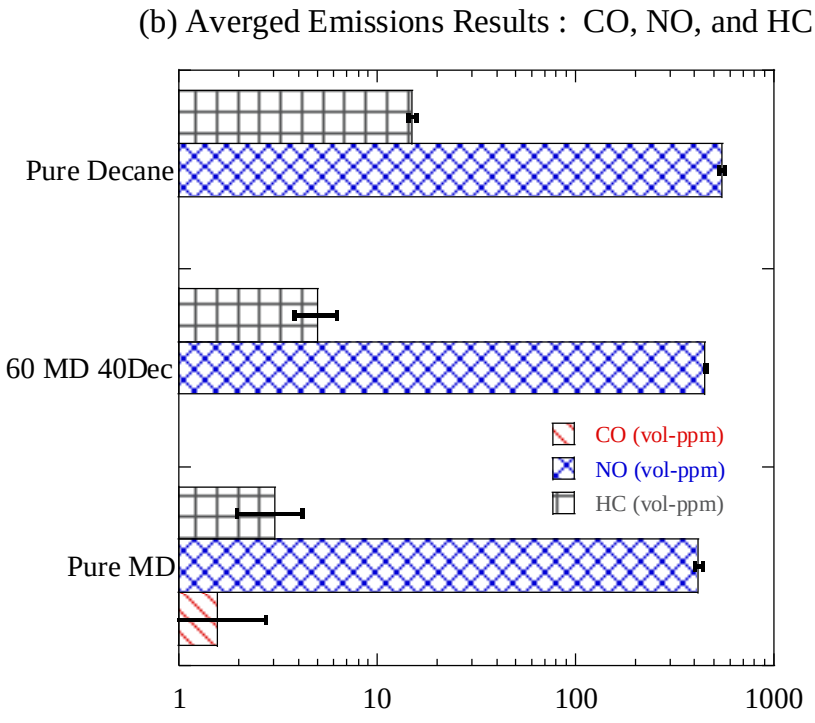

Figure 3.9: (a) Oxygen and carbon dioxide concentrations in the raw FIT exhaust (b) Nitric oxide, hydrocarbons, and carbon monoxide concentrations in the raw FIT exhaust. All at $T_{air} \approx 812.7\ K$.

3.3-4 Methyl Decanoate, *n*-Decane, & Blend Ignition Delay Simulation Investigation

Figs. 3.10(a) and 3.10(b) compare the experimental and simulated pressure traces for neat fuels and binary fuel blends of $R_B = 60$, respectively. For the pure fuels and the LLNL mechanisms [96, 119], the agreement between the experimental and simulated pressure traces is reasonable considering that physical effects related to the spray, vaporization, and non-uniform fuel distributions are not included in the simulations. The mechanism of Ranzi et al. [120] is used for the blend simulations. As such, Fig. 3.10(b), shows an over prediction of ignition delay. It must be mentioned that this mechanism has been validated for high temperature conditions only.

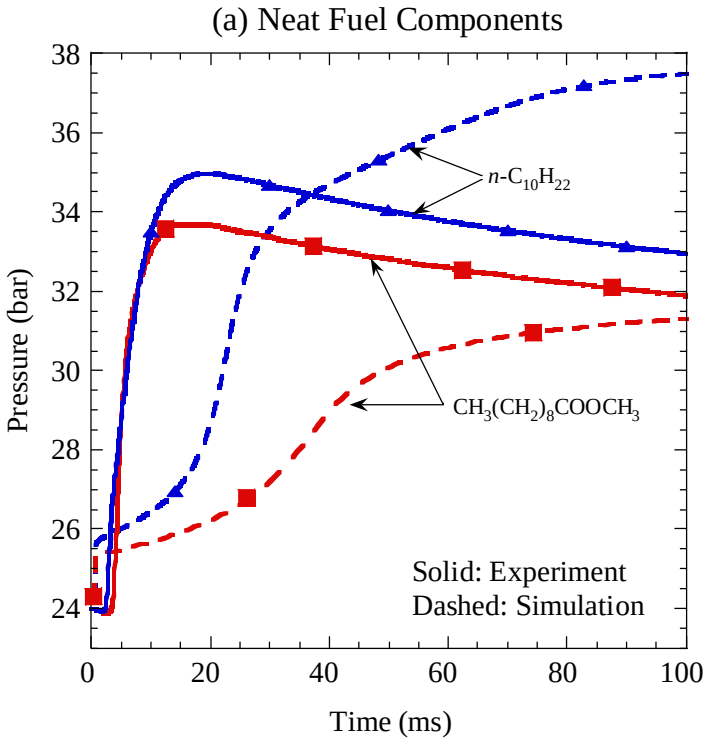

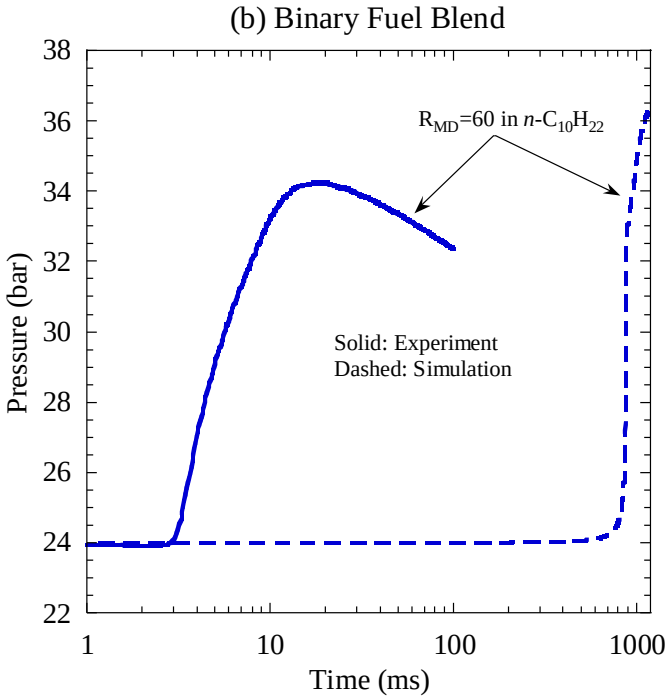

Figure 3.10: (a) Comparison of experimental and simulated pressure traces for n-decane ($\phi = 0.136$) [119] and methyl decanoate ($\phi = 0.115$) [96] all at T ≈ 812.7 K. (b) Comparison of experimental and simulated pressure trace for n-decane/methyl decanoate ($\phi = 0.120$) with R_{MD}=60 and all at T ≈ 812.7 K [120].

Figures 3.11(a) and 3.11(b) compare the experimental and simulated overall and first-stage ignition delay times as a function of air temperature for n-decane and methyl decanoate respectively. The simulations exhibit both first and overall ignition delays. With exception of the lowest temperature test for methyl decanoate, only single stage ignition was observed for the experiments. For the *n*-decane fuel the overall ignition delay predictions using the LLNL mechanism [119] were generally higher a by a factor of eight. This could be a consequence of the non-homogeneity within the FIT, with the actual ignition occurring early in fuel rich pockets in the vicinity of the fuel spray. A similar trend holds for the methyl decanoate fuel for the overall ignition delay and also the single data point for the first-stage delay when compared to the simulations [96]. The slope of the Arrhenius plots of the overall ignition delays for both the fuels were however quite similar.

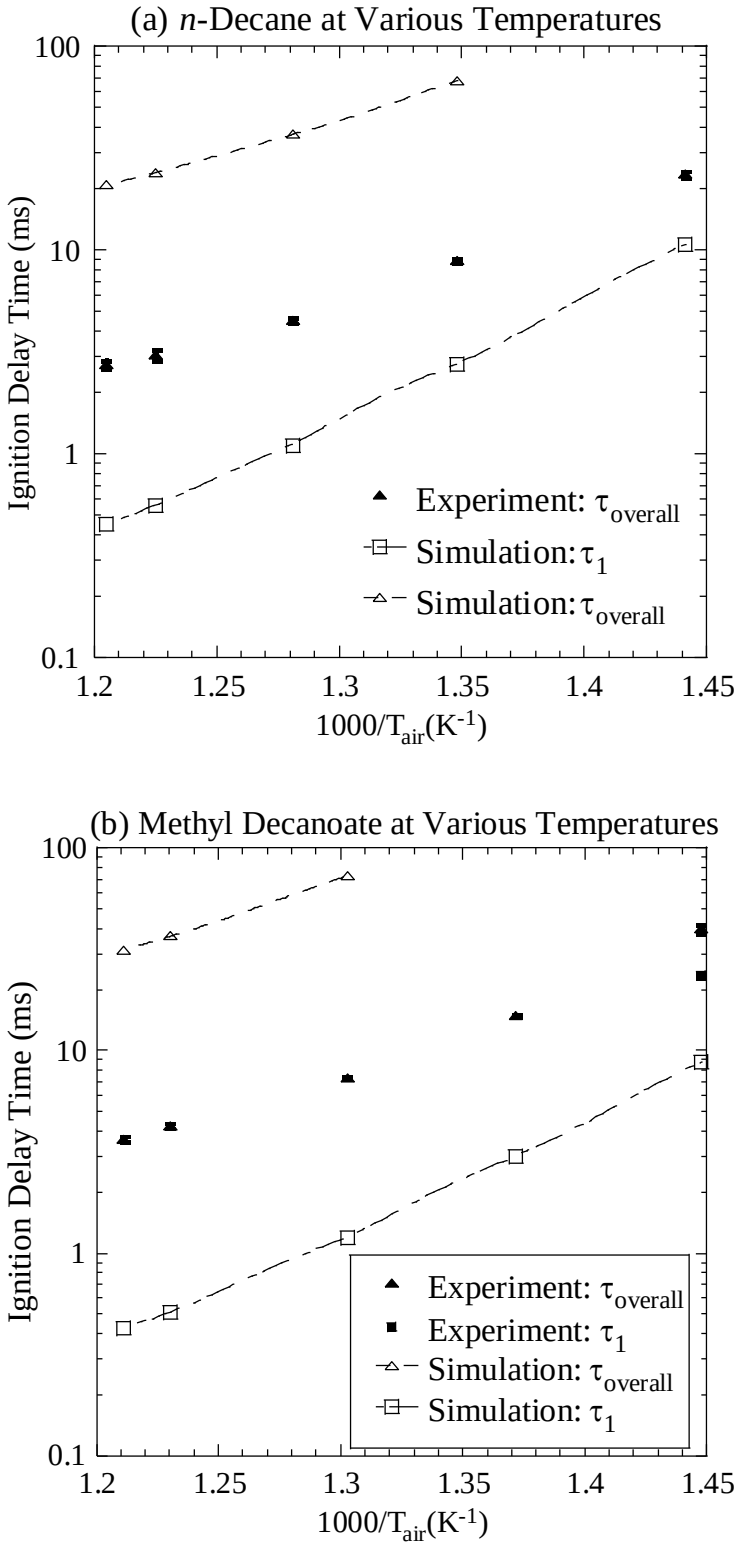

Figure 3.11: Overall ignition delay comparison between experimental and simulated results for (a) n-decane and (b) methyl decanoate.

3.4 Concluding Remarks on *n*-decane / methyl decanoate study

Autoignition characteristics of *n*-decane, methyl decanoate, and their binary blends have been obtained in a constant volume combustion chamber at a fixed fuel injection duration. Addition of methyl decanoate to *n*-decane was found to slightly reduce reactivity of the blend. A slight inhibition effect of methyl decanoate was observed for the overall ignition delay times. The fuel blend tests helped establish a working correlation for DCN as a function of volumetric blending ratio for methyl decanoate / *n*-decane blends. The DCN representative correlation will be useful in determining what mixture of bio-fuel one can use in a certain system.

In addition, the dependence of ignition delay on the oxidizer temperature was obtained for the two pure fuels. No NTC behavior was observed for the temperature range tested. Two stage ignition was observed for both fuels at lower temperatures. It was determined that physical effects from experiments with short ignition delay times might mask this two stage ignition behavior.

Exhaust gas composition measurements were conducted for the pure fuels and 60% methyl decanoate blend. Nitric oxide production was found to be sensitive to the extent of completion of combustion.

The experimental results were also compared to homogeneous constant volume simulations. The simulated results over-predicted the experimental overall delays for both the fuels, but the slopes with respect to temperature variation were quite similar. Products of combustion were analyzed for the pure fuels as well as their blends. The mechanism used for the 60% methyl deaconate blend drastically over predicted the ignition delay time. This is likely because it hasn't been validated for low temperature autoignition. This revels the need for a large *n*-alkane/ methyl ester mechanism for low temperature conditions.

Chapter 4 : Temperature Dependence on Ignition Delay Times of Canola, Corn, and Soy Derived Bio-Diesel

4.1 Biodiesel Study Foreword

First generation plant based feedstocks are increasingly being used for biodiesel production [87]. Typical first generation feedstocks available in the United States are soybean and corn based. The United States produces 35.8% of the world's corn and 33.3% of the world's soybean crops [123]. The definitions, standards, advantages, and other information regarding biodiesel is given in the introduction of chapter 3. While autoignition parameters like DCN have been moderately investigated, there are limited-no studies on the effect of varying the initial thermodynamic conditions on the ignition delay times of theses fuels. This work fills in such a gap and provides the influence of oxidizer temperature on ignition delay.

The work herein is an addition to the study carried out by Stuhlman et al. [5] which was presented at the 2017 WSSCI fall meeting. The study involved the autoignition response of canola, corn and soybean derived biodiesel. The study analyzed the autoignition trend of three different biodiesels at the FIT calibration temperature of ~812 K. A qualitative ranking in the ignition delay times and DCNs was seen. It was suspected that the ranking was due to the different degrees of unsaturation possessed by the biodiesels' major components. This work expands upon the initial study by including three times more data at temperatures from 680 K -812 K. The initial results that are not amended are given in the Appendix.

4.2 Corn, Canola, and Soybean Biodiesel Properties

The canola, corn, and soybean biodiesel fuels were produced in-house for the experimentation of this study. These biofuels were made through transesterification. Refer to the Appendix for additional information on the biodiesel production method. The chain length and degree of unsaturation are molecular traits that affect the ignition delays and DCNs of a fuel. The three biofuels produced for this study have almost identical chain lengths, but differ in terms of the degree of unsaturation.

The five major Fatty Acid Methyl Esters (FAME's) present in biodiesels tested in this work are shown in Fig. 4.1 and the compositional profile (vol-%) is given in in Table 4.1 . The last two rows in Table 4.1 gives the average degree of unsaturation (ADU) and average chain length (ACL) for one representative unit of the respective biofuel; this estimation was found using the following equations.

$$AVG_{degree\ of\ unsaturation}(ADU) = \sum_{i=1}^{6} Unsaturation_i \ x \ \left(\frac{Composition_i}{100}\right) \qquad (4.1)$$

$$AVG_{Chain\ length}(ACL) = \sum_{i=1}^{6} Length_i \ x \ \left(\frac{Composition_i}{100}\right) \qquad (4.2)$$

Table 4.1: Compositional profiles (vol-%) of the total methyl esters for the plant-derived biodiesels [5].

Fatty Acid	Chain Length	Unsaturation	*i*	Canola	Corn	Soybean
C16:0	16	0	1	4.1	11.7	11.1
C18:0	18	0	2	1.8	1.5	4.2
C18:1	18	1	3	65.4	30.9	22.1
C18:2	18	2	4	18.8	54.4	54.2
C18:3	18	3	5	7.6	1	7.9
C20:1	20	1	6	1	0	0
ADU				1.27	1.43	1.54
ACL				17.70	17.68	17.69

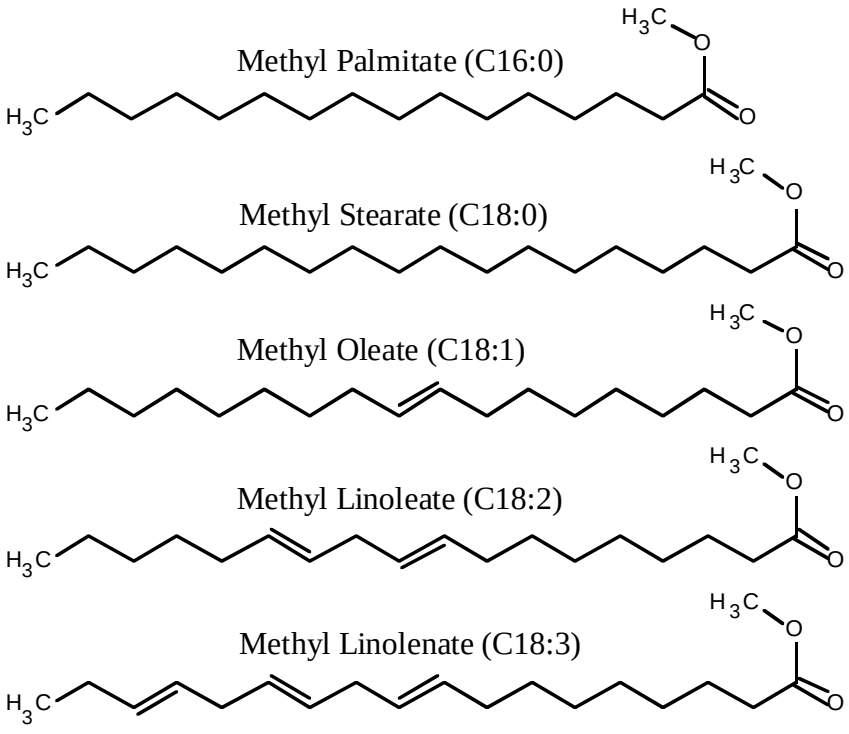

Figure 4.1: Chemical structures of the major neat components for the three plant-derived biofuels [5].

4.3 Results and Discussion

4.3-1 Amended Initial Results of the Stuhlman et al. Study [5]

Fig. 4.2(a) and 4.2(b) show the overall ignition delay times and DCNs of the biodiesels, respectively as a function of the average degree of unsaturation (ADU) found from Equation 4.1 and given in Table 4.1. The x-axis of the graphs in Fig. 4.2 was considered to be suitable since the average chain length among the different biofuels changed very little. Note that the ignition delay times in Fig. 4.2(a) are the overall ignition delay times, not the onset of ignition delay times used for the DCN calculation. The overall ignition delay times show a monotonic non-linear increase in ignition delay time with increasing ADU. The calculated DCNs based on the 0.2 bar pressure rise criterion are shown in Fig. 4.2(b); this plot shows a near linear decrease in DCN with increasing ADU.

(a) Ignition Dealy Times for the Various Biofuels

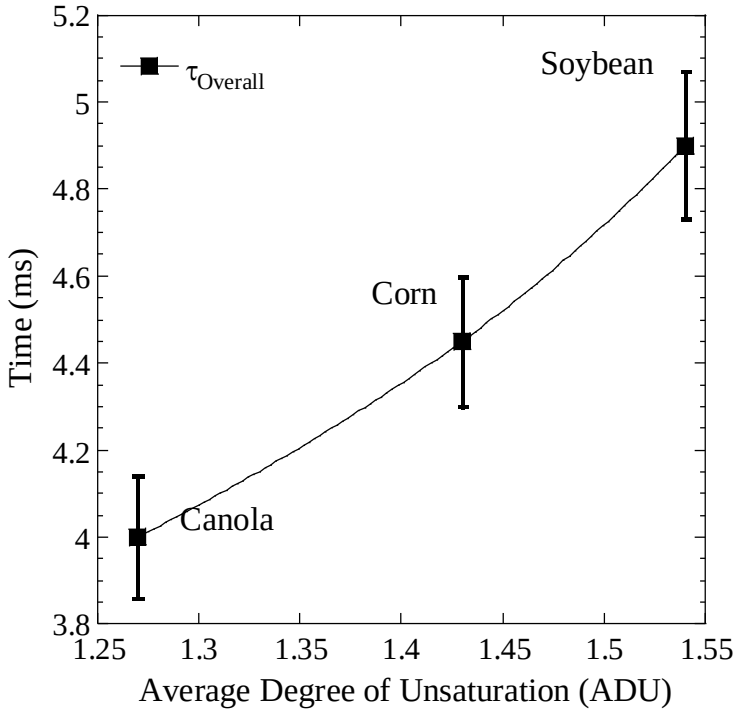

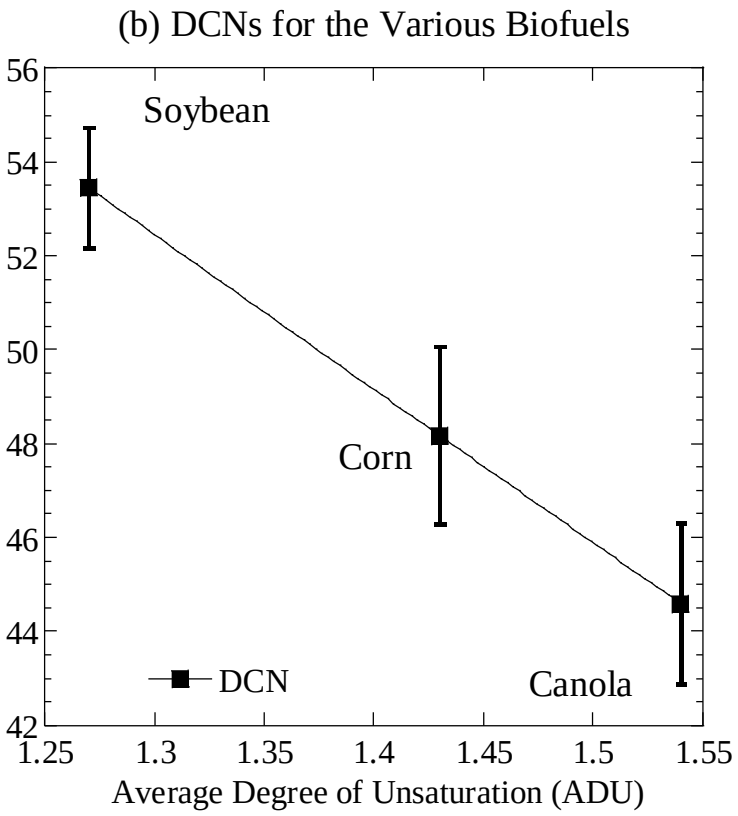

Figure 4.2: (a) Overall ignition delay times of the soybean, corn, and canola biodiesel. (b) Derived cetane numbers of the soybean, corn, and canola biodiesel.

The DCN trend in Fig. 4.2(b) can be explained by examining the makeup of the three biodiesels shown in Table 4.2. Note that the CNs of the pure constituents were obtained from work of Yanowitz et al.[124], and represent the average for the ASTM D613 (CFR) values reported in the compendium. The fuel with the highest amount of unsaturation, in terms of the double bonds, exhibits the lowest DCN. Based on the composition profile in Table 4.2, the soy biodiesel has the highest C18:2 and C18:3 content, followed by corn and canola. It is the inhibiting effect of these multiple double bonds that leads to reduced reactivity and a lower DCN. Even if one were to include the C18:1 in the analysis, the ranking remains the same in terms of the weighted average of the number of ‘double bonds’ present in each biodiesel. To aid in the comparison between the current work and the work present in the literature, the

following equation is proposed. It is simply an average based on the CNs presented by Yanowitz et al.[124] and the biodiesel fatty acid composition.

$$Average\ Cetane\ Number\ (ACN) = \sum_{i=1}^{5} CN[120]_i\ x\ \left(\frac{Composition_i}{100}\right) \qquad (4.3)$$

Table 4.2 (b) shows that the ACN follows the same trend as the work presented here. However, the range of the ACNs (2.2 CN units) is much shorter compared to the DCNs (10.4 DCN units).

Table 4.2: (a) Cetane Numbers of the biodiesel components and compositions of the biodiesels. (b) The experimental DCN found here and the Average Cetane Number (CAN) based on (a) [5].

(a) Yanowitz et al. CNs and Methyl Ester Composition				
Component	CN	Percent Methyl Ester in Biodiesel		
		Canola	Corn	Soybean
Methyl Palmitate (C16:0)	74	4.1	11.7	11.1
Methyl Stearate (C18:0)	81	1.8	1.5	4.2
Methyl Oleate (C18:1)	56	65.4	30.9	22.1
Methyl Linoleate (C18:2)	42	18.8	54.4	54.2
Methyl Linolenate (C18:3)	46	7.6	1	7.9

(b) Experimental DCN Comparison		
	Current Work (DCN)	ACN
Canola	54.3	52.5
Corn	47.5	50.4
Soy	43.9	50.3

4.3-2 Initial Oxidizer Temperature Effect on Biodiesels

The biodiesels were tested at three additional initial oxidizer temperatures. This was done so that the ignition delay ranking of the biodiesels could be further investigated. The pressure traces of the soybean, corn, and canola biofuels are presented in Fig. 4.3(a), (b), & (c) respectively. In general, the different biofuels behave similarly when subjected to different temperatures; that is, a monotonic increasing trend in the ignition delay time with decreeing initial oxidizer temperatures.

From Fig. 4.3 (a), (b), & (c), there is a general decreasing trend in the maximum chamber pressure with decreasing initial oxidizer temperature. This is suspected to be because of the decreasing equivalence ratio trend with decreasing initial temperature; this being based on the assumptions of the ideal gas law and a constant injected mass of fuel for a given biodiesel between initial air temperatures. However, the exception to this trend is for initial air temperatures of 767 ~K. Surprisingly, at this initial air temperature all the biodiesels had their chamber pressure maximums. The reason for this is unknown. Additionally, a similar finding was observed for the works given in Chapter 2 & 3. The normalness of this occurrence may indicate that the assumptions used to formulate the expected trend are not entirely valid or are incomplete. This needs further investigating. One interesting note is that the magnitude of the maximum chamber pressure, at an initial oxidizer temperature of 767 K, changes for the different biofuels. The soybean peak pressure was 33.5 bar, corn 33.7 bar, and canola 34.1 bar; surprisingly the maximum chamber pressure ranking (soybean <corn<canola), is consistent with the DCN ranking believed to be linked to effective degree of unsaturation of the biodiesel.

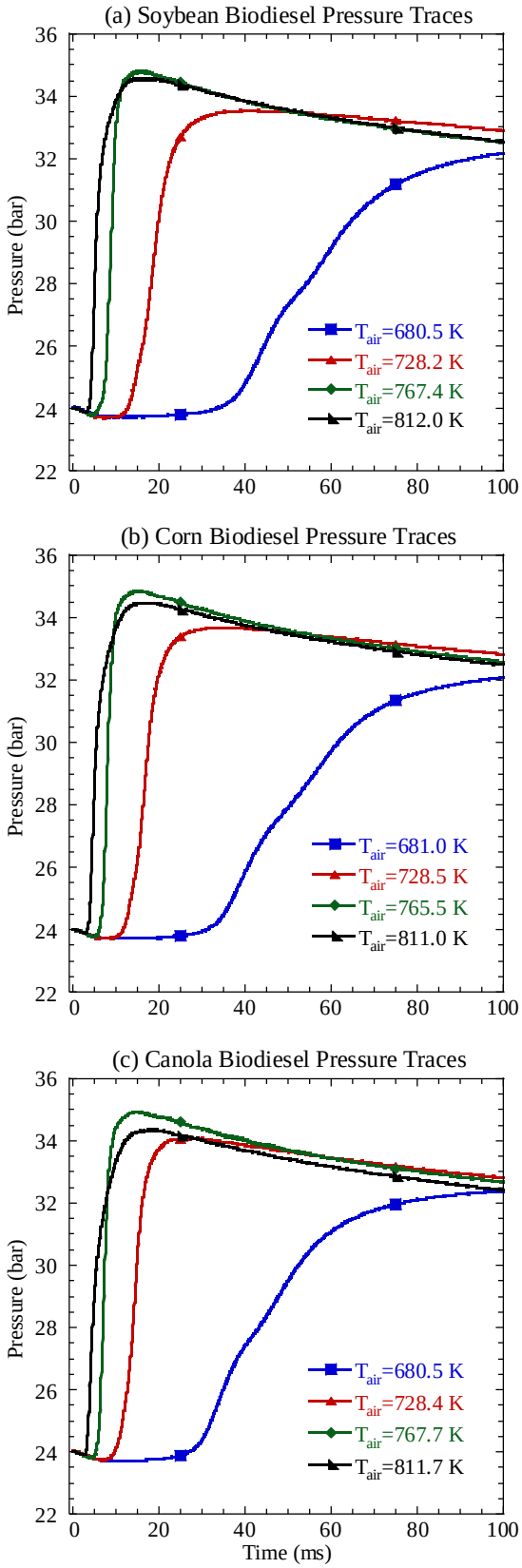

Figure 4.3: Averaged pressure traces with varying initial oxidizer temperatures for (a) soybean biodiesel, (b) corn biodiesel, and (c) canola biodiesel

Fig. 4.3 also showed that all the biodiesels exhibited a two-stage ignition behavior for the coldest initial air temperature experiments at ~680.7 K. Additionally, the soy and corn biodiesels showed two stage behavior at initial air temperatures of ~728 K. To better display the two-stage behavior, the individual & averaged pressure traces, along with the average rate of pressure rise is shown for Canola at 680.5 K and soybean at 728.2 K in Fig. 4.4(a) & (b) respectively. Note the distinct differences between in the two-stage ignition behavior resultant from the different oxidizer temperatures. The average rate of pressure rise in Fig. 4.4 (a) shows the first stage ignition event having a larger rate of pressure rise maximum than the overall ignition event. The opposite is seen for the higher temperature test shown in Fig. 4.4 (b); the first stage ignition event, consistent with first rate of pressure rise maximum, is smaller than the overall ignition delay.

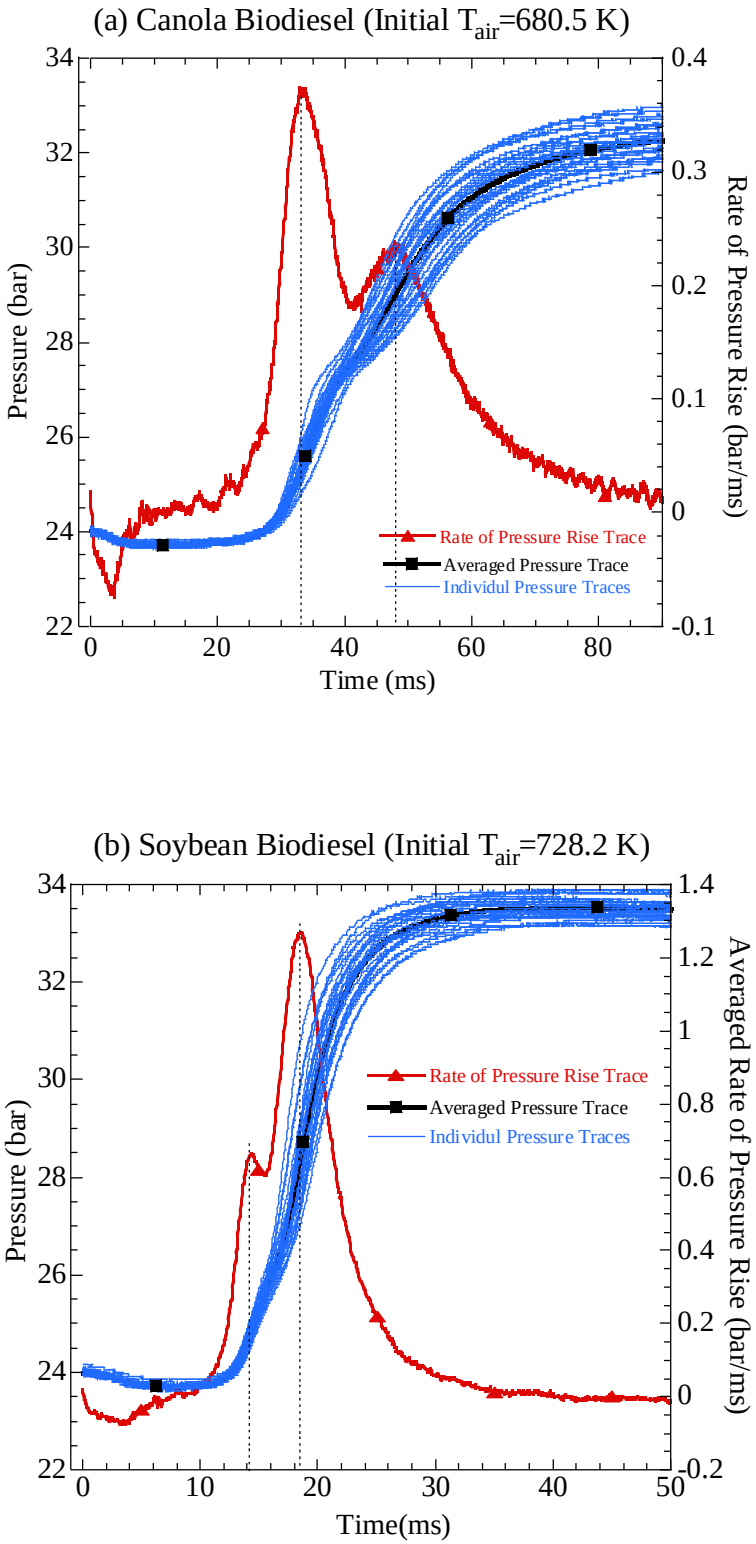

Figure 4.4:Individual and averaged pressure traces, as well as the rate of pressure rise for (a) canola biodiesel at T_{air}=680 K, and (b) soybean biodiesel at T_{air}=728 K.

All the ignition delays form the biodiesel experiments are shown in Fig. 4.5. Note the inverse temperature x axis and the y axis log scale. Overall, the ignition delay time ranking of the different biofuels with respect to temperature is maintained, with the exception of the overall ignition delay time of the corn and soybean biodiesels at the lowest initial oxidizer temperature. Overall the trend is nonlinear, perhaps indicative of being near the NTC region.

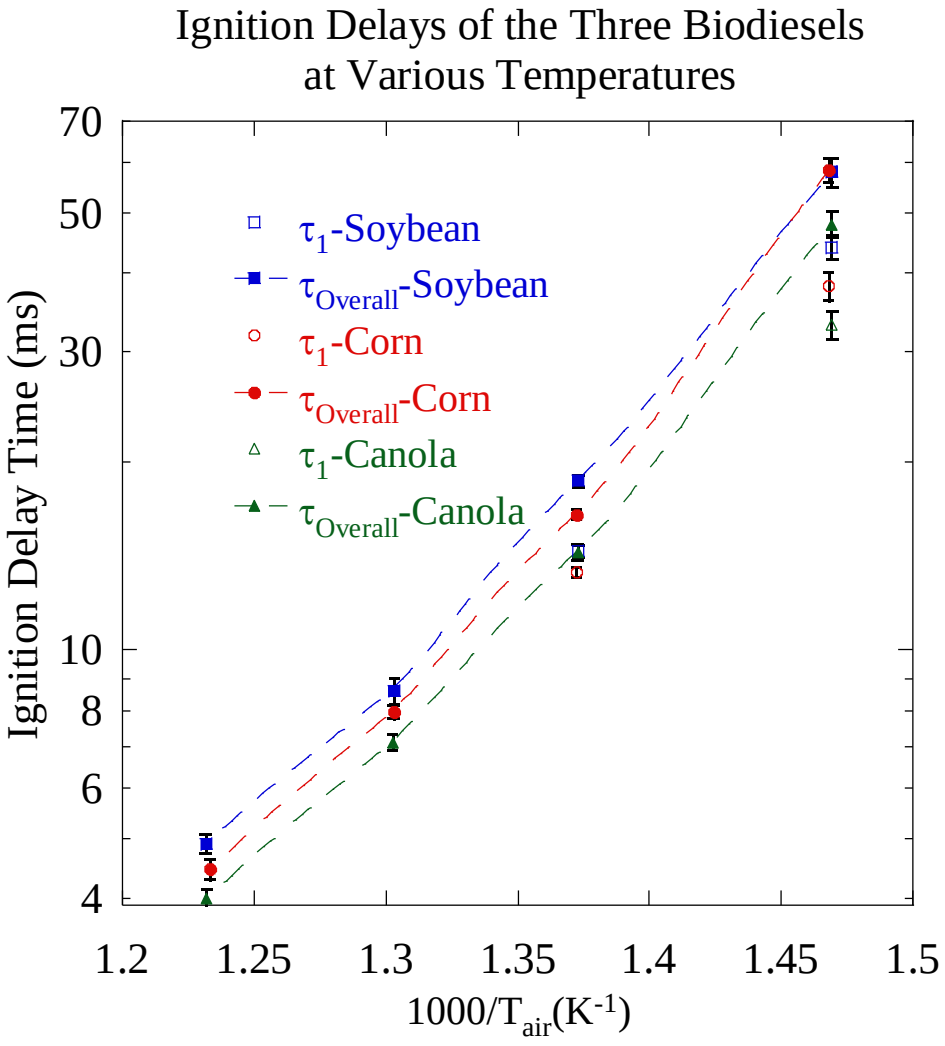

Figure 4.5: First stage ignition and overall ignition events of the biodiesels at different temperatures.

4.4 Conclusions Regarding Biodiesel Study

The autoignition characteristics of three biodiesels produced from three plant derived feedstock have been obtained in a constant volume combustion chamber at a fixed fuel injection duration and various oxidizer temperatures. It was found that the biodiesel derived from canola was the most reactive followed by corn and soy. Similar post combustion pressure rises were observed for the three biodiesels. However, there was a discernible difference in the burn rate for the three fuels with soy-derived biodiesel exhibiting the highest peak value for the rate of pressure rise, followed by corn and canola. These findings are significant because it gives some indication of what feedstock might hold a higher value, in the sense of auto ignition propensity.

From the various oxidizer tests, two stage ignition behavior was seen for the lower temperature tests, ~680 K. The ignition delay time trend was found to be consistent with the amount and degree of unsaturated components present in a particular biodiesel; additionally, the ignition delay ranking was preserved throughout other initial air temperature tests.

.

References

[1] G. Joshi, J. K. Pandey, S. Rana, D. S. Rawat, Challenges and opportunities for the application of biofuel, Renewable and Sustainable Energy Reviews 79 (Supplement C) (2017) 850-866.

[2] T. M. Y. khan, A. E. Atabani, I. A. Badruddin, A. Badarudin, M. S. Khayoon, S. Triwahyono, Recent scenario and technologies to utilize non-edible oils for biodiesel production, Renewable and Sustainable Energy Reviews 37 (Supplement C) (2014) 840-851.

[3] S. N. Naik, V. V. Goud, P. K. Rout, A. K. Dalai, Production of first and second generation biofuels: A comprehensive review, Renewable and Sustainable Energy Reviews 14 (2) (2010) 578-597.

[4] R. Slade, A. Bauen, Micro-algae cultivation for biofuels: Cost, energy balance, environmental impacts and future prospects, Biomass and Bioenergy 53 (2013) 29-38.

[5] C. D. S. Stuhlman, R. Leathers, K. Kumar, D. Shrestha, S. Beyerlein and C.J. Sung, Ignition Delay Times and Derived Cetane Numbers of Canola, Corn, and Soy Derived Bio-Diesel, Fall Technical Meeting of the Western States Section of the Combustion Institute, University of Wyoming, Laramie, Paper 29KI-0043 (2017).

[6] ASTM D7170-09, Standard test method for determination of derived cetane number (DCN) of diesel fuel oils – fixed range injection period, constant volume combustion chamber method, West Conshohocken, PA, 2008,

[7] DIN 73372, Injection nozzles, size T and U, Berlin, Germany, 1978,

[8] Waukesha Engine Dresser: Fuel Ignition Tester User Manual, Waukesha, Wisconsin 53188, 2006

[9] Horiba, Automotive Emissions Analyzer MEXA-584L Instruction Manual, 2008

[10] CHEMKIN-PRO

[11] J. C. Allen, W. J. Pitz, B. T. Fisher, Experimental and computational study of n-heptane autoignition in a direct-injection constant-volume combustion chamber, Journal of Engineering for Gas Turbines and Power-Transactions of the ASME 136 (9) (2014).

[12] G. E. Bogin, E. Osecky, J. Y. Chen, M. A. Ratcliff, J. Luecke, B. T. Zigler, A. M. Dean, Experiments and Computational Fluid Dynamics Modeling Analysis of Large n-Alkane Ignition Kinetics in the Ignition Quality Tester, Energy Fuels 28 (7) (2014) 4781-4794.

[13] M. Uyttebroek, W. Van Hecke, K. Vanbroekhoven, Sustainability metrics of 1-butanol, Catalysis Today 239 (Supplement C) (2015) 7-10.

[14] C. Jin, M. F. Yao, H. F. Liu, C. F. F. Lee, J. Ji, Progress in the production and application of n-butanol as a biofuel, Renewable & Sustainable Energy Reviews 15 (8) (2011) 4080-4106.

[15] S. Belletante, L. Montastruc, S. Negny, S. Domenech, Optimal design of an efficient, profitable and sustainable biorefinery producing acetone, butanol and ethanol: Influence of the in-situ separation on the purification structure, Biochemical Engineering Journal 116 (2016) 195-209.

[16] W. R. D. Trindade, R. G. dos Santos, Review on the characteristics of butanol, its production and use as fuel in internal combustion engines, Renewable & Sustainable Energy Reviews 69 (2017) 642-651.

[17] B. C. Adam Schubert, Wendy Rosen, in: Butamax Advanced Biofuels LLC: WILMINGTON, Del., 2017.

[18] I. L. R. Bec, Y. Zhu, D. F. Davidson, R. K. Hanson, Shock Tube Measurements of Ignition Delay Times for the Butanol Isomers Using the Constrained-Reaction-VolumeStrategy, Int. J. Chem. Kinet. 46 (8) (2014) 433-442.

[19] G. Black, H. J. Curran, S. Pichon, J. M. Simmie, V. Zhukov, Bio-butanol: Combustion properties and detailed chemical kinetic model, Combustion and Flame 157 (2) (2010) 363-373.

[20] Z. Geng, L. L. Xu, H. Li, J. X. Wang, Z. Huang, X. C. Lu, Shock Tube Measurements and Modeling Study on the Ignition Delay Times of n-Butanol/Dimethyl Ether Mixtures, Energy Fuels 28 (6) (2014) 4206-4215.

[21] L. Pan, Y. J. Zhang, Z. M. Tian, F. Y. Yang, Z. H. Huang, Experimental and Kinetic Study on Ignition Delay Times of iso-Butanol, Energy Fuels 28 (3) (2014) 2160-2169.

[22] S. S. Vasu, S. M. Sarathy, On the High-Temperature Combustion of n-Butanol: Shock Tube Data and an Improved Kinetic Model, Energy Fuels 27 (11) (2013) 7072-7080.

[23] J. X. Zhang, S. D. Niu, Y. J. Zhang, C. L. Tang, X. Jiang, E. J. Hu, Z. H. Huang, Experimental and modeling study of the auto-ignition of n-heptane/n-butanol mixtures, Combustion and Flame 160 (1) (2013) 31-39.

[24] M. S. Agathou, D. C. Kyritsis, An experimental comparison of non-premixed bio-butanol flames with the corresponding flames of ethanol and methane, Fuel 90 (1) (2011) 255-262.

[25] M. S. Agathou, D. C. Kyritsis, Experimental investigation of bio-butanol laminar non-premixed flamelets, Applied Energy 93 (2012) 296-304.

[26] K. B. Brady, X. Hui, C. J. Sung, Effect of hydrogen addition on the counterflow ignition of n-butanol at atmospheric and elevated pressures, International Journal of Hydrogen Energy 40 (46) (2015) 16618-16633.

[27] H. F. Jin, A. Cuoci, A. Frassoldati, T. Farayelli, Y. Z. Wang, Y. Y. Li, F. Qi, Experimental and kinetic modeling study of PAH formation in methane coflow diffusion flames doped with n-butanol, Combustion and Flame 161 (3) (2014) 657-670.

[28] W. Liu, A. P. Kelley, C. K. Law, Non-premixed ignition, laminar flame propagation, and mechanism reduction of n-butanol, iso-butanol, and methyl butanoate, Proc. Combust. Inst. 33 (2011) 995-1002.

[29] S. M. Sarathy, M. J. Thomson, C. Togbe, P. Dagaut, F. Halter, C. Mounaim-Rousselle, An experimental and kinetic modeling study of n-butanol combustion, Combustion and Flame 156 (4) (2009) 852-864.

[30] P. Singh, X. Hui, C. J. Sung, Soot formation in non-premixed counterflow flames of butane and butanol isomers, Combustion and Flame 164 (2016) 167-182.

[31] J. Beeckmann, L. Cai, H. Pitsch, Experimental investigation of the laminar burning velocities of methanol, ethanol, n-propanol, and n-butanol at high pressure, Fuel 117 (2014) 340-350.

[32] X. L. Gu, Z. H. Huang, Q. Q. Li, C. L. Tang, Measurements of Laminar Burning Velocities and Markstein Lengths of n-Butanol-Air Premixed Mixtures at Elevated Temperatures and Pressures, Energy Fuels 23 (2009) 4900-4907.

[33] X. L. Gu, Z. H. Huang, S. Wu, Q. Q. Li, Laminar burning velocities and flame instabilities of butanol isomers-air mixtures, Combustion and Flame 157 (12) (2010) 2318-2325.

[34] X. Y. Zhang, C. L. Tang, H. B. Yu, Q. Q. Li, J. Gong, Z. H. Huang, Laminar Flame Characteristics of iso-Octane/n-Butanol Blend-Air Mixtures at Elevated Temperatures, Energy Fuels 27 (4) (2013) 2327-2335.

[35] Y. Xu, C. T. Avedisian, Combustion of n-Butanol, Gasoline, and n-Butanol/Gasoline Mixture Droplets, Energy & Fuels 29 (5) (2015) 3467-3475.

[36] H. Ghiassi, I. C. Jaramillo, J. S. Lighty, Kinetics of Soot Oxidation by Molecular Oxygen in a Premixed Flame, Energy & Fuels 30 (4) (2016) 3463-3472.

[37] W. Pan, D. Liu, Effects of hydrogen additions on premixed rich flames of four butanol isomers, International Journal of Hydrogen Energy 42 (6) (2017) 3833-3841.

[38] P. S. Veloo, Y. L. Wang, F. N. Egolfopoulos, C. K. Westbrook, A comparative experimental and computational study of methanol, ethanol, and n-butanol flames, Combustion and Flame 157 (10) (2010) 1989-2004.

[39] P. Dagaut, S. M. Sarathy, M. J. Thomson, A chemical kinetic study of n-butanol oxidation at elevated pressure in a jet stirred reactor, Proc. Combust. Inst. 32 (2009) 229-237.

[40] P. Dagaut, C. Togbe, Oxidation kinetics of butanol-gasoline surrogate mixtures in a jet-stirred reactor: Experimental and modeling study, Fuel 87 (15-16) (2008) 3313-3321.

[41] P. Dagaut, C. Togbe, Oxidation kinetics of mixtures of iso-octane with ethanol or butanol in a jet-stirred reactor: experimental and modeling study, Combustion Science and Technology 184 (7-8) (2012) 1025-1038.

[42] P. Saisirirat, C. Togbe, S. Chanchaona, F. Foucher, C. Mounaim-Rousselle, P. Dagaut, Auto-ignition and combustion characteristics in HCCI and JSR using 1-butanol/n-heptane and ethanol/n-heptane blends, Proc. Combust. Inst. 33 (2011) 3007-3014.

[43] C. Togbe, A. Mze-Ahmed, P. Dagaut, Kinetics of Oxidation of 2-Butanol and Isobutanol in a Jet-Stirred Reactor: Experimental Study and Modeling Investigation, Energy Fuels 24 (2010) 5244-5256.

[44] E. Agbro, A. S. Tomlin, M. Lawes, S. Park, S. M. Sarathy, The influence of n-butanol blending on the ignition delay times of gasoline and its surrogate at high pressures, Fuel 187 (2017) 211-219.

[45] B. W. Weber, K. Kumar, Y. Zhang, C. J. Sung, Autoignition of n-butanol at elevated pressure and low-to-intermediate temperature, Combustion and Flame 158 (5) (2011) 809-819.

[46] Z. Yang, Y. Qian, X. Yang, Y. Wang, Y. Wang, Z. Huang, X. C. Lu, Autoignition of n-Butanol/n-Heptane Blend Fuels in a Rapid Compression Machine under Low-to-Medium Temperature Ranges, Energy Fuels 27 (12) (2013) 7800-7808.

[47] Z. Yang, Y. Wang, X. Yang, Y. Qian, X. C. Lu, Z. Huang, Autoignition of butanol isomers/n-heptane blend fuels on a rapid compression machine in N-2/O-2/Ar mixtures, Science China-Technological Sciences 57 (3) (2014) 461-470.

[48] J. Hou, F. Yan, T. H. Lee, W. Chang, C.-f. F. Lee, Computational Investigation on Soot Mechanism of Diesel and Diesel/n-Butanol Blend in Constant Volume Chamber with Various Ambient Temperatures, Energy & Fuels 31 (1) (2017) 916-931.

[49] R. Li, Z. Liu, Y. Han, M. Tan, Y. Xu, J. Tian, D. Chong, J. Chai, J. Liu, Z. Li, Experimental and Numerical Investigation into the Effect of Fuel Type and Fuel/Air Molar Concentration on Autoignition Temperature of n-Heptane, Methanol, Ethanol, and Butanol, Energy Fuels 31 (3) (2017) 2572-2584.

[50] H. Liu, X. Bi, M. Huo, C.-f. F. Lee, M. Yao, Soot Emissions of Various Oxygenated Biofuels in Conventional Diesel Combustion and Low-Temperature Combustion Conditions, Energy Fuels 26 (3) (2012) 1900-1911.

[51] H. Liu, C.-f. Lee, M. Huo, M. Yao, Comparison of Ethanol and Butanol as Additives in Soybean Biodiesel Using a Constant Volume Combustion Chamber, Energy Fuels 25 (4) (2011) 1837-1846.

[52] H. Liu, C.-f. F. Lee, M. Huo, M. Yao, Combustion Characteristics and Soot Distributions of Neat Butanol and Neat Soybean Biodiesel, Energy Fuels 25 (7) (2011) 3192-3203.

[53] M. E. Baumgardner, S. M. Sarathy, A. J. Marchese, Autoignition characterization of primary reference fuels and n-heptane/n-butanol mixtures in a constant volume combustion device and homogeneous charge compression ignition engine, Energy & Fuels 27 (12) (2013) 7778-7789.

[54] G. E. Bogin, A. DeFilippo, J. Y. Chen, G. Chin, J. Luecke, M. A. Ratcliff, B. T. Zigler, A. M. Dean, Numerical and Experimental Investigation of n-Heptane Autoignition in the Ignition Quality Tester (IQT), Energy Fuels 25 (12) (2011) 5562-5572.

[55] F. M. Haas, A. Ramcharan, F. L. Dryer, Relative Reactivities of the Isomeric Butanols and Ethanol in an Ignition Quality Tester, Energy Fuels 25 (9) (2011) 3909-3916.

[56] E. Papajak, P. Seal, X. F. Xu, D. G. Truhlar, Thermochemistry of radicals formed by hydrogen abstraction from 1-butanol, 2-methyl-1-propanol, and butanal, J. Chem. Phys. 137 (10) (2012) 13.

[57] D. Katsikadakos, C. W. Zhou, J. M. Simmie, H. J. Curran, P. A. Hunt, Y. Hardalupas, A. Taylor, Rate constants of hydrogen abstraction by methyl radical from n-butanol and a comparison of CanTherm, MultiWell and Variflex, Proc. Combust. Inst. 34 (2013) 483-491.

[58] C. W. Zhou, J. M. Simmie, H. J. Curran, Rate constants for hydrogen-abstraction by (O) over dotH from n-butanol, Combustion and Flame 158 (4) (2011) 726-731.

[59] P. Zhang, S. J. Klippenstein, C. K. Law, Ab Initio Kinetics for the Decomposition of Hydroxybutyl and Butoxy Radicals of n-Butanol, J. Phys. Chem. A 117 (9) (2013) 1890-1906.

[60] B. L. Deng, J. Q. Fu, D. M. Zhang, J. Yang, R. H. Feng, J. P. Liu, K. Li, X. Q. Liu, The heat release analysis of bio-butanol/gasoline blends on a high speed SI (spark ignition) engine, Energy 60 (2013) 230-241.

[61] A. Elfasakhany, Experimental study on emissions and performance of an internal combustion engine fueled with gasoline and gasoline/n-butanol blends, Energy Conversion and Management 88 (2014) 277-283.

[62] Y. Zhang, A. L. Boehman, Oxidation of 1-butanol and a mixture of n-heptane/1-butanol in a motored engine, Combustion and Flame 157 (10) (2010) 1816-1824.

[63] M. A. Fayad, A. Tsolakis, D. Fernandez-Rodriguez, J. M. Herreros, F. J. Martos, M. Lapuerta, Manipulating modern diesel engine particulate emission characteristics through butanol fuel blending and fuel injection strategies for efficient diesel oxidation catalysts, Applied Energy 190 (2017) 490-500.

[64] S. Yu, T. Y. Gao, M. P. Wang, L. G. Li, M. Zheng, Ignition control for liquid dual-fuel combustion in compression ignition engines, Fuel 197 (2017) 583-595.

[65] C. Zhang, C. H. Zhang, L. Xue, Y. Y. Li, Combustion characteristics and operation range of a RCCI combustion engine fueled with direct injection n-heptane and pipe injection n-butanol, Energy 125 (2017) 439-448.

[66] F. Lujaji, A. Bereczky, M. Mbarawa, Performance Evaluation of Fuel Blends Containing Croton Oil, Butanol, and Diesel in a Compression Ignition Engine, Energy Fuels 24 (8) (2010) 4490-4496.

[67] A. Zare, T. A. Bodisco, M. N. Nabi, F. M. Hossain, Z. D. Ristovski, R. J. Brown, Engine Performance during Transient and Steady-State Operation with Oxygenated Fuels, Energy & Fuels 31 (7) (2017) 7510-7522.

[68] J. R. Agudelo, M. Lapuerta, O. Moyer, A. L. Boehman, Autoignition of Alcohol/C7-Esters/n-Heptane Blends in a Motored Engine under HCCI Conditions, Energy & Fuels 31 (3) (2017) 2985-2995.

[69] B. Q. He, M. B. Liu, J. Yuan, H. Zhao, Combustion and emission characteristics of a HCCI engine fuelled with n-butanol-gasoline blends, Fuel 108 (2013) 668-674.

[70] B. Q. He, J. Yuan, M. B. Liu, H. Zhao, Combustion and emission characteristics of a n-butanol HCCI engine, Fuel 115 (2014) 758-764.

[71] B. Q. He, J. Yuan, M. B. Liu, H. Zhao, Low-Temperature Combustion Characteristics of a n-Butanol/Isooctane HCCI Engine, Energy Fuels 28 (6) (2014) 4183-4192.

[72] S. Visakhamoorthy, J. Z. Wen, S. Sivoththaman, C. R. Koch, Numerical study of a butanol/heptane fuelled Homogeneous Charge Compression Ignition (HCCI) engine utilizing negative valve overlap, Applied Energy 94 (2012) 166-173.

[73] K. Kumar, Y. Zhang, C. J. Sung, W. J. Pitz, Autoignition response of n-butanol and its blends with primary reference fuel constituents of gasoline, Combustion and Flame 162 (6) (2015) 2466-2479.

[74] S. M. Sarathy, S. Vranckx, K. Yasunaga, M. Mehl, P. Oßwald, W. K. Metcalfe, C. K. Westbrook, W. J. Pitz, K. Kohse-Höinghaus, R. X. Fernandes, H. J. Curran, A comprehensive

chemical kinetic combustion model for the four butanol isomers, Combustion and Flame 159 (6) (2012) 2028-2055.

[75] D. M. A. Karwat, S. W. Wagnon, M. S. Wooldridge, C. K. Westbrook, On the Combustion Chemistry of n-Heptane and n-Butanol Blends, The Journal of Physical Chemistry A 116 (51) (2012) 12406-12421.

[76] iso-Octane, Version 3. https://combustion.llnl.gov/mechanisms/alkanes/iso-octane-version-3 (1-15-2017)

[77] H. J. Curran, P. Gaffuri, W. J. Pitz, C. K. Westbrook, A comprehensive modeling study of iso-octane oxidation, Combustion and Flame 129 (3) (2002) 253-280.

[78] M. Mehl, H. J. Curran, W. J. Pitz, C. K. Westbrook, Chemical kinetic modeling of component mixtures relevant to gasoline, 4th European Combustion Meeting, Vienna, Austria, LLNL-CONF410968, 2009.

[79] M. Mehl, W. J. Pitz, M. Sjöberg, J. E. Dec, Detailed kinetic modeling of low-temperature heat release for PRF fuels in an HCCI engine, SAE 2009 International Powertrains, Fuels and Lubricants Meeting, Florence, Italy, SAE Paper No. 2009-01-1806., 2009.

[80] Neutrium SPECIFIC ENERGY AND ENERGY DENSITY OF FUELS. https://neutrium.net/properties/specific-energy-and-energy-density-of-fuels/ (10-30-2017)

[81] ASTM D7170-09, Standard test method for determination of derived cetane number (DCN) of diesel fuel oils – fixed range injection period, constant volume combustion chamber method, West Conshohocken, PA, 2009,

[82] ASTM D6890-04, Standard Test Method for Determination of Ignition Delay and Derived Cetane Number (DCN) of Diesel Fuel Oils by Combustion in a Constant Volume Chamber, West Conshohocken, PA, 2004,

[83] S. Tanaka, F. Ayala, J. C. Keck, J. B. Heywood, Two-stage ignition in HCCI combustion and HCCI control by fuels and additives, Combustion and Flame 132 (1) (2003) 219-239.

[84] J. Hou, F. W. Yan, T. H. Lee, W. N. Chang, C. F. F. Lee, Computational Investigation on Soot Mechanism of Diesel and Diesel/n-Butanol Blend in Constant Volume Chamber with Various Ambient Temperatures, Energy Fuels 31 (1) (2017) 916-931.

[85] R. N. Dahms, G. A. Paczko, S. A. Skeen, L. M. Pickett, Understanding the ignition mechanism of high-pressure spray flames, Proc. Combust. Inst. 36 (2) (2017) 2615-2623.

[86] Z. H. Li, W. J. Wang, Z. Huang, M. A. Oehlschlaeger, Autoignition of Methyl Decanoate, a Biodiesel Surrogate, under High-Pressure Exhaust Gas Recirculation Conditions, Energy Fuels 26 (8) (2012) 4887-4895.

[87] Energy Information Administration Monthly Energy Review September 2016, Biodiesel and Other Renewable Fuels Overview, 2016.

[88] ASTM D6751-07a, Standard Specification for Biodiesel Fuel Blend Stock (B100) for Middle Distillate Fuels, West Conshohocken, PA, 2007, www.astm.org

[89] T. Issariyakul, A. K. Dalai, Biodiesel from vegetable oils, Renewable & Sustainable Energy Reviews 31 (2014) 446-471.

[90] A. C. Hansen, D. C. Kyristis, C.-f. F. Lee, in: Biomass to Biofuels, A. A. Vertes; N. Qureshi; H. P. Blaschek; H. Yukawa, (Eds.) John Wiley & Sons, Ltd: 2010; pp 27-50.

[91] M. Mittelbach, C. Remschmidt, in: Biodiesel the comprehensive handbook, 1 ed.; Mittelbach, Martin (Publisher): Graz, 2004; pp 109-183.

[92] G. Knothe, J. Van Gerpen, The Biodiesel Handbook, Taylor & Francis, 2005

[93] U. S. E. P. A. Report, A Compreensive Analysus of Biodiesel Impacts on Exhaust Emissions, 420-P-02-001 (2002).

[94] J. Krahl, K. Baum, U. Hackbarth, H. E. Jeberien, A. Munack, C. Schütt, O. Schröder, N. Walter, J. Bünger, M. M. Müller, A. Weigel, Gaseous compounds, ozone precursors, particle number and particle size distributions, and mutagenic effects due to biodiesel, 2001

[95] X. W. Cheng, H. K. Ng, S. Y. Gan, J. H. Ho, K. M. Pang, Development and validation of a generic reduced chemical kinetic mechanism for CFD spray combustion modelling of biodiesel fuels, Combustion and Flame 162 (6) (2015) 2354-2370.

[96] O. Herbinet, W. J. Pitz, C. K. Westbrook, Detailed chemical kinetic oxidation mechanism for a biodiesel surrogate, Combustion and Flame 154 (3) (2008) 507-528.

[97] W. J. Wang, S. Gowdagiri, M. A. Oehlschlaeger, Comparative Study of the Autoignition of Methyl Decenoates, Unsaturated Biodiesel Fuel Surrogates, Energy Fuels 27 (9) (2013) 5527-5532.

[98] D. R. Haylett, D. F. Davidson, R. K. Hanson, Ignition delay times of low-vapor-pressure fuels measured using an aerosol shock tube, Combustion and Flame 159 (2) (2012) 552-561.

[99] W. J. Wang, M. A. Oehlschlaeger, A shock tube study of methyl decanoate autoignition at elevated pressures, Combustion and Flame 159 (2) (2012) 476-481.

[100] M. F. Campbell, D. F. Davidson, R. K. Hanson, Ignition delay times of very-low-vapor-pressure biodiesel surrogates behind reflected shock waves, Fuel 126 (2014) 271-281.

[101] I. E. Gerasimov, D. A. Knyazkov, A. M. Dmitriev, L. V. Kuibida, A. G. Shmakov, O. P. Korobeinichev, Experimental and Numerical Study of the Structure of a Premixed Methyl Decanoate/Oxygen/Argon Flame, Combustion Explosion and Shock Waves 51 (3) (2015) 285-292.

[102] Y. L. Wang, Q. Y. Feng, F. N. Egolfopoulos, T. T. Tsotsis, Studies of C-4 and C-10 methyl ester flames, Combustion and Flame 158 (8) (2011) 1507-1519.

[103] K. Seshadri, T. F. Lu, O. Herbinet, S. B. Humer, U. Niemann, W. J. Pitz, R. Seiser, C. K. Law, Experimental and kinetic modeling study of extinction and ignition of methyl decanoate in laminar non-premixed flows, Proc. Combust. Inst. 32 (2009) 1067-1074.

[104] S. M. Sarathy, M. J. Thomson, W. J. Pitz, T. Lu, An experimental and kinetic modeling study of methyl decanoate combustion, Proc. Combust. Inst. 33 (2011) 399-405.

[105] P. Dievart, S. H. Won, J. Gong, S. Dooley, Y. G. Ju, A comparative study of the chemical kinetic characteristics of small methyl esters in diffusion flame extinction, Proc. Combust. Inst. 34 (2013) 821-829.

[106] D. Alviso, J. C. Rolon, P. Scouflaire, N. Darabiha, Experimental and numerical studies of biodiesel combustion mechanisms using a laminar counterflow spray premixed flame, Fuel 153 (2015) 154-165.

[107] S. Dooley, M. Uddi, S. H. Won, F. L. Dryer, Y. G. Ju, Methyl butanoate inhibition of n-heptane diffusion flames through an evaluation of transport and chemical kinetics, Combustion and Flame 159 (4) (2012) 1371-1384.

[108] P. A. Glaude, O. Herbinet, S. Bax, J. Biet, V. Warth, F. Battin-Leclerc, Modeling of the oxidation of methyl esters-Validation for methyl hexanoate, methyl heptanoate, and methyl decanoate in a jet-stirred reactor, Combustion and Flame 157 (11) (2010) 2035-2050.

[109] A. J. Marchese, T. L. Vaughn, K. Kroenlein, F. L. Dryer, Ignition delay of fatty acid methyl ester fuel droplets: Microgravity experiments and detailed numerical modeling, Proc. Combust. Inst. 33 (2011) 2021-2030.

[110] Y. C. Liu, T. Farouk, A. J. Savas, F. L. Dryer, C. T. Avedisian, On the spherically symmetrical combustion of methyl decanoate droplets and comparisons with detailed numerical modeling, Combustion and Flame 160 (3) (2013) 641-655.

[111] C. E. Dumitrescu, A. S. Cheng, E. Kurtz, C. J. Mueller, A Comparison of Methyl Decanoate and Tripropylene Glycol Monomethyl Ether for Soot-Free Combustion in an Optical Direct-Injection Diesel Engine, Journal of Energy Resources Technology-Transactions of the Asme 139 (4) (2017).

[112] C. E. Dumitrescu, A. S. Cheng, E. Kurtz, C. J. Mueller, Asme, A COMPARISON OF METHYL DECANOATE AND TRIPROPYLENE GLYCOL MONOMETHYL ETHER FOR SOOT-FREE COMBUSTION IN AN OPTICAL DIRECT INJECTION DIESEL ENGINE, 2016

[113] A. S. Cheng, C. E. Dumitrescu, C. J. Mueller, Investigation of Methyl Decanoate Combustion in an Optical Direct-Injection Diesel Engine, Energy Fuels 28 (12) (2014) 7689-7700.

[114] J. P. Szybist, A. L. Boehman, D. C. Haworth, H. Koga, Premixed ignition behavior of alternative diesel fuel-relevant compounds in a motored engine experiment, Combustion and Flame 149 (1-2) (2007) 112-128.

[115] M. K. Le, R. L. Zhang, L. Z. Rao, S. Kook, E. R. Hawkes, The development of hydroxyl and soot in a methyl decanoate-fuelled automotive-size optical diesel engine, Fuel 166 (2016) 320-332.

[116] B. Mohan, W. M. Yang, W. B. Yu, K. L. Tay, S. K. Chou, Numerical investigation on the effects of injection rate shaping on combustion and emission characteristics of biodiesel fueled CI engine, Applied Energy 160 (2015) 737-745.

[117] S. R. Hoffman, J. Abraham, A comparative study of n-heptane, methyl decanoate, and dimethyl ether combustion characteristics under homogeneous-charge compression-ignition engine conditions, Fuel 88 (6) (2009) 1099-1108.

[118] K. Kumar, Y. Zhang, C.-J. Sung, W. J. Pitz, Autoignition response of n-butanol and its blends with primary reference fuel constituents of gasoline, Combustion and Flame 162 (6) (2015) 2466-2479.

[119] C. K. Westbrook, W. J. Pitz, O. Herbinet, H. J. Curran, E. J. Silke, A comprehensive detailed chemical kinetic reaction mechanism for combustion of n-alkane hydrocarbons from n-octane to n-hexadecane, Combustion and Flame 156 (1) (2009) 181-199.

[120] E. Ranzi, A. Frassoldati, R. Grana, A. Cuoci, T. Faravelli, A. P. Kelley, C. K. Law, Hierarchical and comparative kinetic modeling of laminar flame speeds of hydrocarbon and oxygenated fuels, Prog. Energy Combust. Sci. 38 (4) (2012) 468-501.

[121] ANSYS® Academic Research, Release 18.1, CHEMKIN PRO, ANSYS, Inc.

[122] N. I. S. a. Technology NIST chemistry WebBook, SRD 69. http://webbook.nist.gov/cgi/cbook.cgi?ID=C110429&Units=SI&Mask=E

[123] U. S. D. o. Agriculture Production, Supply, and Distribution Reports. https://apps.fas.usda.gov/psdonline/app/index.html#/app/downloads (10-30-2017)

[124] J. Yanowitz, M. A. Ratcliff, R. L. McCormick, J. D. Taylor, M. J. Murphy, Compendium of Experimental Cetane Numbers, NREL/TP--5400-67585 United States 10.2172/1345058 NREL English, ; National Renewable Energy Lab. (NREL), Golden, CO (United States), 2017